Characterization of Pattern Recognition Receptor Responses Against Materials for Cell Encapsulation

By

Eunha Kim

B.S. & M.A. Molecular, Cell, and Developmental Biology
University of California, Los Angeles, 2006

Submitted to the Department of Biology
in Partial Fulfillment of the Requirements for the Degree of

Doctor of Philosophy

at the

MASSACHUSETTS INSTUTUTE OF TECHNOLOGY

February 2015

Signature redacted

Signature of Author _____
Eunha Kim
Department of Biology
February 2, 2015

Signature redacted

Certified by _____
Robert S. Langer, Sc.D.
Institute Professor
Thesis Supervisor

Signature redacted

_____
Daniel G. Anderson, Ph.D.
Associate Professor of Chemical Engineering
Thesis Supervisor

Signature redacted

Accepted by _____
Amy E. Keating, Ph.D.
Associate Professor of Biology
Co-Chairman, Graduate Committee

This doctoral thesis was successful defended in public on Thursday, September 11th 2014 at 9:00AM in the Koch Institute Auditorium, Koch Institute for Integrative Cancer Research at MIT in partial fulfillment of the degree of Doctor of Philosophy in Biology at the Massachusetts Institute of Technology.

This thesis has been examined by the following Thesis Committee:

Thesis Supervisor
Robert S. Langer, Sc.D
Institute Professor
Massachusetts Institute of Technology

Daniel G. Anderson, Ph.D.
Associate Professor of Chemical Engineering
Massachusetts Institute of Technology

Thesis Committee
Amy E. Keating, Ph.D.
Associate Professor of Biology
Massachusetts Institute of Technology

Jianzhu Chen, Ph.D.
Professor of Biology
Massachusetts Institute of Technology

Michael Hemann, Ph.D.
Associate Professor of Biology
Massachusetts Institute of Technology

External Thesis Committee
Angela Koehler, Ph.D.
Assistant Professor Biological Engineering
Massachusetts Institute of Technology

Characterization of Pattern Recognition Receptor Responses Against Materials for Cell Encapsulation

By

Eunha Kim

Submitted to the Department of Biology on February 2, 2015
in Partial Fulfillment of the Requirement for the Degree of Doctor of Philosophy in Biology

Abstract

Islet transplantation has significant potential for the treatment of type I diabetes, but an immunoprotective barrier is necessary to protect the donor tissue from host rejection and to eliminate the need for systemic immunosuppressive therapy. Cell encapsulation is an attractive technology to enable donor cell transplantation, but clinical success has remained elusive due to immunological responses to the encapsulated materials. Alginate is the leading material for the microencapsulation of islet cells, successfully creating a barrier between the host immune system and implanted islet cells. However, inflammatory monocytes and macrophages initiate a cascade of immunological responses to the implanted materials, leading to a chronic inflammation that results in fibrosis of the implants and hypoxic death of the islet cells. These macrophages may sense alginate via pattern recognition receptors (PRRs), such as toll-like receptors (TLRs) and NOD-like receptors (NLRs). However, which PRRs are involved, how they recognize alginate, and whether alginate material characteristics and compositions can elicit different responses are not very well understood. To better understand the PRR mediated immune response to alginate, we devised an *in vitro* system to study the activation of PRRs against several commercially available alginates. Here, we report that alginate compositions and material characteristics can influence which PRRs activate and how strongly they can provoke PRR mediated immune response, and that direct cell-to-material contact is a crucial step in initiating such response.

Thesis Supervisor: Robert S Langer, Sc.D.
Title: Institute Professor

Thesis Supervisor: Daniel G. Anderson, Ph.D.
Title: Associate Professor of Chemical Engineering

Acknowledgement

"Success is not final, failure is not fatal: it is the courage to continue that counts."
~ Winston Churchill

First and foremost, I am extremely grateful to my thesis advisors, professors Robert Langer and Daniel Anderson for their unwavering support, guidance, generosity, and patience, and for giving me freedom and flexibility to pursue the projects that befit my needs and interests. I had just joined the lab about a month ago when I was diagnosed with cancer. During my cancer journey, many had recommended that I give up pursuing a Ph.D. Without my advisers' understanding, patience, and support, my persistence alone would not have been enough to finish this dissertation. At times, I faced seemingly impossible obstacles to continue pursuing a Ph.D. But, my advisors supported my determination. Numerous times, I sat with Dan and crafted a doable plan for me to get my Ph.D. Many times, I had no idea whether I could really finish it or not. Many times I hit the rock bottom, and was tempted to give it all up to focus on my health. But, I just knew that I could not give up because I could not have the regret of not finishing the Ph.D. program. After all those struggles, I am here with the final product of the Ph.D. program. Graduate school was extremely difficult for me, and I don't think I could have finished it without my advisers' support. No words can describe my gratitude to my advisers who fostered my development as a graduate student. Also, to the members of my committee, Amy Keating, Jianzhu Chen, and Mike Hemann, for their thoughtful advice, encouragement, at times harsh challenges, and for always making sure that I remain on the track to finish this Ph.D. My life as a graduate student would not have been the same without the enormous help and support from everyone.

To my lab mates, too many to name, Rose Kanasty, Christina Cortez, Nikita Malavia and Fan Yang, just to name a few, thank you. Thank you for being there for me when I broke down in tears from the burdens of fighting cancer, trying to make progress in the lab, and dealing with the death of my cancer buddies. I am incredibly fortunate to have found such an amazing group of friends in the lab. Also, the work described here would truly not have been possible without the collaboration with Arturo Vegas, Omid Veiseh, and Josh Doloff. No words can adequately describe my gratitude to these three who have fostered my development as a scientist and have supported me academically to finish this dissertation.

I also need to thank my medical team, especially Dr. Michael Kane, Dr. Lydia Schapira, Dr. Michelle Gadd, Dr. AnnKathryn Goodman, Dr. Amy Colwell, Dr. Haleh Rokni, and many others for keeping me alive and sane.

Finally, to my family and my guardian Robert Zurcher for supporting me through this long journey of pursuing a higher education so that I could be the first one with a doctorate degree in my family. And, I want to thank my fellowship buddies John Cassady and Sacha Prashad, and my labmate Brian Timko for proofreading this dissertation. Last but not least, HHMI for providing me the five-year Gilliam Fellowship for Advanced Studies.

Life is full of uncertainty, but whatever life throws at me, I know will *never ever* give up.

To R. Zurcher

Table of Contents

Chapter 1

Introduction

~~~ CHAPTER OUTLINE ~~~

- *Diabetes Overview*
- *Historical Development of Diabetes Treatment*
  - *Discovery of endocrine role of pancreas*
  - *Experimental usage of insulin*
  - *Sequencing, synthesis & characterization of Insulin*
  - *Development of insulin analogs*
- *Insulin Biosynthesis and Processing*
- *Glucose Homeostasis*
- *Classification and Treatments of Diabetes*
- *Islet Transplantation*
- *Principles & Materials for Cell Encapsulation*
- *Progress of Alginate Cell Encapsulation*
- *Challenges of Encapsulated Islet Transplantation*
- *Future of Islet Encapsulation*

"In diabetes the thirst is greater for the fluid dries the body ... For the thirst there is need of a powerful remedy, for in kind it is the greatest of all sufferings, and when a fluid is drunk, it stimulates the discharge of urine. "
~ Aretaeus of Cappadocia, 1st century AD

Diabetes Overview

Diabetes mellitus is a metabolic disease characterized by hyperglycemia stemming from inadequate production and/or utilization of insulin. According to International Diabetes Federation, there were 382 million people living with diabetes worldwide in 2013; furthermore, they estimated that by the end of 2013, diabetes could cause 5.1 million deaths and cost the US $548 billion in healthcare spending, making diabetes one of the most prevalent, costly, and debilitating disease in the world (**Figure 1**).
Diabetes generally falls in to one of two categories: type 1 and type 2. Type 1 is an autoimmune disease caused by cellular-mediated autoimmune destruction of the β-cells in the islets of Langerhans in the pancreas, usually leading to absolute insulin deficiency. Unlike type 1 diabetes, type 2 diabetes patients usually have intact β-cells, yet they have insulin resistance with relative insulin deficiency (Drouin et al., 2009).

Discovery of insulin revolutionized the treatment of diabetes. Prior to the discovery of insulin, most juvenile type 1 diabetes patients, shortly after diagnosis, died of ketoacidosis (White, 1932). Frederick Banting, a surgeon, and John Macleod, a professor of physiology, discovered insulin in 1921 and were awarded the Nobel Prize in Medicine in October 1923 (Banting and Best, 1922). Insulin therapy significantly reduced immediate risks of diabetes; however, chronic complications continue to prevail and are the primary cause of

diabetic mortality (Raju, 2006). Persistent chronic hyperglycemia can cause failure of vital organs, leading to various complications such as cardiovascular, cerebrovascular, peripheral vascular diseases, nephropathy, retinopathy, neuropathy, and increased risk of foot amputation. Occurrence and progression of diabetic complications can be reduced if hyperglycemia is strictly controlled with precise insulin therapy; however, doing so with currently available treatments is proven to be difficult (Deedwania and Fonseca, 2005; Sheetz, 2002).

An alternative to insulin replacement therapy that has shown increasingly promising results is a cell replacement therapy using beta cells from the islets of Langerhans. However, there are several technical barriers to be overcome before cell replacement therapy of diabetes can become a reality. The main barrier is to overcome any immune responses against transplanted cells. Despite its long history, cell replacement therapy still has a long way to go before it can become clinically applicable. The effort to make a cell-based cure for diabetes a success will continue to provide significant milestones, not only for the cure of diabetes, but also for other regenerative medicine applications.

Historical Development of Diabetes Treatment

Discovery of endocrine role of pancreas

1869 Paul Langerhans, a medical student, discovered "clumps of cells" within pancreas, which later were named the islet of Langerhans (**Figure 2**) (Langerhans, 1869; Morrison, 1937).

1889 Oscar Minkowski and Joseph von Mering performed the complete pancreatectomy on two dogs and examined their urine for sugar. They demonstrated that pancreas is a gland, which can prevent the hyperglycemia when implanted under the skin of a depancreatized dog, and established classic experimental study of diabetes and its metabolic deviations (Von Mering and Minkowski, 1889; Minkowski, 1989).

1900 E. L. Opie described hyalinization in the islets of Langerhans in diabetic people, and discovered that the islet of Langerhans produce insulin and that the destruction of these cells resulted in diabetes (Opie, 1900).

Experimental usage of insulin

1916 Nicolae Paulescu, a Romanian physiologist, developed the first pancreatic extract that lowered blood sugar in diabetic dogs. He, however, failed to show its application in human diabetes (Paulesco, 1921).

1921 Frederick Banting, John Macleod, Charles Best, and J.B. Collip produced successful insulin extract for the treatment of human diabetes. A 14-year-old boy named Leonard Thompson was the first person to receive the extract to correct the metabolic acidosis at the Toronto General Hospital in Canada in January of 1922. Banting and Macleod were awarded the Nobel Prize in Medicine in October 1923 (Banting and Best, 1922; Banting et al., 1922; Best and Scott, 1923).

Sequencing, synthesis & characterization of Insulin

1923 George Walden, a chemical engineer at the Eli Lilly Company, observed that maintenance of the isoelectric point of insulin allowed a maximum extraction of

insulin from animal pancreases. Eli Lilly became the first insulin manufacturer (Bliss, 1982).

1925 First international insulin unit defined (1 unit = 0.125mg of standard material) (Schade et al., 1983)

1926 Crystalline insulin in concentrations of 10, 20, and 40 units per milliliter became available worldwide

1936 Hans Christian Hagedorn discovered that the action of insulin can be prolonged when zinc is added to protamine insulin (P.Z.I)(Deckert, 2000).

1939 Reiner, Searle, and Lang developed Globin insulin with shorter duration of action than P.Z.I. (protamine zinc insulin) (Mosenthal, 1944; Reiner et al., 1939)

1950 Insulin isophane NPH (neutral protamine Hagedorn), an intermediate acting insulin, with controlled amounts of protamine was developed by Novo Nordisk Company (Schade et al., 1983)

1951 The amorphous Lente insulin (IZS), an intermediate acting insulin, was developed by acetate buffering of zinc insulin. The proportion of zinc in the preparation changed the duration, onset, and peak action of insulin (Hallas-Mo, 1956).

1955 Frederick Sanger and coworkers sequenced Insulin, and it was the first protein to be fully sequenced. Sanger received the Nobel Prize in Chemistry in 1958 (Stretton, 2002).

1960 Rosalyn Yalow and Solomon Berson developed radioimmunoassasy (RIA), and demonstrated insulin metabolism in humans with radioactive iodine isotope labeled insulin (Berson and Yalow, 1968; Berson et al., 1956).

1963-1966 Insulin became the first human protein to be chemically synthesized in laboratories (Katsoyannis et al., 1966; Kung et al., 1966; Meienhofer et al., 1963).

1967 Donald Steiner discovered that insulin was synthesized as a single polypeptide, proinsulin precursor, not as two separate A- and B- chains, and a portion of the proinsulin (C-peptide) was cleaved out after its biosynthesis (Steiner and Oyer, 1967a; Steiner et al., 1967a).

1967 William Kelly and Richard Lillehei performed the first pancreas transplant. A duct ligated segmental pancreas along with kidney and duodenum, from cadaver donor, was transplanted into a 28-year-old woman, and insulin independence was achieved; however, she deceased from pulmonary embolism three months later (Kelly et al., 1967).

1969 Dorothy Crowfoot Hodgkin, a British biochemist and the Nobel laureate of Chemistry, deciphered the structure of insulin by x-ray crystallography (Adams et al., 1969).

1971 Insulin receptors discovered and its interaction with insulin defined (Cuatrecasas, 1969, 1971; Freychet et al., 1971).

1973 U100 (100 units per milliliter) insulin became the standardized insulin for human use in the United States in order to reduce dosage errors and promote better accuracy in administration (Schade et al., 1983).

1974 Highly purified animal insulin was manufactured with new chromatographic purification techniques. Eli Lilly Company introduced "single peak" insulin, using soft gels and scale-up of insulin purification on Sephadex G-50. It was termed as

"single peak" because it gave a single peak in analytical gel filtration. Novo Company introduced monocomponent (MC) insulin, which was purified ion exchange chromatography. MC insulin gave a single band in electrophoresis (Root et al., 1972; Walsh, 2005).

1975 Fully synthetic insulin (CGP12831) was synthesized in the laboratories of Ciba-Geigy in Basel (Teuscher, 1979).

1976 Serum C-peptide became a clinical tool to access pancreatic beta cell function (Rubenstein et al., 1977)

1977 The insulin gene was cloned (Cordell et al., 1979; Ullrich et al., 1977).

1978 Open-loop insulin pump delivery system was invented (Pickup et al., 1979). Also, Genentech used a genetically modified plasmid of *E. coli* bacteria to synthesize insulin. Insulin became the first human protein to be manufactured with recombinant DNA technology (Goeddel et al., 1979).

1980 The human insulin gene was sequenced (Bell et al., 1980). Recombinant DNA human insulin was first tested on 17 non-diabetic volunteers in England, and the potency was compared with porcine insulin (Keen et al., 1980).

1981 Insulin receptor kinase activity was described (Kahn et al., 1981).

1982 FDA approved recombinant human insulin, HumulinR (rapid), and HumulinN (NPH), manufactured by Eli Lilly Company, for the U.S. market.

1989 Islet cells were successfully transplanted into a type I diabetes patient for the first time (Scharp et al., 1990).

Development of insulin analogs

1996 FDA approved a short-acting insulin analog, lispro (Humalog) developed by Eli Lilly Company. In lispro, the natural sequence of proline at position B28 and lysine at position B29 is reversed. This modified amino acid sequence of lispro, decreased the tendency of insulin to self-associate and increased the rate of absorption after subcutaneous injection (DiMarchi et al., 1994; Howey et al., 1994).

2000 The "Edmonton Protocol" was devised to improve results of islet transplantation (Shapiro et al., 2000).

2001 Long acting insulin analog glargine, developed by Aventis Pharma, was approved for clinical use in the U.S. and Europe. Glargine has two arginine residues added at the C-terminal end of the B-chain, and asparagine at the position A21 is substituted with glycine. Glargine has longer duration of action with reduced peak insulin effect (Jones, 2000; Vajo et al., 2013).

2004 Rapid acting insulin analog glulisine, developed by Aventis Pharma, was approved for clinical use in the U.S. In glulisine, the natural sequence of asparagine at position B3 is substituted by lysine, and lysine at position B29 is substituted by glutamic acid (Becker, 2007; Becker and Frick, 2008).

2006 Fatty acid acylated detemir insulin analog (Levemir), developed by Novo Nordisk, approved for clinical use in the U.S. Insulin detemir is a long-acting analog for maintaining the basal level of insulin.

2013 Insulin degludec (Tresiba) is an ultra-long acting insulin analog, developed by Novo Nordisk. Insulin degludec has single amino acid deletion and is conjugated to

hexadecanedioic acid via γ-L-glutamyl spacer at the B29 lysine. It is approved in the Europe and Japan, but not yet in the U.S.

Insulin biosynthesis and processing

Insulin is a small peptide hormone (MW ~6kDa) produced by beta cells in the islet of Langerhans in the pancreas (**Figure 2**). It consists of two polypeptide chains (A and B chains) linked together by two disulfide bonds. An additional disulfide bond exist within the A chain (**Figure 3**) (Levine and Mahler, 1964; Ryle et al., 1955). Insulin is a highly conserved protein with a minimal variation among species. The sequences of amino acids varies between species, but certain segments, especially the positions of three disulfide bonds, are highly conserved, making insulin from one species likely active in another species (Steiner et al., 1985). Indeed, pig insulin has been used to treat diabetes in human (Greene et al., 1983; Richter and Neises, 2003). In most species, the A chain is composed of 21 amino acids, and the B chain of 30 amino acids (Steiner et al., 1985). This two-chain structure was identified in 1955, but it wasn't until 1967 that the precursor of insulin (proinsulin) is a single-chain peptide (Ryle et al., 1955; Steiner and Oyer, 1967b; Steiner et al., 1967b).

In human, there is a precursor of proinsulin – preproinsulin encoded by the *INS* gene on chromosome 11 (Owerbach et al., 1980). The first 24 amino acids of preproinsulin form a hydrophobic signal peptide, which signals the translocation of nascent chain of preproinsulin into the rough endoplasmic reticulum (RER) (Blobel and Dobberstein, 1975). Proinsulin is synthesized in the RER, where the protein gets folded into the correct

conformation, and its disulfide bonds are oxidized. Proinsulin is then transported into the trans Golgi network, where endopeptidases cleave off C-peptide. Resulting two peptide A- and B-chains, linked by two disulfide bonds, are then packaged into immature granules where it gets further processed by carboxypeptidaseE, which removes two pairs of basic residues, producing mature insulin. Mature insulin is then packaged into secretory vesicles, awaiting for metabolic signals to be exocytosed (**Figure 3**; **Figure 4**) (Eskridge and Shields, 1983; Patzelt et al., 1978; Rhodes and Alarcón, 1994; Walter and Johnson, 1994).

Insulin molecules have a tendency to self-associate and form dimers in solution because of the hydrogen bonding between the C-termini of B-chains. Moreover, insulin dimers assemble into hexamers in the presence of zinc ions (**Figure 5**). This assembly and disassembly of dimers and hexamers has an important clinical ramification. The active form of insulin is monomers, but insulin is stored in the pancreas as a hexamer, awaiting release in response to external stimuli. Hexamers diffuse poorly whereas monomeric and dimeric insulin diffuse more readily into blood (Brange and Langkjoer, 1993; Derewenda et al., 1989; Dodson et al., 1979). When the secretory vesicle containing insulin is released into the bloodstream, the instant dilution causes hexamers to break up into the active form of monomer quickly (Brange et al., 1990; Sleigh, 1998). However, injected insulin, which at its storage concentration predominantly exists as hexamers, does not diffuse as readily, hence delaying absorption and entry into circulation (Brange et al., 1990). A number of fast-acting insulin analogs were developed by decreasing the tendency to self-associate while maintaining its normal receptor binding affinity. Lispro is an insulin analog, which

has B28 (proline) and B29 (lysine) amino acids at the C-terminus of the B-chain reversed. This modification decreases the tendency to self-associate and increases the rate of absorption after subcutaneous injection without affecting receptor binding (DiMarchi et al., 1994; Howey et al., 1994). Aspart insulin is another example of short acting insulin analog. In Aspart insulin, proline at the B28 position of the B-chain, the amino acid residue that participates in self-association, is replaced with negatively charged aspartic acid. This negative charge eliminates self-association because of charge repulsion (Heinemann et al., 1993; Kang et al., 1991).

Glucose homeostasis

Insulin is a principal hormonal messenger in fuel homeostasis in human. The basic circulating units of fuels are glucose and free fatty acids, which are stored intracellularly as glycogen in skeletal muscles and liver and triglycerides in adipose tissue, respectively (Cahill, 1976). When food is ingested, insulin levels increases to promote glycogen synthesis in liver and muscle and lipid formation in adipocytes. In starvation state, insulin release from the beta cells decreases, and the alpha cells in the islet of Langerhans (**Figure 2**) start to release glucagon, which stimulates break down of glycogen stored in liver and muscle (Cryer and Gerich, 1985).

Glucose homeostasis is a complex mechanism that regulates release of insulin from beta cells in response to changes in blood glucose concentration. The principle objective of glucose homeostasis is to maintain normoglycemia, and the concentration of blood glucose is more closely controlled than any other fuels in circulation because both hypoglycemia

and hyperglycemia can be detrimental. The brain, for instance, is a vital organ that has a continuous need for fuel but does not have fuel storage capacity. It cannot utilize fatty acids as a fuel source either, though it can use energy derived from fatty acids in a prolonged starvation state; therefore, it relies solely on blood glucose. Other vital organs, such as heart, also have continuous need for fuels, but they can utilize fatty acids directly as needed. Hence, in hypoglycemic state, central nervous function becomes the most impaired vital organ. Hyperglycemia is detrimental as well because it causes glycosuria and contributes to the complication of diabetes (Cahill, 1976; Cryer and Gerich, 1985).

Release of insulin from beta cells in the islets of Langerhans is a biphasic process. The first phase release is rapid, and the amount of initial release, triggered in response to increased blood glucose level, is dependent on the amounts available in storage. Once stored insulin is depleted, second phase of slow and sustained release is triggered independently of glucose. During this latter phase, release of insulin is slow because insulin has to be synthesized, processed, and packaged into vesicles. Furthermore, beta cells have to replenish depleted insulin in the initial fast response phase (Curry et al., 1968; O'Connor et al., 1980; Porte and Pupo, 1969).

Initial release phase is initiated when glucose enters the beta cells through the type 2 glucose transporters (GLUT2). Upon entry, glucose is phosphorylated by the enzyme glucokinase and is metabolized in glycolysis and the Krebs cycle, producing high-energy ATP molecules and increasing intracellular ATP/ADP ratio. The increased ATP/ADP ratio closes ATP sensitive potassium channel, preventing potassium ions from leaving the cells, which in turn depolarize the cell surface membrane. This depolarization opens voltage

gated Ca^{2+} channels, increasing intracellular calcium ion concentration, which in turn activates phospholipase C.

Phospholipase C cleaves the membrane-bound phospholipid phosphatidyl inositol 4,5-biphosphate (PIP_2) into inositol 1,4,5-triphosphate (IP_3) and diacylglycerol (DAG). DAG remains within the plasma membrane and activates protein kinase C (PKC), while IP_3 diffuses into the cytosol and binds to IP3-gated Ca^{2+} Channel in the plasmamembrane of the endoplasmic reticulum (ER). This allows release of Ca^{2+} from the ER via IP3-gated Ca^{2+} channel, further increasing the intracellular Ca^{2+} concentration. Significantly released intracellular Ca^{2+} triggers exocytosis of previously synthesized insulin stored in secretory vesicles (**Figure 6**) (Hiriart and Aguilar-Bryan, 2008; Matschinky et al., 1993; Rana and Hokin, 1990).

Insulin circulates in the blood stream until it binds to transmembrane insulin receptors, which belong to a family of tyrosine kinase receptors and play an important role in the regulation of glucose homeostasis. Activated insulin receptors promote uptake of glucose via type 4 glucose transporters (GLUT4) into various tissues, such as skeletal muscles and adipose tissues, and increase glycogen, lipid, and protein synthesis. Role of insulin is also implicated in various gene regulations via control of amino acid uptake and modification of numerous enzyme activities. (**Figure 7**) (Bergamini et al., 2007; Dimitriadis et al., 2011; Gupta et al., 1992; Ward and Lawrence, 2009).

Classification and Treatments of Diabetes

Currently etiological classification of diabetes mellitus falls into four categories – type 1, type 2, other specific types, and gestational diabetes mellitus (GDM) (**Table 1**). Most common forms of diabetes are type 1 and type 2 diabetes. Other specific types of diabetes encompass a variety of types of diabetes associated with particular diseases or syndromes with a distinct etiology. Gestational diabetes mellitus is glucose intolerance associated with varying degrees of hyperglycemia with the onset during pregnancy (Drouin et al., 2009; Gavin and Alberti, 1997).

Type 1 diabetes is generally caused by destruction of beta cells; therefore, individuals with this disease require insulin for survival. Idiopathic forms of type I diabetes is further divided into type 1A and type 1B (Gavin and Alberti, 1997). Type 1A is characterized by the presence of islet autoantibodies (anti-GAD, anti-islet cell, or anti-insulin antibodies), which leads to insulitis and selective destruction of islet beta cells, and almost always progresses to severe insulin deficiency. Type 1A is also strongly associated with human leukocytes antigen (HLA) alleles (Foulis et al., 1991; Nepom and Kwok, 1998; Noble et al., 1996; Todd, 1999). Type 1B comprises a minority of type 1 diabetes patients. They are presented with severe insulin deficiency but without evidence of autoimmune destruction of beta cells (Sacks et al., 2011).

Type 2 diabetes is the most common form of diabetes and is characterized by defective insulin action and secretion with no autoimmune destruction of beta cells. Type 2 diabetes patients usually have insulin resistance and relative insulin deficiency. Their plasma insulin concentration is typically normal or elevated, yet not sufficient to control blood

glucose within normal range because of insulin resistance. They often don't require insulin for survival, although some may require insulin for glycemic control due to progressive beta cell failure, which can occur with increasing duration of diabetes (Gavin and Alberti, 1997). Some people with type 2 diabetes can regulate blood glucose level with life style change, diet and exercise alone, but many require diabetes medications, such as metformin and sulfonylureas (**Table 2**).

Typical diabetes treatments include oral medications, insulin injections, dietary restrictions, exercise, and intense self-monitoring of blood glucose; however, these only provide a short-term relief (Beck et al., 2007). Despite the impressive progress in treating diabetes, most people with diabetes continue to develop disabling complications, most of which are directly linked to hyperglycemia. Several advancements have been made to decrease complications and to treat diabetes more effectively, such as gene therapy and closed-loop insulin delivery systems. The combination of a glucose sensor and an insulin pump can mechanically replace beta cell function and provide patients with normoglycemia (Steil, 2004; Yechoor and Chan, 2005). However, the most promising and attractive alternative treatment option, especially for type 1 diabetes, remains to be replacing the missing beta cells with pancreas, islet, or beta cell transplants. This concept was tested clinically, though unsuccessfully, as early as 1893 in Bristol, England when pieces of sheep pancreas were transplanted subcutaneously to a 15-year-old boy with diabetes (Williams, 1894). In 1967, the pancreas transplant from a cadaver donor was transplanted into a 28-year-old woman for the first time, and the patient achieved insulin independence; however, she deceased from pulmonary embolism three months later (Kelly

et al., 1967). The first successful islet transplantation into a type 1 diabetes patient was in 1989 (Scharp et al., 1990). Beta cell replacement with pancreas, islet, or beta cell transplants can result in long-term relief, providing a glucose homeostasis for an extended period of time; however, success is limited by the host graft rejection because they can fail without life long systemic immunosuppression, which can cause many adverse effects such as renal failure (Gallagher et al., 2011).

Islet transplantation

Pancreas transplantation is an invasive complex surgery; and therefore, regardless of surgical method, it inevitably comes with a high risk of morbidity and mortality. Despite the risks and life-long immunosuppression, pancreas transplantation still remains the best alternative choice for patients, especially those with type 1 diabetes, who do not respond to conventional treatments. Islet transplantation is an attractive alternative to pancreas transplantation, since it is a much less invasive procedure (Vardanyan et al., 2010). Methods to isolation of islet cells were first reported by Lacy and Kostianovsky in 1967, and since then several studies reported that islet transplantation can successfully reverse hyperglycemia in both small and large animals (Lacy and Kostianovsky, 1967; Sutherland et al., 1993). Subsequently, Scharp et al. demonstrated in 1981 that islet allografts successfully reversed the diabetic state of type 1 diabetes patients, unveiling the promising future islet transplantation holds for treating diabetes patients (Scharp et al., 1991). Frustrated with less than optimal outcomes of earlier islet cell transplantation trials, the Edmonton protocol was developed by a group of researchers in Edmonton, Alberta, Canada

in 1999 (Shapiro et al., 2000). Although the results of the Edmonton protocol are spectacularly better than any of the previous islet transplantation trials, patients still have to receive immunosuppressive therapy.

Despite the conceptual simplicity of the procedure, progress in making islet transplantation a reliable therapy has been hindered by two major barriers. The first drawback is the source of the islet cells, which cannot be expanded *in vitro* - this is beyond the scope of this chapter; however, there are numerous reports of exploring different sources of islet cells and even unlocking possibilities of islet cell regeneration from stem cells. Another major obstacle for islet transplantation is the process of transplant rejection and autoimmunity from destroying transplanted islet cells. To avoid graft rejection, patients are again required to take life-long immunosuppressive drugs (Halban et al., 2010; Weir, 2013). In an attempt to control transplant rejection and autoimmunity, safer and more effective immunosuppressive drugs are being developed. However, it still does not eliminate the fact that patients still need to be on life-long immunosuppressive therapy. Recently, it was found that autoimmune destruction of islet cells can be prevented by creating a barrier between lymphocytes and transplanted islet cells. This concept of creating an immunobarrier, if successful, will completely eliminate the use of immunosuppressive drugs and maintain the long-term islet graft function. For this reason, transplantation of encapsulated islet cells has created high expectations for treating type 1 diabetes (Murua et al., 2008; Orive et al., 2003b; Weir, 2013; Zimmermann et al., 2001).

Principles & Materials of Cell Encapsulation

Cell encapsulation techniques consist of enclosing therapeutic cells within a semi-permeable polymeric matrix, which will allow bi-direction diffusions of nutrients, oxygen and waste, and secretion of therapeutic products while preventing immune cells from destroying the enclosed cells (**Figure 2**) (Orive et al., 2003b). Several materials, such as polysulphone (PS), poly(ethylene glycol) (PEG), dimethylaminoethy methacrylate-methyl methacrylate copolymer, and poly(vinyl alcohol), have been explored to achieve the purpose of encapsulation. Successful islet encapsulation was demonstrated with PS by blending it with poly-vinylpyrrolidone or sodium-dodecyl-sulfate ; however, this encapsulation technique hindered proper islet cell function by limiting insulin diffusion. Encapsulating with hydroxy-methylated PS showed some promising results (Figliuzzi et al., 2005; Lembert et al., 2001; Petersen et al., 2002), but, the encapsulated cells had reduced viability and function due to polymer degradation , as well as fragility and limited permeability of the capsules (Xie et al., 2005). Additionally, amniotic membranes, nano-porous microsystems, silica, and synthetic extracellular matrix consisting of poly(N-isopropyl-acrylamide) and acrylic acid copolymers have also been explored. However, the properties and manufacturing methods of these materials limit their applicability (Vernon et al., 2000) (Boninsegna et al., 2003; Desai et al., 2004; Mahgoub et al., 2004).

Alginate, generally extracted from various brown algae (*Phaeophyceae*) has shown the most promising results. Alginate is a family of linear co-polymers of β-D-mannuronic acid (M) and α-L-guluronic acid (G) with highly variable G and M sequences and compositions (**Figure 9a**) (Andersen et al., 2012). The percentage of M and G blocks and the length of

each block vary,depending on the source of extraction. Currently, more than 200 different alginates are being commercially manufactured. As an ionic polysaccharide, alginate can form hydrogels in the presence of divalent cations, such as barium and calcium ions. Hydrogels are highly hydrated three-dimensional networks of hydrophilic polymers, and due to their structural similarity to the extracellular matrices in the body, they are often biocompatible. Only the G-blocks of alginate are known to participate in intermolecular cross-linking with calcium ions (**Figure 9b**), while the M-blocks can also participate when cross-linked with barium ions (Lee and Mooney, 2012). These associations of alginate chains and divalent cations constitute the junction zone, known as the "egg box model," responsible for the gelation (**Figure 9c**). In the egg box model, oxygen atoms are involved in the coordination of the divalent cations (Grant et al., 1973; Mackie et al., 1983). Encapsulating cells with alginate is relatively easy. The cross-linking of alginate happens almost instantaneously simply by mixing the cells with a solution of sodium alginate and dripping them into a solution of calcium or barium (**Figure 10**) (Chaikof, 1999; Zimmermann et al., 2007). This cross-linking is efficient at near physiological conditions; and therefore, the cells entrapped inside are highly viable and functional. It is this gelation property of alginate that has gained high interests for the application of cell encapsulation (Andersen et al., 2012; Zimmermann et al., 2007).

Progress of Alginate Cell Encapsulation

The first use of a semi-permeable membrane to prevent graft failure was reported in 1954 (Algire et al., 1954). Subsequently, the concept of cell encapsulation was defined

when T.M.S Chang proposed the use of biocompatible polymer microcapsules to provide immune-protection of transplanted cells (Chang, 1964). In 1980, this cell encapsulation concept was successfully implanted to mobilize xenograft islets cells. Lim and Sun demonstrated that microencapsulated islets with alginate corrected diabetic state for 2 to 3 weeks and remained functionally viable for over 15 weeks in rats (Lim and Sun, 1980). Since then, tremendous advancements have been made in using alginate for various biomedical applications, and alginate remains the leading material for the microencapsulation of islet cells (Zimmermann et al., 2007).

Since the first demonstration of proof-of-concept with encapsulated cells in humans in 1991 (Scharp et al., 1991), many studies have reported varying degrees of success. In 2003, Omer et al. demonstrated that they could reverse diabetic state in immunocompetent mice for more than 20 weeks with alginate encapsulated porcine neonatal pancreatic cell clusters (Omer et al., 2003). In 2007, Calafiore et al. reported two cases where human diabetic patients received human islet microcapsules in the peritoneal cavity under local anesthesia. Without immunosuppression, high blood glucose level was reversed for one year in one of the patients, and for six months in the other patients (Calafiore et al., 2006). In 2007, Elliott et al. reported a single case of a 9.5-year long-term survival of alginate encapsulated porcine islets cells in a 41-year-old type 1 diabetes patient. Though functional, the surviving islet cells were insufficient to reverse the diabetic state after the first year of transplantation (Elliott et al., 2007). In 2009, Tuch et al. transplanted alginate encapsulated human islet cells, which were collected from cadaver pancreases, in four type 1 diabetes patients. They reported that patients did not display any side effect or infection

from receiving islet cells from cadavers, but capsules retrieved after 16 months were completely covered with fibrous tissues and contained necrotized islet cells (Tuch et al., 2009). Most recently, Jacobs-Tulleneers-Thevissen et al. advanced the islet transplantation field by demonstrating that alginate encapsulated human islets remain functional in the peritoneal cavity of mice and of a human type 1 diabetes patients (Jacobs-Tulleneers-Thevissen et al., 2013).

Challenges of Encapsulated Islet Transplantation

Although promising, these studies highlight one of the most serious problems facing this field: implanted capsules, regardless of whether they contain cells inside or not, elicit a foreign body response due to the alginate material itself, forming fibrotic structures around the capsules, which eventually lead the hypoxic death of the islet cells inside (Anderson et al., 2008; Bridges and García, 2008; Franz et al., 2011; Weir, 2013). How these reactions occur is not well understood, although it has been suggested that this foreign body response is a combination of the reactivity to the material itself and/or impurities present within the material. Genetic makeup of the recipients and possibly the immune reaction to the biomolecules released by the encapsulated cells can also influence foreign body responses (Weir, 2013).

The foreign body response is a biomaterial-mediated inflammation, a complex process initiated immediately upon implantation of the material (**Figure 11**). When biomaterials are implanted, various proteins present in the host fluids (blood, lymph, and wound fluids) get adsorbed to the surface of the material. Neutrophils enter the implant site and react to

this material surface coated with diverse protein species in various conformations and adsorbed state by producing various pro-inflammatory cytokines. These neutrophils eventually recruit tissue resident macrophages and undifferentiated monocytes, and subsequently exit the implant site. Macrophages respond to the foreign materials by producing their own set of various inflammatory mediators, which in turn recruit fibroblasts and fuse into multinucleated foreign body giant cells. Recruited fibroblasts start infiltrating the site and form thick collagenous fibrous capsules around the implant, isolating it from the host tissue (Anderson et al., 2008; Bridges and García, 2008; Franz et al., 2011; Grainger, 2013).

Our current understanding of alginate mediated inflammation is that mannuronic acid polymers activate Toll-like receptor 2 (TLR2) and TLR4, which are types of pattern recognition receptors (PRRs), in primary murine macrophages (Flo et al., 2002). A study by Yang and Jones in 2008 also implicated the involvement of TLRs by demonstrating that alginate can stimulate innate immune response via macrophage receptors, leading to NF-κB activation (Yang and Jones, 2009). A number of studies on other biomaterials have implicated the role of TLRs in the foreign body response as well. Grandjean-Laquerriere et al. reported that particles of hydroxyapatite, which is widely used biomaterial to fill bone defects or to coat prosthesis, can induce an inflammatory reaction by activating TLR4 (Grandjean-Laquerriere et al., 2007). Another study by Auquit-Aucbur et al. reported involvement of TLR4 in inflammation around silicone prosthesis (Auquit-Auckbur et al., 2011). Pearl et al. investigated involvement of TLRs in polymethylmethacrylate (PMMA) microparticle induced inflammation by applying the inhibitor of Myeloid Differentiation

primary response gene 88 (MyD88), which is an adaptor protein involved in many of TLR signaling pathways. Although they were able to demonstrate that TLRs are indeed involved in PMMA induced inflammatory reaction, they could not identify which TLRs are involved. Another report on rheumatoid arthritis patients with implants showed upregulation of TLR2 and TLR4 (Myles and Aggarwal, 2011). All these studies clearly implicate TLRs are the mediators of the foreign body response. However, which particular TLRs are involved in macrophage activation in response to alginate microcapsules is currently not well understood. Additionally, some of these studies are plagued by questions of whether the materials are contaminated with pathogen-associated molecular patterns (PAMPs) as alginate is produced not only by brown algae but also by bacteria. Paredes-Juarez et al. reported that PAMPs, predominantly ligands of TLR2, 5, 8, 9, are present in some of the commercial alginates (Paredes-Juarez et al., 2013).

Future of Islet Encapsulation

The cell encapsulation technique, based on the principle of immunoisolation, still remains an attractive therapeutic method with a potential to greatly advance diabetes treatment, possibly curing type 1 diabetes. It undeniably has the potential to protect transplanted beta cells from autoimmune destruction. Many challenges remain to be addressed, and many researchers are collaboratively working on the problems. With continuous research effort, new and improved materials and formulations are on the horizon, which may well lead to greater success of not only for the treatment of diabetes, but for other diseases that require implantation of biocompatible medical devices.

Insulin is not a cure for diabetes; it is a treatment. It enables the diabetic to burn sufficient carbohydrates, so that proteins and fats may be added to the diet in sufficient quantities to provide energy for the economic burdens of life.

~ Sir Frederick G. Banting, 1925

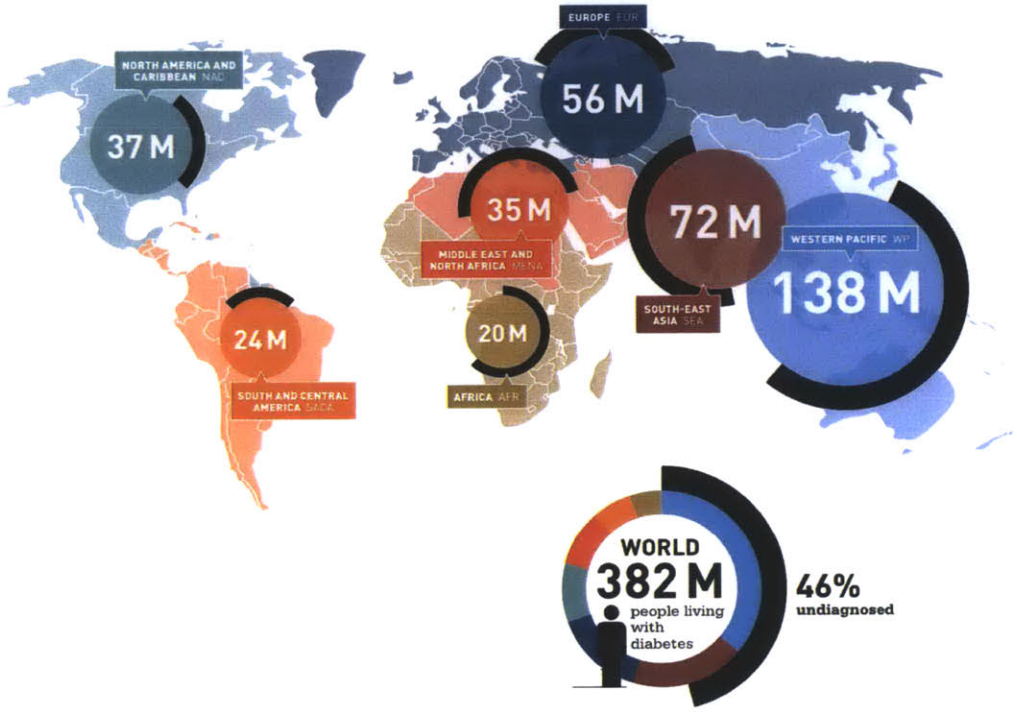

Figure 1. Worldwide diabetes statistics. Figure adopted from IDF Diabetes Atlas, 6th ed. Brussels, Belgium: International Diabetes Federation, 2013.

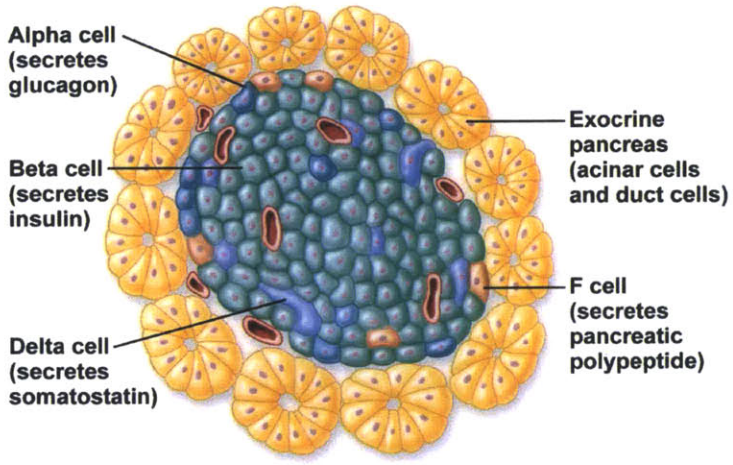

Figure 2. Islet of Langerhans. Located within pancreas, they consist of four distinct cell types – alpha, beta, delta, and F cells. The beta cells are the most common islet cells, and they produce insulin, which is the major hormone responsible for glucose metabolism. The alpha cells produce glucagon which can trigger the release of stored glucose from the liver and fat tissues (©2011 Pearson Education, Inc).

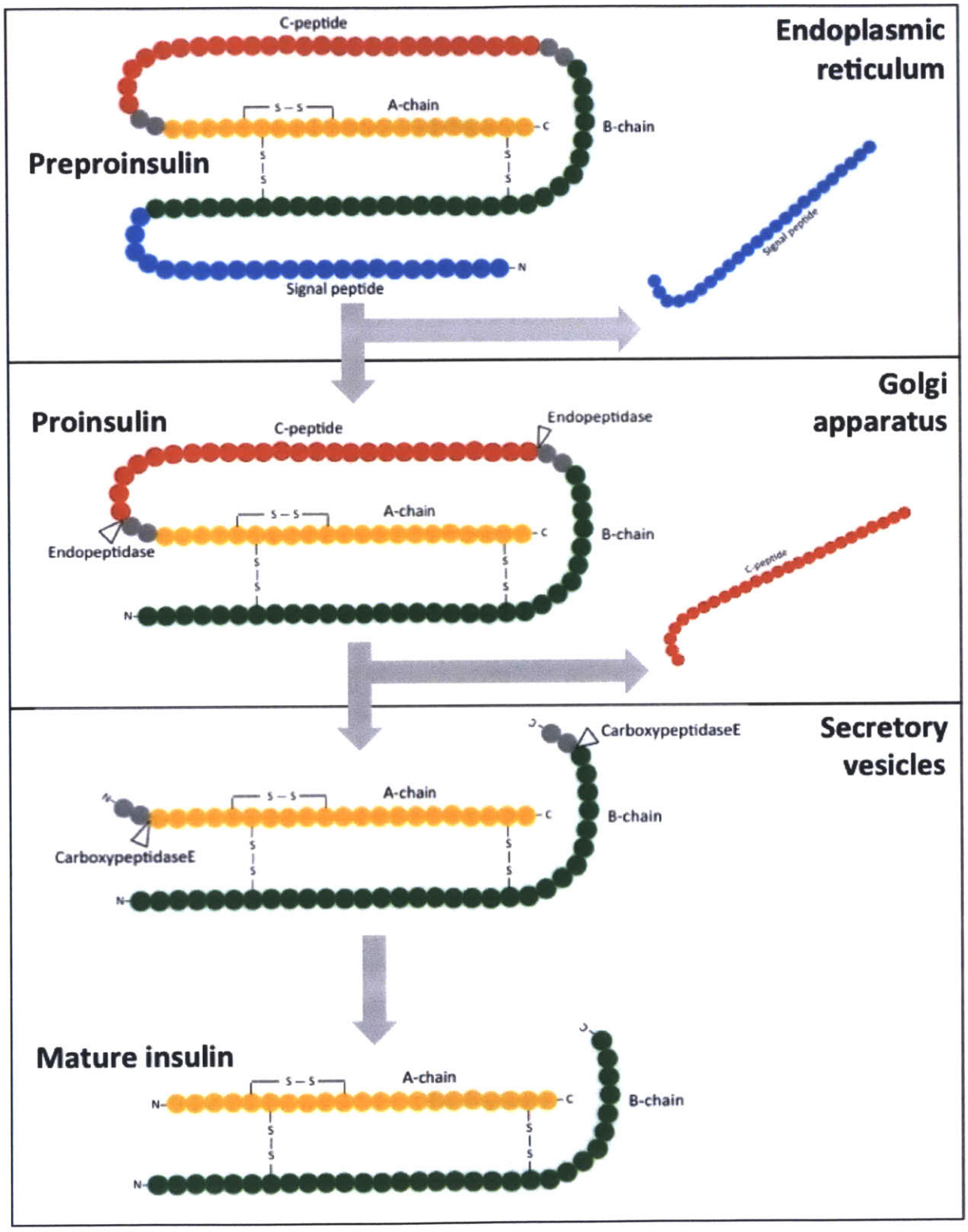
Endoplasmic reticulum
C-peptide
A-chain
B-chain
Preproinsulin
Signal peptide
Golgi apparatus
Proinsulin
Endopeptidase
Secretory vesicles
CarboxypeptidaseE
Mature insulin

Figure 3. Processing of insulin. In human, the initial precursor of insulin is preproinsulin, which consists of four domains – signal peptide, A-chain, B-chain, C-peptide. The signal peptide, the first 24 amino acids at N-terminus of preproinsulin, translocates the nascent protein into the rough endoplasmic reticulum (RER) where the signal peptide gets cleaved off and the protein gets folded into correct conformation, producing proinsulin. Proinsulin is then transported into the Golgi apparatus where C-peptide gets cleaved off by endopeptidases. The resulting two peptide chains (A- and B-chains) are packaged into secretory vesicles where they get further processed by carboxypeptidaseE, which removes two pairs of basic residues, producing mature insulin. Mature insulin in the secretory vesicles then waits for metabolic signals to be exocytosed.

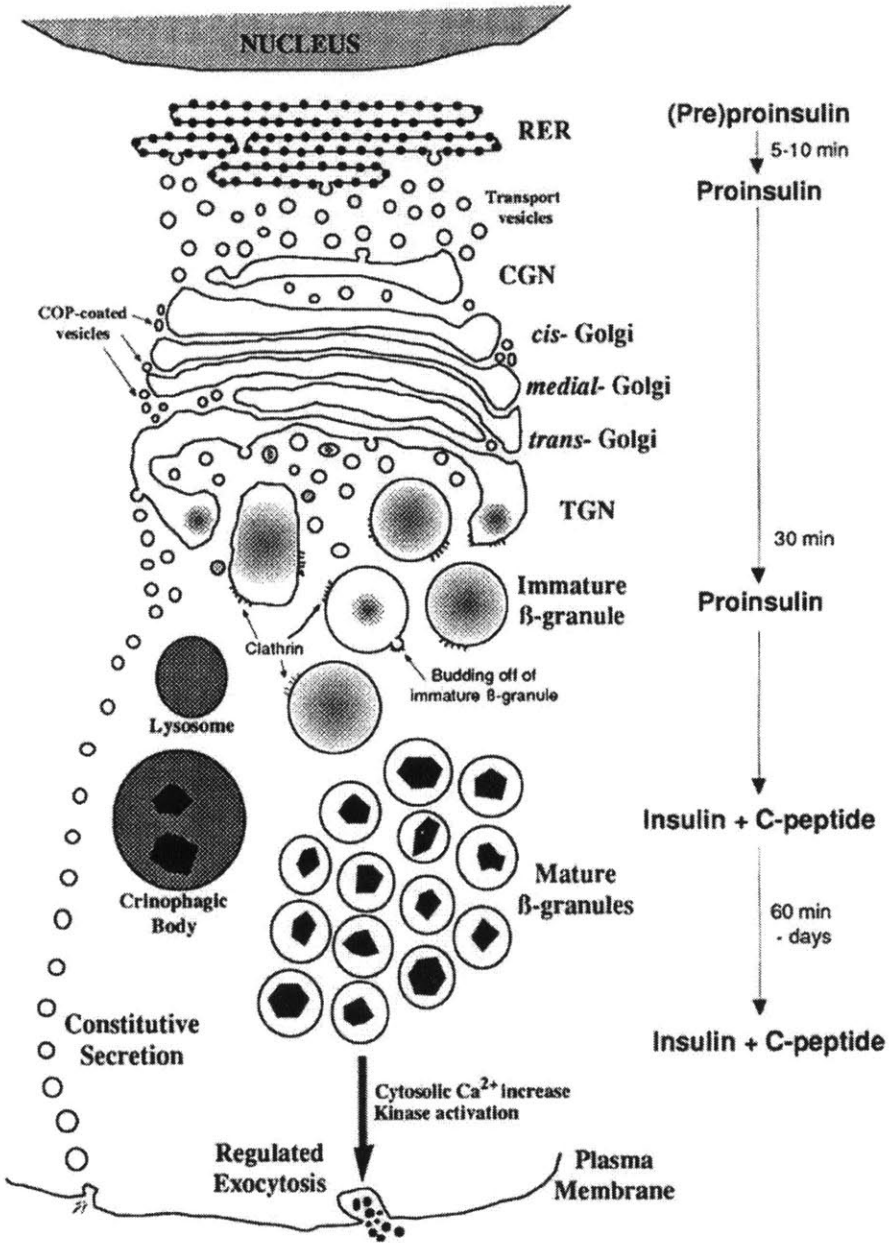

Figure 4. Insulin secretion pathway. Newly made proinsulin in the rough endoplasmic reticulum (RER) is transferred to the *cis*-Golgi network (CGN). Proinsulin is packaged into immature β-granules in the *trans*-Golgi network (TGN). Proinsulin is sent to the β-granule compartment, where the C-peptide is cleaved off to produce insulin. Mature β-granules are held in an intracellular storage compartment awaiting a signal for exocytosis (©2004 Lippincott Williams & Wilkins).

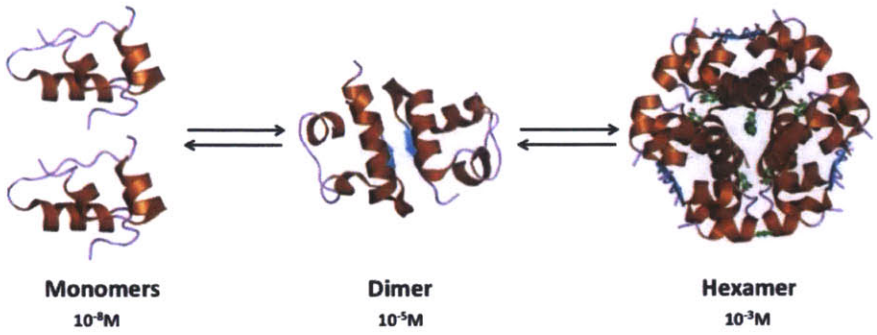

Figure 5. Assembly and disassembly of insulin monomer, dimer, and hexamer. At different concentrations, insulin assembles and disassembles into monomers, dimers, and hexamers. Insulin molecules tend to form dimers in solution due to the hydrogen bonds between the C-termini of B-chains. Furthermore, in the presence of zinc ions, insulin dimers assemble into hexamers.

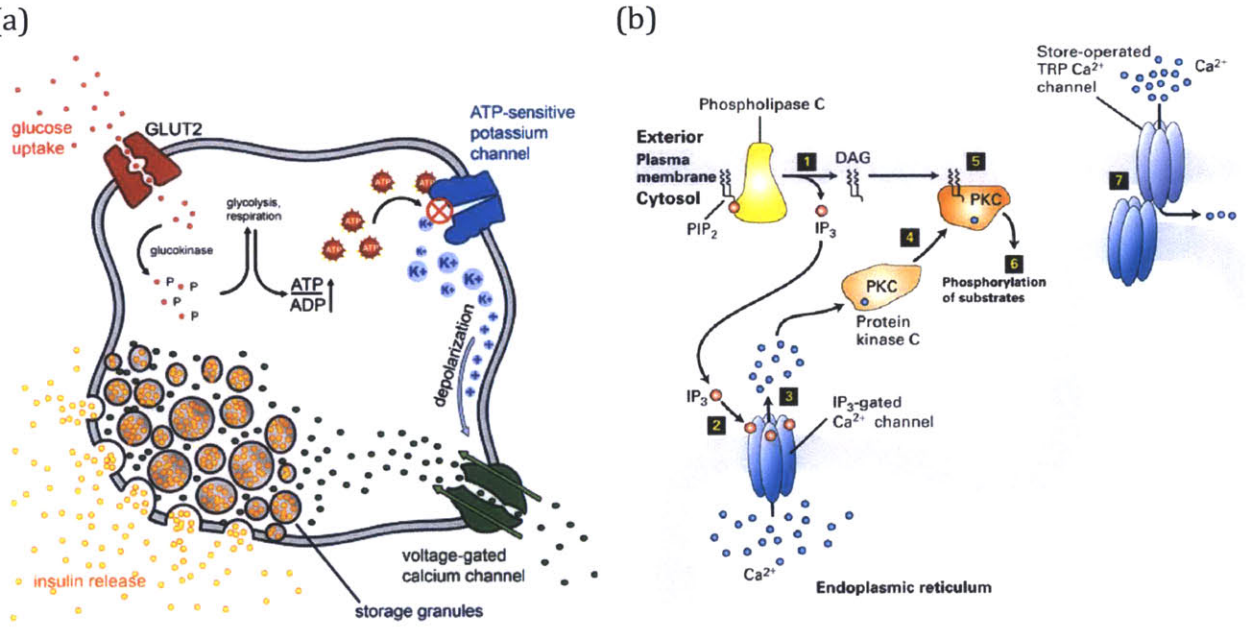

Figure 6. Mechanism of insulin secretion. (a) Insulin secretion in beta cells is triggered by elevated blood glucose. Cells uptake glucose via GLUT2 transporter, and the glycolytic phosphorylation of glucose causes a rise of ATP:ADP ratio. This increased ATP:ADP ratio deactivates the potassium channel, causing depolarization of the membrane, which then leads to opening of calcium channel, allowing inflow of calcium ions and activates phospholipase C. This subsequently leads to exocytosis of stored insulin. (b) Phospholipase C cleaves phospholipid phosphatidyl inositol 4,5-biphosphate (PIP_2) to inositol 1,4,5-triphosphate (IP_3) and diacylglycerol (DAG). DAG activates protein kinase C (PKC), and IP_3 activates IP_3-gated calcium channel, which leads to further increase of intracellular calcium ion concentration (© 2004 Beta Cell Biology Consortium).

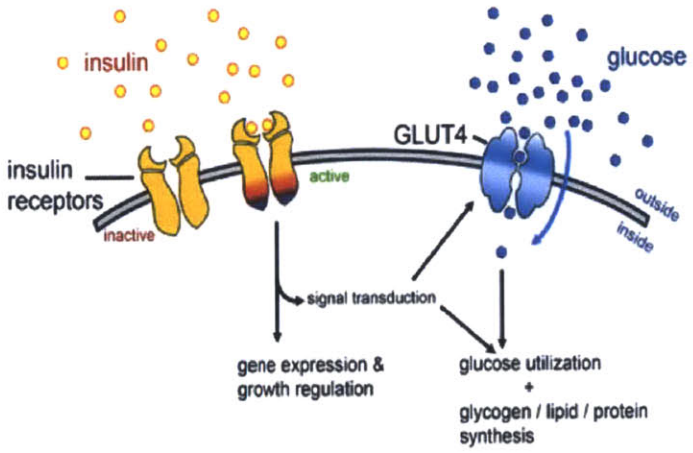

Figure 7. Effect of insulin on glucose uptake and metabolism. Activated insulin receptor promotes uptake of glucose via GLUP4 transporter. Binding of insulin to its receptor also activates a cascade of reactions, such as glycogen/lipid/protein synthesis, glycolysis (© 2004 Beta Cell Biology Consortium).

Table 1. Etiologic classification of diabetes mellitus

I. Type 1 diabetes mellitus	1A (Autoimmune)	β-cell destruction, usually leading to absolute insulin deficiency
	1B (Idiopathic)	
II. Type 2 diabetes mellitus	May range from predominantly insulin resistance with relative insulin deficiency to a predominantly secretory defect with or without insulin resistance	
III. Gestational diabetes mellitus (GDM)		
IV. Other specific types		
Genetic defects of β-cell function		Genetic defects in insulin action
Chromosome 20, HNF4α (MODY1) Chromosome 7, glucokinase (MODY2) Chromosome 12, HNF1α (MODY3) Chromosome 13, IPF1 (MODY4) Chromosome 17, HNF3β (MODY5) Mitochondrial DNA, A3243G mutation Others		Type A insulin resistance Leprechaunism Rabson-Mendenhall syndrome Lipoatrophic diabetes Others
Other genetic syndromes sometimes associated with diabetes		Drug- or chemical- induced
Down syndrome Friedreich ataxia Huntington disease Klinefelter syndrome Laurence-Moon-Biedl syndrome Myotonic dystrophy Porphyria Prader-Willi syndrome Turner syndrome Wolfram syndrome Other		Nicotinic acid Glucocorticoids Thyroid hormone α-adrenergic agonists β-adrenergic agonists Thiazides Phenytoin Pentamidine Pyriminil (Vacor) Interferon-α Others
Endocrinopathies		Diseases of the exocrine pancreas
Cushing syndrome Acromegaly Pheochromocytoma Glucagonoma Hyperthyroidism Somatostatinoma Others		Fibrocalculous pancreatopathy Pancreatitis Trauma/pancreatectomy Neoplasia Cystic fibrosis Hemochromatosis Wolcott-Rallison syndrome Others
Uncommon forms of immune-mediated diabetes		Infections
Insulin autoimmune syndrome (antibodies to insulin) Anti-insulin receptor antibodies "Stiff-man" syndrome Others		Congenial rubella Cytomegalovirus Others

Adapted from Joslin's Diabetes Mellitus. 14th ed. In: Bennett, PH and Knowler, WC. *Definition, Diagnosis and Classification of Diabetes Mellitus and Glucose Homeostasis.* Lippincott Williams & Wilkins, 2005:333-334

Table 2. Diabetes medications

Groups		Mechanism of Action	Medications
Sensitizers (Biguanides)		Reduce gluconeogenesis and hepatic glucose output via increasing AMPK signaling	Metformin (Glucophage) Metformin liquid (Riomet) Metformin extended release (Glucophage XR, Fortamet, Glumetza)
Thiazolidinediones (TZDs)		Binds to PPAR-γ in fat and muscle to reduce insulin resistance	Pioglitazone (Actos)
Secretagogues	Sulfonylureas	Stimulates insulin release by pancreatic beta cells by inhibiting the K_{ATP} channel	Glimepiride (Amaryl) Glyburide (Diabeta Micronase) Glipizide (Glucotrol, Glucotrol XL) Micronized glyburide (Glynase)
	Meglitinides	Act on the same K_{ATP} channel as sulfonylureas but at a different binding site (short acting)	Repaglinide (Prandin) Nateglinide (Starlix)
Alpha-glucosidase inhibitors		Slows the absorption of carbohydrate into the bloodstream by decreasing production of enzymes needed to digest carbohydrates in small intestine	Miglitol (Glyset) Acarbose (Precose/Glucobay)
Dipeptidyl peptidase-4 (DPP-4) inhibitors		Increase blood concentration of the incretin GLP-1 by inhibiting its degradation by depeptidyl peptidase-4 (DDP-4)	Sitagliptin (Januvia) Saxagliptin (Onglyza) Linagliptin (Tradjenta)
Glycosurics (SLGT-2 inhibitors)		Blocks the re-uptake of glucose in the renal tubules, promoting loss of glucose in the urine	Canagliflozin (Invokana), dapagliflozin (Farxiga)
Bile acid sequestrants		Works with other diabetes medication to lower blood glucose	Colesevelam (Welchol)

Adapted from Joslin Diabetes Center (http://www.joslin.org/info/oral-diabetes_medications_summary_chart.html)

Table 3. Chemical composition of alginates from various most commonly used industrial sources.

Source	F_G	F_M	F_{GG}	F_{MM}	F_{GM} F_{MG}	F_{GGG}	F_{GGM}	F_{MGM}	$N_{G>1}$
Durvillea antarctica	0.32	0.68	0.16	0.51	0.17	0.11	0.05	0.12	4
Laminaria japonica	0.35	0.65	0.18	0.48	0.17				
Ascophyllum nodosum	0.39	0.61	0.23	0.46	0.16	0.17	0.07	0.09	5
Lessonia nigrescens	0.41	0.59	0.22	0.40	0.19	0.17	0.05	0.14	6
Laminaria digitata	0.41	0.59	0.25	0.43	0.16	0.20	0.05	0.11	6
Macrocystis pyrifera	0.42	0.58	0.20	0.37	0.21	0.16	0.04	0.02	6
Laminaria hyperborea (leaf)	0.49	0.51	0.31	0.32	0.19	0.25	0.05	0.13	8
Laminaria hyperborea (stipe)	0.63	0.37	0.52	0.26	0.11	0.48	0.05	0.07	15

Adapted from Andersen et al., 2012.

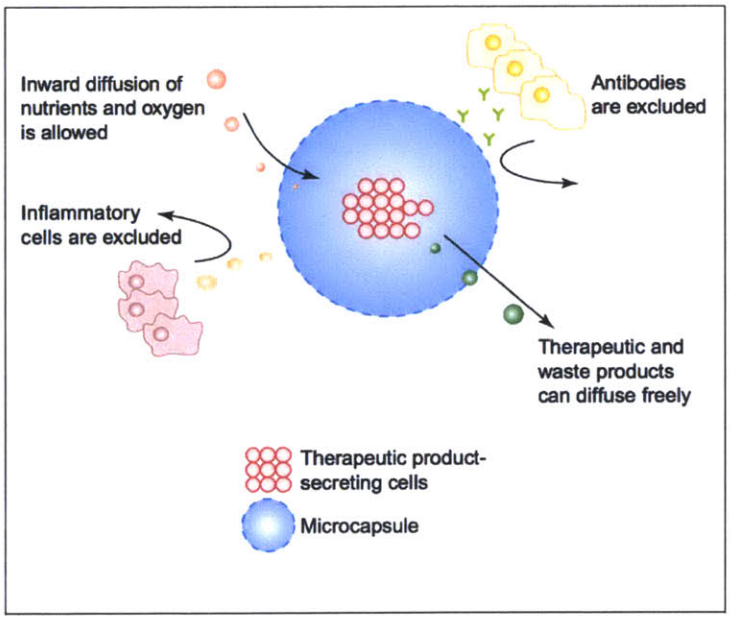

Figure 8. Principles of cell encapsulation. Cells are enclosed within a semi-permeable polymeric matrix, which can circumvent host immune rejection. The matrix allows in-flow of oxygen and nutrients and out-flow of therapeutic and waste products, while preventing immune cells and antibodies come in direct contact with the enclosed cells. Figure adapted from Orive et al., 2003.

(a)

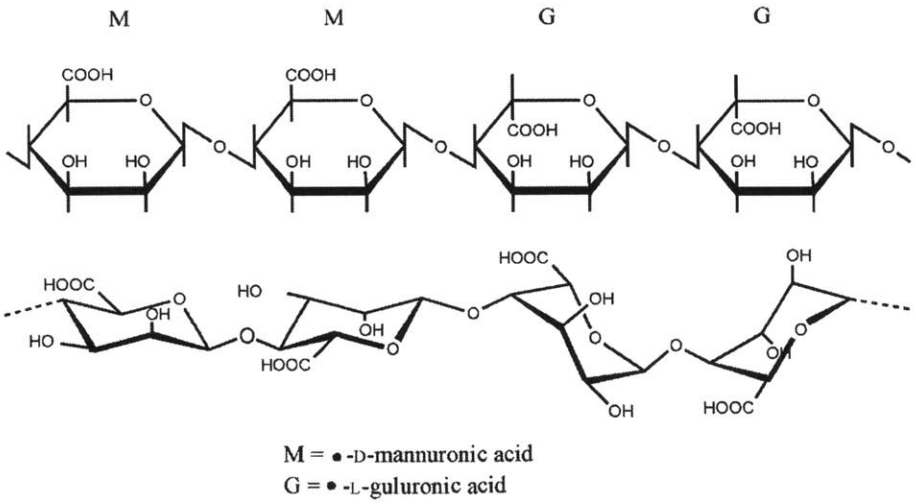

(b)

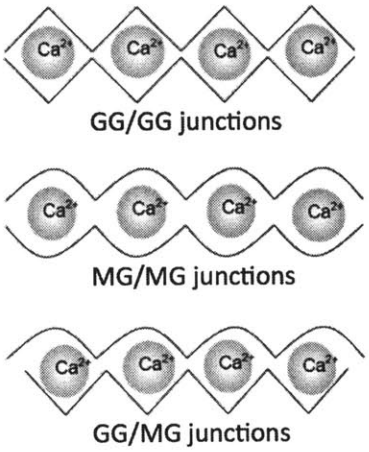

(c)

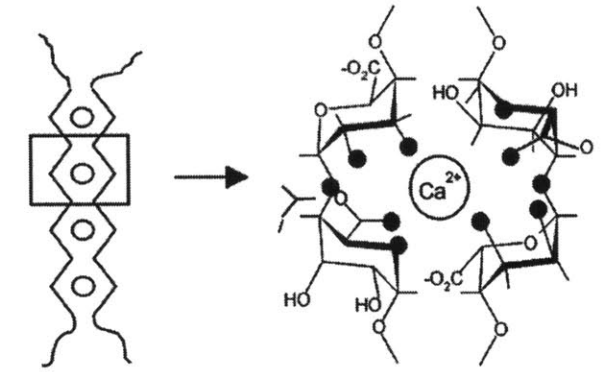

Figure 9. Schematic diagrams of alginate. (a) Chemical structure of alginate MMGG block; (b) alginate crosslinked with calcium; (c) Schematic drawing and calcium coordination of the "egg box model" as described for the pair of guluronate chains in calcium alginate junction zones. Dark circles represent the oxygen atoms involved in the coordination of the calcium ion. (Andersen et al., 2012; Braccini and Perez, 2001)

(a) (b)

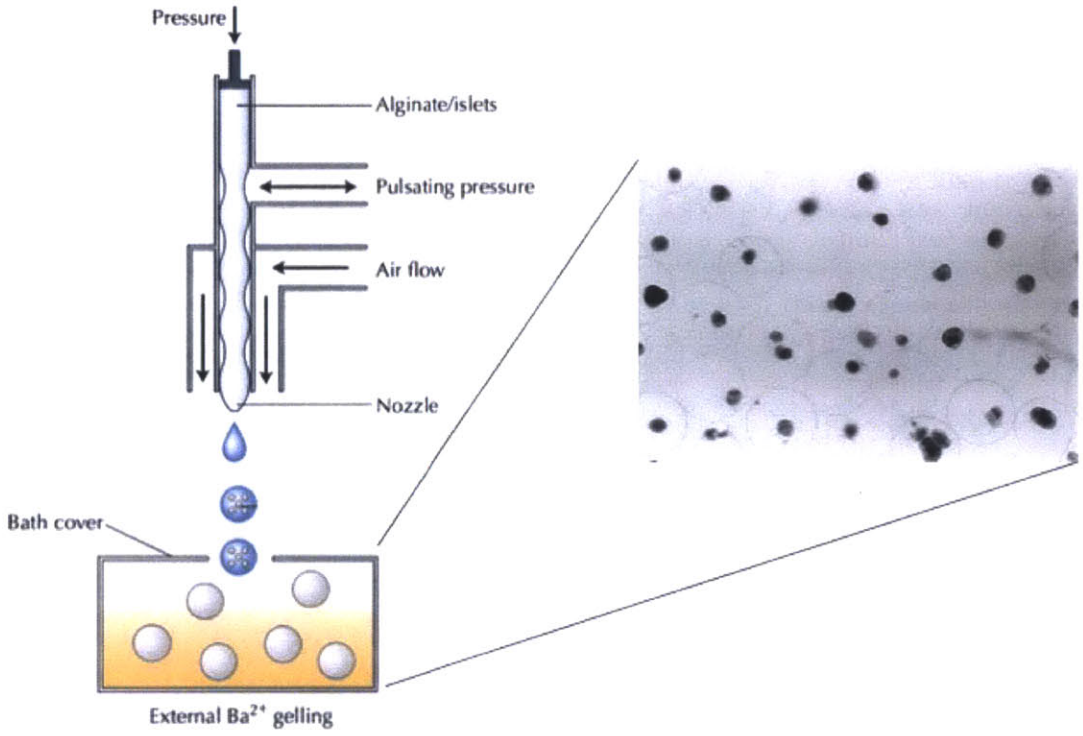

Figure 10. Schematic diagram of islet encapsulation. (a) An air-jet droplet generator is used to encapsulate islet cells with alginate; (b) Rat islet cells encapsulated in alginate hydrogel. Figure adapted from Zimmermann et al., 2007 and Chaikof, 1999.

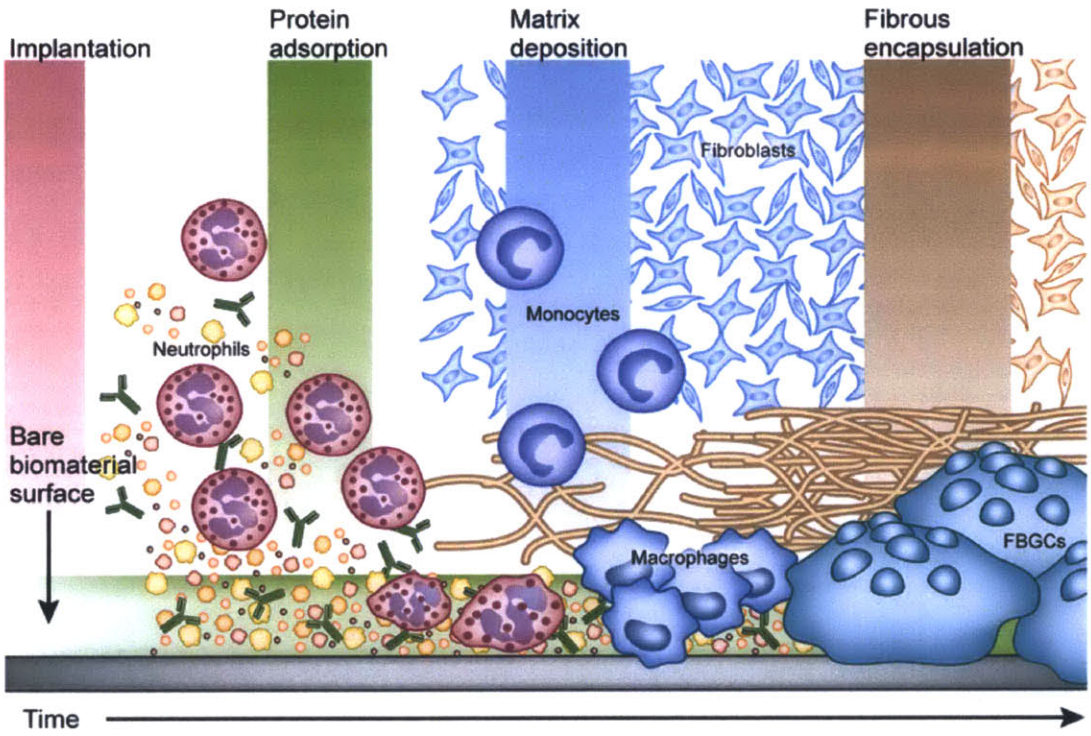

Figure 11. Foreign body response to implanted biomaterial. Diverse adsorbed protein layers, which happens instantaneously upon implantation of the material, on the implant surface recruit neutrophils. Neutrophils produce various inflammatory mediators and recruit macrophages and monocytes. Within days, neutrophils exit the site, and macrophages start recruiting fibroblasts. Some macrophages fuse to create foreign body giant cells. Fibroblasts start forming thick collagenous layers on the implant. Figure adapted from Grainger, 2013.

References

Adams, M.J., Blundell, T.L., Dodson, E.J., Dodson, G.G., Vijayan, M., Baker, E.N., Harding, M.M., Hodgkin, D.C., Rimmer, B., and Sheat, S. (1969). Structure of Rhombohedral 2 Zinc Insulin Crystals. Nature *224*, 491–495.

Algire, G.H., Weaver, J.M., and Prehn, R.T. (1954). Growth of cells in vivo in diffusion chambers. I. Survival of homografts in immunized mice. J. Natl. Cancer Inst. *15*, 493–507.

Andersen, T., Strand, B.L., Formo, K., Alsberg, E., and Christensen, B.E. (2012). Chapter 9 Alginates as biomaterials in tissue engineering. In Carbohydrate Chemistry: Volume 37, (The Royal Society of Chemistry), pp. 227–258.

Anderson, J.M., Rodriguez, A., and Chang, D.T. (2008). Foreign body reaction to biomaterials. Semin. Immunol. *20*, 86–100.

Auquit-Auckbur, I., Caillot, F., Arnoult, C., Menard, J.F., Drouot, L., Courville, P., Tron, F., and Musette, P. (2011). Role of toll-like receptor 4 in the inflammation reaction surrounding silicone prosthesis. Acta Biomater *7*, 2047–2052.

Banting, F.G., and Best, C.H. (1922). The internal secretion of the pancreas. J Lab Clin Med *7*, 251–266.

Banting, F.G., Best, C.H., and Collip, J.B. et al (1922). The effect produced on diabetes by extracts of pancreas. Trans Assoc Am Physicians 1–11.

Beck, J., Angus, R., Madsen, B., Britt, D., Vernon, B., and Nguyen, K.T. (2007). Islet encapsulation: strategies to enhance islet cell functions. Tissue Eng. *13*, 589–599.

Becker, R. (2007). Insulin glulisine complementing basal insulins: a review of structure and activity. Diabetes Technol Ther *9*, 109–121.

Becker, R., and Frick, A. (2008). Clinical pharmacokinetics and pharmacodynamics of insulin glulisine. Clin Pharmacokinet *47*, 7–20.

Bell, G.I., Pictet, R.L., Rutter, W.J., Cordell, B., Tischer, E., and Goodman, H.M. (1980). Sequence of the human insulin gene. Nature *284*, 26–32.

Bergamini, E., Cavallini, G., Donati, A., and Gori, Z. (2007). The role of autophagy in aging: its essential part in the anti-aging mechanism of caloric restriction. Ann. N. Y. Acad. Sci. *1114*, 69–78.

Berson, S.A., and Yalow, R.S. (1968). General principles of radioimmunoassay. Clin. Chim. Acta *22*, 51–69.

Berson, S.A., Yalow, R.S., Bauman, A., Rothschild, M.A., and Newerly, K. (1956). Insulin-I131 metabolism in human subjects: demonstration of insulin binding globulin in the circulation of insulin treated subjects. J. Clin. Invest. *35*, 170–190.

Best, C.H., and Scott, D.A. (1923). The preparation of insulin. J. Biol. Chem *57*, 709–723.

Bliss, M. (1982). The discovery of insulin (Chicago: University of Chicago Press).

Blobel, G., and Dobberstein, B. (1975). Transfer of proteins across membranes. I. Presence of proteolytically processed and unprocessed nascent immunoglobulin light chains on membrane-bound ribosomes of murine myeloma. J. Cell Biol. *67*, 835–851.

Boninsegna, S., Bosetti, P., Carturan, G., Dellagiacoma, G., Dal Monte, R., and Rossi, M. (2003). Encapsulation of individual pancreatic islets by sol–gel SiO2: J. Biotechnol. *100*, 277–286.

Brange, J., and Langkjoer, L. (1993). Insulin structure and stability. Pharm. Biotechnol. *5*, 315–350.

Brange, J., Owens, D.R., Kang, S., and Vølund, A. (1990). Monomeric insulins and their experimental and clinical implications. Diabetes Care *13*, 923–954.

Bridges, A.W., and García, A.J. (2008). Anti-inflammatory polymeric coatings for implantable biomaterials and devices. J. Diabetes Sci. Technol. *2*, 984–994.

Cahill, G.J. (1976). Starvation in man. Clin Endocrinol Metab *5*, 397–415.

Calafiore, R., Basta, G., Luca, G., Lemmi, A., Montanucci, M.P., Calabrese, G., Racanicchi, L., Mancuso, F., and Brunetti, P. (2006). Microencapsulated pancreatic islet allografts into nonimmunosuppressed patients with type 1 diabetes: first two cases. Diabetes Care *29*, 137–138.

Chaikof, E.L. (1999). Engineering and material considerations in islet cell transplantation. Annu. Rev. Biomed. Eng. *1*, 103–127.

Chang, T.M.. (1964). Semipermeable microcapsules. Science (80-.). *146*, 524–525.

Cordell, B., Bell, G., Tischer, E., DeNoto, F.M., Ullrich, A., Pictet, R., Rutter, W.J., and Goodman, H.M. (1979). Isolation and characterization of a cloned rat insulin gene. Cell *18*, 533–543.

Cryer, P., and Gerich, J. (1985). Glucose counterregulation hypoglycemia and intensive insulin therapy in diabetes mellitus. N Engl J Med *313*, 232–241.

Cuatrecasas, P. (1969). Interaction of insulin with the cell membrane: the primary action of insulin. Proc. Natl. Acad. Sci. U. S. A. *63*, 450–457.

Cuatrecasas, P. (1971). Insulin-receptor interactions in adipose tissue cells: direct measurement and properties. Proc. Natl. Acad. Sci. U. S. A. *68*, 1264–1268.

Curry, D., Bennett, L., and Grodsky, G. (1968). Dynamics of insulin secretion by the perfused rat pancreas. Endocrinology *83*, 572–584.

Deckert, T. (2000). Protamine insulin (Hening, Denmark: Poul Kristensen Publishing Co,).

Deedwania, P.C., and Fonseca, V.A. (2005). Diabetes, prediabetes, and cardiovascular risk: shifting the paradigm. Am. J. Med. *118*, 939–947.

Derewenda, U., Derewenda, Z., Dodson, G.G., Hubbard, R.E., and Korber, F. (1989). Molecular structure of insulin: the insulin monomer and its assembly. Br. Med. Bull. *45*, 4–18.

Desai, T.A., West, T., Cohen, M., Boiarski, T., and Rampersaud, A. (2004). Nanoporous microsystems for islet cell replacement. Adv. Drug Deliv. Rev. *56*, 1661–1673.

DiMarchi, R.D., Chance, R.E., Long, H.B., Shields, J.E., and Slieker, L.J. (1994). Preparation of an insulin with improved pharmacokinetics relative to human insulin through consideration of structural homology with insulin-like growth factor I. Horm. Res. *41 Suppl 2*, 93–96.

Dimitriadis, G., Mitrou, P., Lambadiari, V., Maratou, E., and Raptis, S.A. (2011). Insulin effects in muscle and adipose tissue. Diabetes Res. Clin. Pract. *93 Suppl 1*, S52–S59.

Dodson, E.J., Dodson, G.G., Hodgkin, D.C., and Reynolds, C.D. (1979). Structural relationships in the two-zinc insulin hexamer. Can. J. Biochem. *57*, 469–479.

Drouin, P., Blickle, J.F., Charbonnel, B., Eschwege, E., Guillausseau, P.J., Plouin, P.F., Daninos, J.M., Balarac, N., and Sauvanet, J.P. (2009). Diagnosis and classification of diabetes mellitus. Diabetes Care *32 Suppl 1*, S62–S67.

Elliott, R.B., Escobar, L., Tan, P.L.J., Muzina, M., Zwain, S., and Buchanan, C. (2007). Live encapsulated porcine islets from a type 1 diabetic patient 9.5 yr after xenotransplantation. Xenotransplantation *14*, 157–161.

Eskridge, E.M., and Shields, D. (1983). Cell-free processing and segregation of insulin precursors. J. Biol. Chem. *258*, 11487–11491.

Figliuzzi, M., Cornolti, R., Plati, T., Rajan, N., Adobati, F., Remuzzi, G., and Remuzzi, A. (2005). Subcutaneous xenotransplantation of bovine pancreatic islets. Biomaterials *26*, 5640–5647.

Flo, T.H., Ryan, L., Latz, E., Takeuchi, O., Monks, B.G., Lien, E., Halaas, O., Akira, S., Skjak-Braek, G., Golenbock, D.T., et al. (2002). Involvement of toll-like receptor TLR2 and TLR4 in cell activation by mannuronic acid polymers. J Biol Chem *277*, 35489–35495.

Foulis, A., McGill, M., and Farquharson, M. (1991). Insulitis in type 1 (insulin-dependent) diabetes mellitus in man - macrophages, lymphocytes, and interferon-gamma containing cells. J Pathol *165*, 97–103.

Franz, S., Rammelt, S., Scharnweber, D., and Simon, J.C. (2011). Immune responses to implants - a review of the implications for the design of immunomodulatory biomaterials. Biomaterials *32*, 6692–6709.

Freychet, P., Roth, J., and Neville, D.M. (1971). Insulin receptors in the liver: specific binding of (125 I)insulin to the plasma membrane and its relation to insulin bioactivity. Proc. Natl. Acad. Sci. U. S. A. *68*, 1833–1837.

Gallagher, M.P., Goland, R.S., and Greenbaum, C.J. (2011). Making progress: preserving beta cells in type 1 diabetes. Ann. N. Y. Acad. Sci. *1243*, 119–134.

Gavin, J., and Alberti, K. (1997). Report of the expert committee on the diagnosis and classification of diabetes mellitus. Diabetes Care *20*.

Goeddel, D.V., Kleid, D.G., Bolivar, F., Heyneker, H.L., Yansura, D.G., Crea, R., Hirose, T., Kraszewski, A., Itakura, K., and Riggs, A.D. (1979). Expression in Escherichia coli of chemically synthesized genes for human insulin. Proc. Natl. Acad. Sci. U.S.A. *76*, 106–110.

Grainger, D.W. (2013). All charged up about implanted biomaterials. Nat Biotechnol *31*, 507–509.

Grandjean-Laquerriere, A., Tabary, O., Jacquot, J., Richard, D., Frayssinet, P., Guenounou, M., Laurent-Maquin, D., Laquerriere, P., and Gangloff, S. (2007). Involvement of toll-like receptor 4 in the inflammatory reaction induced by hydroxyapatite particles. Biomaterials *28*, 400–404.

Grant, G.T., Morris, E.R., Rees, D.A., Smith, P.J.C., and Thom, D. (1973). Biological interactions between polysaccharides and divalent cations: The egg-box model. FEBS Lett. *32*, 195–198.

Greene, S.A., Smith, M.A., Cartwright, B., and Baum, J.D. (1983). Comparison of human versus porcine insulin in treatment of diabetes in children. Br. Med. J. (Clin. Res. Ed). *287*, 1578–1579.

Gupta, A.K., Clark, R. V., and Kirchner, K.A. (1992). Effects of insulin on renal sodium excretion. Hypertension *19*, I78–I78.

Halban, P.A., German, M.S., Kahn, S.E., and Weir, G.C. (2010). Current status of islet cell replacement and regeneration therapy. J. Clin. Endocrinol. Metab. *95*, 1034–1043.

Hallas-Mo, K. (1956). The Lente Insulins. Diabetes *5*, 7–14.

Heinemann, L., Heise, T., Jorgensen, L.N., and Starke, A.A. (1993). Action profile of the rapid acting insulin analogue: human insulin B28Asp. Diabet. Med. *10*, 535–539.

Hiriart, M., and Aguilar-Bryan, L. (2008). Channel regulation of glucose sensing in the pancreatic beta-cell. Am J Physiol Endocrinol Metab *295*, E1298–E1306.

Howey, D.C., Bowsher, R.R., Brunelle, R.L., and Woodworth, J.R. (1994). [Lys(B28), Pro(B29)]-human insulin. A rapidly absorbed analogue of human insulin. Diabetes *43*, 396–402.

Jacobs-Tulleneers-Thevissen, D., Chintinne, M., Ling, Z., Gillard, P., Schoonjans, L., Delvaux, G., Strand, B.L., Gorus, F., Keymeulen, B., Pipeleers, D., et al. (2013). Sustained function of alginate-encapsulated human islet cell implants in the peritoneal cavity of mice leading to a pilot study in a type 1 diabetic patient. Diabetologia *56*, 1605–1614.

Jones, R. (2000). Insulin glargine (Aventis Pharma). Drugs Investig. Drugs J. *3*, 1081–1087.

Kahn, C.R., Baird, K.L., Flier, J.S., Grunfeld, C., Harmon, J.T., Harrison, L.C., Karlsson, F.A., Kasuga, M., King, G.L., Lang, U.C., et al. (1981). Insulin receptors, receptor antibodies, and the mechanism of insulin action. Recent Prog. Horm. Res. *37*, 477–538.

Kang, S., Creagh, F.M., Peters, J.R., Brange, J., Vølund, A., and Owens, D.R. (1991). Comparison of subcutaneous soluble human insulin and insulin analogues (AspB9, GluB27; AspB10; AspB28) on meal-related plasma glucose excursions in type I diabetic subjects. Diabetes Care *14*, 571–577.

Katsoyannis, P.G., Tometsko, A., and Zalut, C. (1966). Insulin peptides XII. Human insulin generation by combination of synthetic A and B chains. J Am Chem Soc *88*, 186.

Keen, H., Glynne, A., and Pickup, J.C. et al (1980). Human insulin produced by recombinant DNA technology: safety and hypoglycaemic potency in healthy men. Lancet *ii*, 398–401.

Kelly, W.D., Lillehei, R.C., Merkel, F.K., Idezuki, Y., and Goetz, F.C. (1967). Allotransplantation of the pancreas and duodenum along with the kidney in diabetic nephropathy. Surgery *61*, 827–837.

Kung, Y.T., Da, Y.C., and Huang, W.T. et al (1966). Total synthesis of crystallilne insulin. Sci Sin *15*, 544.

Lacy, P.E., and Kostianovsky, M. (1967). Method for the isolation of intact islets of Langerhans from the rat pancreas. Diabetes *16*, 35–39.

Langerhans, P. (1869). Beitrage zur mikroskopischen Anatomie der Bauchspeicheldruse. Med Diss.

Lee, K.Y., and Mooney, D.J. (2012). Alginate: properties and biomedical applications. Prog Polym Sci *37*, 106–126.

Lembert, N., Wesche, J., Petersen, P., Zschocke, P., Enderle, A., Planck, H., and Ammon, H.P. (2001). Macroencapsulation of rat islets without alteration of insulin secretion kinetics. Exp. Clin. Endocrinol. Diabetes *109*, 116–119.

Levine, R., and Mahler, R. (1964). Productino, Secretion, and Availability of Insulin. Annu. Rev. Med. *15*, 413–432.

Lim, F., and Sun, A.M. (1980). Microencapsulated islets as bioartificial endocrine pancreas. Science (80-.). *210*, 908–910.

Mackie, W., Perez, S., Rizzo, R., Taravel, F., and Vignon, M. (1983). Aspects of the conformation of polyguluronate in the solid state and in solution. Int. J. Biol. Macromol. *5*, 329–341.

Mahgoub, M.A., Ammar, A., Fayez, M., Edris, A., Hazem, A., Akl, M., and Hammam, O. (2004). Neovascularization of the amniotic membrane as a biological immune barrier. Transplant. Proc. *36*, 1194–1198.

Matschinky, F., Liang, Y., Wang, L., Froguel, P., Velho, G., Cohen, D., Permutt, M., Tanizawa, Y., Jetton, T., and Kesavan, P. (1993). Glucokinase as pancreatic beta-cell glucose sensor and diabetes gene. J Clin Invest *92*, 2092–2098.

Meienhofer, J., Schnabel, E., and Bremer, H. et al (1963). Synthesis der Insulinketten und ihre Kombination zu insulactiven Präparaten. Z Naturforsch *18*.

Von Mering, J., and Minkowski, O. (1889). Diabetes Mellitus nach Pankreasexstirpation. Zentralbl Klin Med *10*, 393–394.

Minkowski, O. (1989). Historical development of the theory of pancreatic diabetes (introduction and translation by R. Levine). Diabetes *38*, 1–6.

Mørch, Y.A., Donati, I., Strand, B.L., and Skjåk-Braek, G. (2007). Molecular engineering as an approach to design new functional properties of alginate. Biomacromolecules *8*, 2809–2814.

Morrison, H. (1937). Translation and introductory essay. Langerhans P. Contributions to the microscopic anatomy of the pancreas. Bull Inst Hist Med *5*, 259–269.

Mosenthal, H.O. (1944). Globin insulin with zinc in the treatment of diabetes mellitus. J. Am. Med. Assoc. *125*, 483.

Murua, A., Portero, A., Orive, G., Hern??ndez, R.M., de Castro, M., and Pedraz, J.L. (2008). Cell microencapsulation technology: Towards clinical application. J. Control. Release *132*, 76–83.

Myles, A., and Aggarwal, A. (2011). Expression of Toll-like receptors 2 and 4 is increased in peripheral blood and synovial fluid monocytes of patients with enthesitis-related arthritis subtype of juvenile idiopathic arthritis. Rheumatology (Oxford). *50*, 481–488.

Nepom, G., and Kwok, W. (1998). Perspectives in diabetes: molecularbasis for HLA-DQ association with IDDM. Diabetes *47*, 1177–1184.

Noble, J., Valdes, A., Cook, M., Klitz, W., Thomson, G., and Erlich, H. (1996). The role of HLA class II genes in insulin-dependent diabetes mellitus: molecular analysis of 180 Caucasian, multiplex families. Am J Hum Genet *59*, 1134–1148.

O'Connor, M., Landahl, H., and Grodsky, G. (1980). Comparison of storage- and signal-limited models of pancreatic insulin secretion. Am J Physiol *238*, R378–R389.

Omer, A., Duvivier-Kali, V.F., Trivedi, N., Wilmot, K., Bonner-Weir, S., and Weir, G.C. (2003). Survival and maturation of microencapsulated porcine neonatal pancreatic cell clusters transplanted into immunocompetent diabetic mice. Diabetes *52*, 69–75.

Opie, E.L. (1900). The relstion of disbetes mellitus to lesions of the pancreas: hyaline degeneration of the islands of Langerhans. J Exp Med *5*.

Orive, G., Gascón, A.R., Hernández, R.M., Igartua, M., and Luis Pedraz, J. (2003). Cell microencapsulation technology for biomedical purposes: novel insights and challenges. Trends Pharmacol. Sci. *24*, 207–210.

Owerbach, D., Bell, G.I., Rutter, W.J., and Shows, T.B. (1980). The insulin gene is located on chromosome 11 in humans. Nature *286*, 82–84.

Paredes-Juarez, G.A., de Haan, B.J., Faas, M.M., and de Vos, P. (2013). The role of pathogen-associated molecular patterns in inflammatory responses against alginate based microcapsules. J Control Release *172*, 983–992.

Patzelt, C., Labrecque, A.D., Duguid, J.R., Carroll, R.J., Keim, P.S., Heinrikson, R.L., and Steiner, D.F. (1978). Detection and kinetic behavior of preproinsulin in pancreatic islets. Proc. Natl. Acad. Sci. U. S. A. *75*, 1260–1264.

Paulesco, N.C. (1921). Action de l'extrait pancréatique injecté dans le sang, chez un animal diabétique. C R Soc Biol *85*, 555–559.

Petersen, P., Lembert, N., Zschocke, P., Stenglein, S., Planck, H., Ammon, H.P.., and Becker, H.. (2002). Hydroxymethylated polysulphone for islet macroencapsulation allows rapid diffusion of insulin but retains PERV. Transplant. Proc. *34*, 194–195.

Pickup, J.C., Keen, H., Parsons, J.A., and Alberti, K.G. (1979). Technology of pre-programmable insulin delivery systems: continuous subcutaneous insulin infusion. Horm. Metab. Res. Suppl. 49–51.

Porte, D., and Pupo, A. (1969). Insulin responses to glucose: evidence for a two pool system in man. J Clin Invest *48*, 2309–2318.

Raju, T.N.K. (2006). A mysterious something: the discovery of insulin and the 1923 Nobel Prize for Frederick G. Banting (1891-1941) and John J.R. Macleod (1876-1935). Acta Paediatr. *95*, 1155–1156.

Rana, R.S., and Hokin, L.E. (1990). Role of phosphoinositides in transmembrane signaling. Physiol Rev *70*, 115–164.

Reiner, L., Searle, D.S., and Lang, E.H. (1939). Insulin preparations with prolonged activity: I. Globin insulin. Proc. Soc. Exper. Biol. Med. *40*, 171.

Rhodes, C.J., and Alarcón, C. (1994). What beta-cell defect could lead to hyperproinsulinemia in NIDDM? Some clues from recent advances made in understanding the proinsulin-processing mechanism. Diabetes *43*, 511–517.

Richter, B., and Neises, G. (2003). "Human" insulin versus animal insulin in people with diabetes mellitus. Cochrane Database Syst. Rev. CD003816.

Root, M.A., Chance, R.E., and Galloway, J.A. (1972). Immunogenicity of insulin. Diabetes *21*, 657–660.

Rubenstein, A.H., Kuzuya, H., and Horwitz, D.L. (1977). Clinical Significance of Circulating C-Peptide in Diabetes Mellitus and Hypoglycemic Disorders. Arch. Intern. Med. *137*, 625.

Ryle, A.P., Sanger, F., Smith, L.F., and Kitai, R. (1955). The disulphide bonds of insulin. Biochem. J. *60*, 541–556.

Sacks, D.B., Arnold, M., Bakris, G.L., Bruns, D.E., Horvath, A.R., Kirkman, M.S., Lernmark, A., Metzger, B.E., and Nathan, D.M. (2011). Guidelines and recommendations for laboratory analysis in the diagnosis and management of diabetes mellitus. Diabetes Care *34*, e61–e99.

Schade, D., Santiago, J., Skyler, J., and Al., E. (1983). Haycock P. History of insulin therapy. In Intensive Insulin Therapy, (Princeton, NJ: Excerpta Medica), pp. 1–19.

Scharp, D.W., Lacy, P.E., Santiago, J. V, McCullough, C.S., Weide, L.G., Falqui, L., Marchetti, P., Gingerich, R.L., Jaffe, A.S., and Cryer, P.E. (1990). Insulin independence after islet transplantation into type I diabetic patient. Diabetes *39*, 515–518.

Scharp, D.W., Lacy, P.E., Santiago, J. V, McCullough, C.S., Weide, L.G., Boyle, P.J., Falqui, L., Marchetti, P., Ricordi, C., and Gingerich, R.L. (1991). Results of our first nine intraportal islet allografts in type 1, insulin-dependent diabetic patients. Transplantation *51*, 76–85.

Shapiro, A., Lakey, J., Ryan, E., Korbutt, G., Toth, E., Warnock, G., Kneteman, N., and Rajotte, R. (2000). Islet transplantation in seven patients with type I diabetes mellitus using a glucocorticoid-free immunosuppressive regimen. N Engl J Med *343*, 230–238.

Sheetz, M.J. (2002). Molecular Understanding of Hyperglycemia's Adverse Effects for Diabetic Complications. JAMA *288*, 2579.

Sleigh, S. (1998). Insulin preparations and analogues: structure and properties -. J. Diabetes Nurs. *2*, 150–154.

Steil, G. (2004). Closed-loop insulin delivery—the path to physiological glucose control. Adv. Drug Deliv. Rev. *56*, 125–144.

Steiner, D.F., and Oyer, P.E. (1967a). The biosynthesis of insulin and a probable precursor of insulin by a human islet cell adenoma. Proc. Natl. Acad. Sci. U.S.A. *57*, 473–480.

Steiner, D.F., and Oyer, P.E. (1967b). The biosynthesis of insulin and a probable precursor of insulin by a human islet cell adenoma. Proc. Natl. Acad. Sci. U. S. A. *57*, 473–480.

Steiner, D.F., Cunningham, D., Spigelman, L., and Aten, B. (1967a). Insulin biosynthesis: evidence for a precursor. Science (80-.). *157*, 697–700.

Steiner, D.F., Cunningham, D., Spigelman, L., and Aten, B. (1967b). Insulin biosynthesis: evidence for a precursor. Science *157*, 697–700.

Steiner, D.F., Chan, S.J., Welsh, J.M., and Kwok, S.C. (1985). Structure and evolution of the insulin gene. Annu. Rev. Genet. *19*, 463–484.

Stretton, A.O.W. (2002). The First Sequence: Fred Sanger and Insulin. Genetics *162*, 527–532.

Sutherland, D.E.R., Gores, P.F., Farney, A.C., Wahoff, D.C., Matas, A.J., Dunn, D.L., Gruessner, R.W.G., and Najarian, J.S. (1993). Evolution of kidney, pancreas, and islet transplantation for patients with diabetes at the University of Minnesota. Am. J. Surg. *166*, 456–491.

Teuscher, A. (1979). The biological effect of purely synthetic human insulin in patients with diabetes mellitus. Schweiz Med Wochenschr *109*, 743–747.

Todd, J. (1999). From genome to aetiology in a multifactorial disease, type 1 diabetes. Bioassays *21*, 164–174.

Tuch, B.E., Keogh, G.W., Williams, L.J., Wu, W., Foster, J.L., Vaithilingam, V., and Philips, R. (2009). Safety and viability of microencapsulated human islets transplanted into diabetic humans. Diabetes Care *32*, 1887–1889.

Ullrich, A., Shine, J., Chirgwin, J., Pictet, R., Tischer, E., Rutter, W., and Goodman, H. (1977). Rat insulin genes: construction of plasmids containing the coding sequences. Science (80-.). *196*, 1313–1319.

Vajo, Z., Fawcett, J., and Duckworth, W.C. (2013). Recombinant DNA Technology in the Treatment of Diabetes: Insulin Analogs.

Vardanyan, M., Parkin, E., Gruessner, C., and Rodriguez Rilo, H.L. (2010). Pancreas vs. islet transplantation: a call on the future. Curr. Opin. Organ Transplant. *15*, 124–130.

Vernon, B., Kim, S.W., and Bae, Y.H. (2000). Thermoreversible copolymer gels for extracellular matrix. J. Biomed. Mater. Res. *51*, 69–79.

Walsh, G. (2005). Therapeutic insulins and their large-scale manufacture. Appl Microbiol Biotechnol *67*, 151–159.

Walter, P., and Johnson, A.E. (1994). Signal sequence recognition and protein targeting to the endoplasmic reticulum membrane. Annu. Rev. Cell Biol. *10*, 87–119.

Ward, C.W., and Lawrence, M.C. (2009). Ligand-induced activation of the insulin receptor: a multi-step process involving structural changes in both the ligand and the receptor. Bioessays *31*, 422–434.

Weir, G.C. (2013). Islet encapsulation: advances and obstacles. Diabetologia *56*, 1458–1461.

White, P. (1932). Diabetes in childhood and adolescence (Philadelphia: Lea & Febiger).

Williams, P. (1894). Notes on diabetes treated with extract and by grafts of sheep's pancreas. **BMJ 1303–1304.**

Xie, D., Smyth, C.A., Eckstein, C., Bilbao, G., Mays, J., Eckhoff, D.E., and Contreras, J.L. (2005). Cytoprotection of PEG-modified adult porcine pancreatic islets for improved xenotransplantation. Biomaterials *26*, 403–412.

Yang, D., and Jones, K.S. (2009). Effect of alginate on innate immune activation of macrophages. J. Biomed. Mater. Res. A *90*, 411–418.

Yechoor, V., and Chan, L. (2005). Gene therapy progress and prospects: gene therapy for diabetes mellitus. Gene Ther. *12*, 101–107.

Zimmermann, H., Shirley, S.G., and Zimmermann, U. (2007). Alginate-based encapsulation of cells: past, present, and future. Curr Diab Rep *7*, 314–320.

Zimmermann, U., Cramer, H., Jork, A., Thürmer, F., Zimmermann, H., Fuhr, G., Hasse, C., and Rothmund, M. (2001). Microencapsulation-Based Cell Therapy. In Biotechnology Set, pp. 547–571.

Chapter 2

Characterization of Pattern Recognition Receptor Responses Against Materials for Cell Encapsulation

The content of this chapter in whole is currently in preparation for publication.

The content of this chapter in part is published to Journal of Advanced Materials:

O'Shea, T.M., Aimetti, A.A., Kim, E., Yesilyurt, V., and Langer, R. Synthesis and Characterization of a Library of *in situ* Curing, Non-swelling Ethoxylated Polyol Thiol-ene Hydrogels for Tailorable Macromolecule Delivery. Advanced Materials (2014). DOI:10.1002/adma.201403724

~~~ CHAPTER OUTLINE ~~~

"Life [with diabetes] is short, disgusting and painful."
~ Aretaeus of Cappadocia, 1st century AD

Abstract

Islet transplantation has tremendous potential for the treatment of type I diabetes, but an immunoprotective barrier is necessary to protect the donor tissue from host rejection and to eliminate the need for systemic immunosuppressive therapy. Cell encapsulation is an attractive technology to enable donor cell transplantation, but clinical success has remained elusive due to immunological responses to the encapsulated materials. Alginate is the leading material for the microencapsulation of islet cells, successfully creating a barrier between the host immune system and implanted islet cells. However, inflammatory monocytes and macrophages initiate a cascade of immunological responses to the implanted materials, leading to a chronic inflammation that results in fibrosis of the implants and hypoxic death of the islet cells. These macrophages may sense alginate via pattern recognition receptors (PRRs), such as toll-like receptors (TLRs) and NOD-like receptors (NLRs). However, which PRRs are involved, how they recognize alginate, and whether alginate material characteristics and compositions can elicit different responses are not very well understood.

To better understand the PRR mediated immune response to alginate, we devised an *in vitro* system to study the activation of PRRs against several commercially available alginates. Here, we report that alginate compositions and material characteristics can influence which PRRs activate and how strongly they can provoke PRR mediated immune response, and that direct cell-to-material contact is a crucial step in initiating such response.

I. Introduction

Type I diabetes mellitus is an autoimmune disease caused by progressive destruction of the insulin secreting pancreatic beta cells in the islets of Langerhans (Drouin et al., 2009). Such destruction is caused by CD4+ and CD8+ auto-reactive T-lymphocytes (Chatenoud, 2008). Current diabetes therapies are insulin injections, monitoring of blood glucose, dietary restriction and exercise; however, these only provide a short-term relief (Beck et al., 2007; Lakey et al., 2006). Alternatively, pancreas or islet cell transplantation provides a long-term relief, maintaining normoglycemia for an extended period of time. However, success of these methods is largely limited by the host graft rejection (Beck et al., 2007; Lakey et al., 2006).

First demonstrated by Algire et al. in 1954, cells encapsulated by a semi-permeable membrane prevented allograft failure in mice (Algire et al., 1954; Lakey et al., 2006). In 1964, T.M.S Chang proposed the idea of incorporating a semi-permeable membrane made of biocompatible polymers to provide immune-protection of transplanted cells (Chang, 1964; Orive et al., 2003a). The premise of his idea was that the membrane would allow bi-directional flow of nutrients, oxygen, and waste products while allowing therapeutic product secretion and preventing the host immune system from destroying the enclosed cells (**Chapter 1, Figure 8**). Subsequently in 1980, Lim and Sun demonstrated for the first time that microencapsulated islets with alginate, naturally occurring polymers extracted from algae, corrected diabetic state for 2 to 3 weeks and remained functionally viable over 15 weeks in rats (Lim and Sun, 1980). Since then, tremendous advancements have been made in technologies using alginate for various 3biomedical applications. Today, alginate

remains the leading material for the microencapsulation of islet cells (Zimmermann et al., 2007).

Alginate is a family of linear co-polymers of β-D-mannuronic acid (M) and α-L-guluronic acid (G) with highly variable G and M sequence and composition (Andersen et al., 2012) (**Chapter 1, Figure 9a**). Commercially available alginate is generally extracted from various brown algae (*Phaeophyceae*). They generally have a high molecular weight, typically in the range of 10^5 to 10^6 Daltons, and the ratio of G and M varies depending on the source (**Chapter 1, Table 3**) (Andersen et al., 2012; Lee and Mooney, 2012; Mørch et al., 2007). As ionic polysaccharides, alginate can form gels in the presence of divalent cations, such as calcium, barium and strontium ions, and this ionic cross-linking is most efficient at physiological condition (Andersen et al., 2012; Braccini and Perez, 2001; Lee and Mooney, 2012). Divalent cations induce linear alginate polymer chain-chain association which constitute the junction zones responsible for gel formation (Braccini and Perez, 2001). This junction zone is known as the "egg box model" (**Chapter 1, Figure 9b and 9c**). It is this gelation property that has gained high interest, as it constitutes the foundation of creating a barrier between the host immune system and the implanted islet cells.

Although the alginate hydrogels provide a protection against host graft rejection and allow diffusion and exchange of oxygen, nutrients, and insulin, there are obstacles to be overcome in order to keep the enclosed cells viable and make this a successful alternative treatment for diabetes. The biggest problem is a foreign body response against the material itself, which is initiated by the inflammatory cell recruitment at the implant site.

This ultimately leads to formation of thick collagenous fibrous tissues around the capsules and hypoxic death of encapsulated islet cells (Lakey et al., 2006; Narang and Mahato, 2006; Orive et al., 2003b; Weir, 2013). Due to these immunological foreign body responses to alginate microcapsules, clinical success of alginate encapsulated islet cell transplantation remained elusive. Various human trials assessing practicability of using alginate to replace diseased cells validated feasibility of cell replacement therapy. However, these studies not only demonstrated short-term success, but also indicated a major hurdle that has to be overcome in order to achieve long-term success (Basta et al., 2011; Calafiore et al., 2006; Hasse et al., 1997).

Foreign body response is one of the major obstacles in making encapsulated islet transplantation a success. Foreign body reaction is a complex cascade of reaction involving protein adsorption, leukocyte recruitment, secretion of various inflammatory cytokines, formation of foreign body giant cells, and eventual fibrous encapsulation of the biomaterials (**Chapter 1, Figure 11**) (Anderson et al., 2008; Bridges and García, 2008; Franz et al., 2011). Biomaterials have long been recognized to induce inflammation, and many studies have confirmed that macrophages play a key role in biomaterial induced inflammation (Omer et al., 2003a; Yang and Jones, 2009). Over the years, it has been shown that sensing pathogen-associated molecular patterns (PAMPs) and responding to them quickly provide a first line of defense, subsequently activating adaptive immune responses (Gallucci and Matzinger, 2001). The consequences of innate immune activation and biomaterial-induced inflammation are remarkably similar, and therefore it has been suggested that alginate can activate pattern recognition receptors (PRRs), which include

families of Toll-like receptors and NOD-like receptors, of the innate immunity (Yang and Jones, 2009). However, the mechanism of PRR activation and which particular PRRs are involved in macrophage activation in response to alginate are currently not well understood.

The our primary goal is to confirm whether PRRs are involved in activating macrophages against alginate, and to gain a better understanding of which PRRs are involved in alginate-induced inflammation *in vitro.* We first established *in vitro* PRR activation assays with several commercially available alginates, and optimized the assays by varying several important experimental parameters. Here, we report that (1) alginate compositions and material characteristics can influence how strongly they can provoke PRR mediated immune response. By testing alginate of different material characteristics and composition, we show that some alginates, but not all, can provoke PRR mediated immune responses. We used clean, sterile, and ultrapure alginates in our studies; and therefore, our data suggest that alginate itself can provoke immune response via PRR activation. As an additional note, we observed that impure alginates could indeed trigger inflammation, as other studies have reported. We also report that (2) direct cell-to-material contact plays a key role in initiating PRR mediated immune response. We compared PRR activations against alginate with adherent cells and non-adherent cells. We confirmed the contact dependency of alginate-induced inflammation by testing adherent and non-adherent cells and by blocking direct cell-to-material contact in two different systems. Lastly, of all alginate we tested, UPVLVG caused the strongest PRR activation, and this led us to investigate the roles of specific PRRs with UPVLVG. We report that (3) of

TLR2, TLR4, TLR5, TLR7, TLR8, and TLR9 we tested, UPVLVG does not seem to activate TLR2, but does activate TLR4, TLR7, TLR8, and TLR9; and that TLR2 and TLR5 responses are likely related to the impurities present in the alginate samples, while TLR 4, 7, 8, 9 responses.

II. Materials and Methods

A. Establishment of the PRR activation assays

1. Cell cultures

All cell lines were obtained from InvivoGen (San Diego, CA). RAW-Blue™ cells, derived from murine macrophage cell line RAW264.7, express many pattern recognition receptors (PRRs), including all toll-like receptors (TLRs), except TLR5, and are stably transfected with a secreted embryonic alkaline phosphatase (SEAP) reporter gene inducible by NF-kB and AP-1 transcription factors. RAW-Blue™ cells were cultured in DMEM medium (4.5g/L glucose, 2mM L-glutamine) supplemented with 10% heat inactivated fetal bovine serum, Pen-Strep (50U/ml), 100ug/ml Normocin™, and 200ug/ml Zeocin™.

2. Alginates

Alginates with different G and M ratios and molecular weights were obtained from several different companies. Alginate SLG20 (MW 75,000-150,000 g/mol, G/M≥1.5), SLG100 (MW 150,000-250,000 g/mol, G/M≥1.5), SLM20 (MW 75,000-150,000 g/mol, G/M≤1), SLM100 (MW 150,000-250,000 g/mol, G/M≤1) are sterile Ultrapure PRONOVA™ sodium alginates purchased from NovaMatrix® (Sandvika, Norway). Alginates UP VLVM (MW < 75,000 g/mol, G/M≤1), UP LVM (MW 75,000-200,000 g/mol, G/M≤1), UP MVM (MW > 200,000 g/mol, G/M≤1), UPVLVG (MW < 75,000 g/mol, G/M≥1.5), UP LVG (MW 75,000-200,000 g/mol, G/M≥1.5), UP MVG (MW > 200,000 g/mol, G/M≥1.5) are Ultrapure PRONOVA™ sodium alginates purchased from NovaMatrix® (Sandvika, Norway). Pharmaceutical grade alginate Protanal® LF10/60

alginate was purchased from FMC BioPolymer (Philadelphia, PA). Crude alginate was purchased from Sigma-Aldrich Co. LLC (St. Louis, MO).

The endotoxin level of all alginates purchased from NovaMatrix® is less than 100EU/g. Endotoxin is a complex lipopolysaccharide (LPS) found in the outer cell membrane of gram-negative bacteria. One Endotoxin Unit (EU) equals approximately 0.1 to 0.2 ng of endotoxin/ml. Increasing evidence suggests that endotoxin can cause a variety of problems for cell culture research. In the presence of high endotoxin, leukocyte cultures can be stimulated to produce various cytokines. Currently FDA requires that endotoxin level of medical devices be less than 0.5EU/ml (Gorbet and Sefton, 2005).

3. Quanti-Blue™ assay

QUANTI-Blue™ is a colorimetric enzyme assay developed by InvivoGen (San Diego, USA) and can be used to detect alkaline phosphatase activity in cell culture media. In the presence of secreted embryonic alkaline phosphatase (SEAP), QUANTI-Blue™ medium turns a purple-blue color, and SEAP activity can be measured by reading the OD at 620-655nm (**Figure 1**).

4. PRR agonists

Following PRR agonists, all of which were purchased from InvivoGen (San Diego, USA), were tested as positive controls: Pam3CSK4 (100ng/ml), Poly(I:C) High Molecular Weight (5μg/ml), LPS-EK Ultrapure (5μg/ml), FLA-ST Ultrapure (100ng/ml), Gardiquimod™ VacciGrade™(10μg/ml), ssRNA40/LyoVec™(5μg/ml), R848 (100ng/ml),

ODN 2006(ODN 7909) (5μM), ODN 1826 (1μM), ORN Sa19 (500ng/ml), Tri-DAP (10μg/ml), L18-MDP (50ng/ml).

Pam3CSK4 (Pam3CysSerLys4) is a synthetic triacylated lipoprotein that mimics the acylated amino terminus of bacterial lipoproteins. Recognition of Pam3CSK4 is mediated by TLR2, which cooperates with TLR1 through their cytoplasmic domain to induce the signaling cascade leading to the NF-κB activation (Aliprantis, 1999; Ozinsky et al., 2000). Cells were stimulated with 100ng/ml of Pam3CSK4.

Poly(I:C) (polyinosinic-polycytidylic acid) is a synthetic analog of double stranded RNA (dsRNA). It is a molecular pattern associated with viral infection and is known to induce type I interferons (IFNs) and other cytokines. Poly(I:C) is recognized by TLR3 receptor. Upon recognition, TRL3 activates the transcription factor interferon regulatory factor 3 (IRAF3), which leads to the type I IFNs (Alexopoulou et al., 2001; Kawai and Akira, 2008; Matsumoto et al., 2002; Yamamoto et al., 2003).

LPS-EK Ultrapure is lipopolysaccharide from *E. coli* K12 strain. It is the major structural component of the outer wall of Gram-negative bacteria. LPS recognition is predominantly mediated by TLR4 (Fujihara et al., 2003; Poltorak, 1998).

FLA-ST Ultrapure is purified Flagellin from *S. typhimurium*. Flagellin is the major component of the flagella of many Gram-negative bacteria, and is recognized by TLR5, resulting in MyD88 mediated NF-κB activation (Hayashi et al., 2001; Mizel et al., 2003).

Gardiquimod™ VacciGrade™ is an imidazoquinoline compound, which acts as a TLR7 agonist (Ma et al., 2010).

ssRNA40/LyoVec™ is a 20-mer phosphothioate protected single-stranded RNA containing a GU rich sequence, complexed with the cationic lipid LyoVec™. TLR7 is known to play an important role in recognizing viral ssRNA in murine cells. In human, TLR8 is known to be the key factor for viral ssRNA (Diebold et al., 2004; Heil et al., 2004).

R848 is an imidazoquinoline compound that can activate immune cells via the TLR7/TLR8 MyD88 depending signaling pathway (Hemmi et al., 2002; Jurk et al., 2002).

ODN 2006 (ODN 7909) and ODN 1826 are synthetic oligonucleotides that contain unmethylated CpG motifs and are recognized by TLR9. ODN 2006 is specific for human TLR9, and ODN 1826 is specific for murine TLR9 (Bauer et al., 2001; Krieg et al., 1995).

ORN Sa19 is a conserved 23S ribosomal RNA sequence (CGGAAAGACC), stabilized by phosphorothioate modification, derived from *S. aureus*, and is shown to induce cytokine production via TLR13 MyD88 dependent manner (Hidmark et al., 2012; Li and Chen, 2012; Oldenburg et al., 2012).

Tri-DAP (L-Ala-γ-D-Glu-mDAP) comprises the iE-DAP(γ-D-Glu-mDAP) dipeptide and an L-Ala residue. Tri-DAP is present in the peptidoglycan (PGN) in a subset of Gram-negative and Gram-positive bacteria, and is recognized by NOD1, leading to activation of NF-κB (Chamaillard et al., 2003; Park et al., 2007).

L18-MDP is a 6-*O*-acyl derivative of muramyl dipeptide (MDP), common peptidoglycan motif to all bacteria, with a stearoyl fatty acid. MDP is known to be recognized by NOD2, and L18-MDP is shown to be 10 times more efficient than MDP to induce NF-κB activation (Girardin et al., 2003).

As a negative control for testing PRR agonists with RAW-Blue™ cells, DMEM medium (4.5g/L glucose, 2mM L-glutamine) supplemented with 10% heat inactivated fetal bovine serum, Pen-Strep (50U/ml), 100ug/ml Normocin™, and 200ug/ml Zeocin™ was used.

5. Synthesis of alginate hydrogels

Alginate solutions were prepared as follows: SLG20 was dissolved at 1.4% weight to volume in 0.8% saline. SLG100 was dissolved at 1.2% weight to volume in 0.8% saline. UPVLVG was dissolved at 5% weight to volume in 0.8% saline. SLM20, SLM100, UPVLVG, UPVLVM, UPLVM, UPMVM, UPMVG, LF10/60, and Crude were dissolved at 2% weight to volume in 0.8% saline. UPVLVG (5%) was blended with SLG100 (3%) to make the UPVLVG/SLG100 (70:30) blend alginate solution.

For the synthesis of flat alginate hydrogel in 96 well plate, 70µl of each alginate solution was aliquoted into individual wells of Corning® Costar® Ultra-Low attachment 96-well purchased from Sigma-Aldrich Co. LLC (St. Louis, MO). 2.4% $BaCl_2$ (135mM $NaCl_2$, 4.7mM KCl, 25mM HEPES, 1.2mM KH_2PO_4, 1.2mM $MgSO_4 \bullet 7H_2O$) and mannitol solution (90g, 50ml 1M HEPES, 2L H_2O) solution were prepared and sterilized by filtration and autoclaving. Cross-linking of alginate was initialed by adding 100µl of $BaCl_2$:mannitol (1:4) to each well. This produced alginate hydrogels approximately 4mm in thickness. After the gelation is complete, excess barium was washed with HEPES and appropriate cell culture media prior to cell seeding.

6. Quantification of SEAP

To assess whether alginate can activate PRRs, cells were plated on alginate hydrogels surface at 100,000 – 200,000 cells/well and incubated overnight at 37°C and 5% CO_2. Activation of PRRs leads to the activation of NF-κB and AP-1 transcription factors and subsequently produces secreted embryonic alkaline phosphatase (SEAP). The SEAP level was monitored using QUANTI-Blue™ detection medium. QUANTI-Blue™ medium was prepared according to manufacture's protocol. Supernatants (50µl) from the cells seeded on alginates were transferred to a new flat bottom 96-well plate, and 150ul of QUANTI-Blue™ medium was added to each well. After 2 hour incubation at 37°C 5% CO_2, the SEAP activity was measured at 650nm using TECAN Infinite M200 (**Figure 1**).

Since decreased SEAP secretion can be either due to the lack of PRR activation or cell death, cell viability assays were performed parallel to all alginate PRR stimulation assays. Cell viability was determined using CellTiter-Glo® Luminescent Cell Viability Assay (Promega, Madison, WI, USA) for all alginate PRR activation assays, and CellTiter 96® AQ_{ueous} One Solution Cell Proliferation Assay (Promega, Madison, WI, USA) for PEG PRR stimulation assay. For CellTiter-Glo® Luminescent Cell Viability Assay, an equal volume of CellTiter-Glo® reagent was added to each well of alginate plates seeded with cells, placed on an orbital shaker for 2 minutes to induce cell lysis, and incubated at room temperature for 10 minutes to stabilized luminescent signal. Supernatants were then transferred to white 96 well plates, and luminescence was recorded using 650nm using TECAN Infinite M200. For CellTiter 96® AQ_{ueous} One Solution Cell Proliferation

Assay, appropriate volume of CellTiter 96® AQueous One Solution Reagent was added into each well of alginate plates seeded with cells. The plate was then incubated 1 to 4 hours at 37°C, 5% CO_2, and the absorbance at 49nm was recorded using TECAN Infinite M200. For each cell viability assay, standard curve was generated to calculate the number of viable cells for each PRR activation assay.

7. Statistical analysis

The QUANTI-Blue™ PRR stimulation assays with all cell lines were all done in 6 to 12 replicas. All data are presented as the mean ± standard deviation of the mean. Statistical significance was calculated using Prism6 (GraphPad Software) one-way ANOVA with Tukey's test. P-value less than 0.001 is designated with three asterisks (***). P-value less than 0.01 was designated with two asterisks (**). P-value less than 0.05 is designated with one asterisk (*). P-value greater than 0.05 is designated with not-significant (ns).

B. Optimization of the immunostimulation assays with alginates

1. Controlled gelation of alginate

Alginate solutions were prepared as stated above. Cross-linking of alginate with barium is an instantaneous process, and therefore when making the hydrogels in the 96well plate, gelation kinetics are uncontrolled, and it produces rough hydrogel surface topology. To control gelation kinetics and to make smooth flat surface hydrogel, 1ml of each alginate solution was aliquoted into individual wells of Corning® Costar® Ultra-Low attachment 24-well purchased from Sigma-Aldrich (St. Louis, MO). Sterile Scaffdex CellCrown™ 24 well plate inserts with 8μm PET filter (Sigma-Aldrich, St. Louis, MO)

were inserted into each well. 2.4% $BaCl_2$ (135mM $NaCl_2$, 4.7mM KCl, 25mM HEPES, 1.2mM KH_2PO_4, 1.2mM $MgSO_4 \bullet 7H_2O$) and mannitol solution (90g, 50ml 1M HEPES, 2L H_2O) solution were prepared and sterilized by filtration and autoclaving. Cross-linking of alginate was initialed by adding 1ml of $BaCl_2$:mannitol (1:4) to each insert. The plate was then placed on a rotary shaker overnight to allow barium solution to slowly diffuse through the PET membrane. Resulting alginate hydrogels were approximately 5mm in thickness with smooth flat surface topology. After the gelation is complete, excess barium washed with HEPES and appropriate cell culture media prior to cell seeding.

2. Synthesis of alginate microcapsules

Electrospray was set up as follows: Alginate is loaded into a 5 mL lure lock syringe (BD, NJ, USA). A blunt tipped needle is attached to the syringe (SAI Infusion Technologies, IL, USA). The syringe is clipped to a vertically oriented syringe pump (Pump 11 Pico Plus, Harvard Apparatus, MA, USA). The syringe pump positions the blunt tipped needle over a glass dish that contains a 20mM barium 5% mannitol cross-linking solution (Sigma Aldrich, MO, USA). An ES series 0-100 KV, 20 Watt high voltage power generator (Gamma ES series, Gamma High Voltage Research, FL, USA) is connected to the blunt tipped needle. A 25 gauge blunt tipped needle (SAI Infusion Technologies) was used with a voltage of 5-7 kV. The settings of the PicoPlus syringe pump are 12.06 mm diameter and 0.2 mL/min flow rate. After the capsules are formed, the capsules are then collected and washed with HEPES buffer (NaCl 15.428g, KCl 0.70g,

$MgCl_2 \cdot 6H_2O$ 0.488g, 50 mL of HEPES (1M) buffer solution (Gibco, Life Technologies, California, USA) in 2L of DiH2O) 4 times. The alginate capsules are stored at 4°C.

3. Kinetics studies of PRR activation with alginates

In order to determine the optimal number of RAW-Blue™ cells and incubation time with QUANTI-Blue™ for SEAP quantification, we investigated kinetic profiles of QUANTI-Blue™ with different cell numbers and incubation times. RAW-Blue™ cells were plated at 100,000 cells/well, 200,000 cells/well, and 500,000 cells/well and treated with various PRR agonists. After 24 hours and 48 hours treatments with agonists, cell culture media of the agonist treat cells were incubated with QUANTI-Blue™ reagents, and absorbance at 655nm was measured at every 2 hours interval for 24 hours. Absorbance values were normalized with untreated cell control values.

4. Cell adhesion assay

In order to determine how many cells are adhered to alginate hydrogels, Vybrant™ Cell Adhesion Assay Kit (Molecular Probes, NY, USA) was used. RAW-Blue™ cells cultured in DMEM medium (4.5g/L glucose, 2mM L-glutamine) supplemented with 10% heat inactivated fetal bovine serum, Pen-Strep (50U/ml), 100ug/ml Normocin™, and 200ug/ml Zeocin™ were washed twice with 1X PBS. Cells were detached and resuspended at 5×10^6 cells/ml in serum free medium: DMEM medium (4.5g/L glucose, 2mM L-glutamine) supplemented with Pen-Strep (50U/ml), 100ug/ml Normocin™, and 200ug/ml Zeocin™. Vybrant™ Cell Adhesion Assay Kit utilizes calcein acetoxymethyl ester (calcein AM), which is nonfluorescent but produces fluorescence once loaded into the cells because it is cleaved by endogenous esterases to produce highly fluorescent

calcein. 5µl of the calcein AM solution (1mM) was added to per ml of cell suspension (final concentration 5µM). The cell suspension was incubated at 37°C for 30 minutes. After the incubation, the cells were washed twice with pre-warmed media (DMEM medium (4.5g/L glucose, 2mM L-glutamine) supplemented with Pen-Strep (50U/ml), 100ug/ml Normocin™, and 200ug/ml Zeocin™) and resuspended at 5×10^6 cells/ml. 100µl of calcein labeled cell suspension was added to each alginate hydrogel containing well in 96 well plate. The plate was incubated at 37°C and 5% CO_2. At each time point (4, 8, 12, and 24 hours), non-adherent cells were removed by careful washing with media. After the final wash, 1X PBS was added, and fluorescence was measured using TECAN Infinite M200 (absorbance 494nm and emission 517nm). The percentage of adhesion was determined by dividing the corrected (background subtracted) fluorescence of adhered cells by the total corrected fluorescence of cells (no alginate, no washing steps).

5. Cell staining and immunofluorescence imaging

RAW-Blue™ cells plated on the alginate hydrogels were incubated overnight at 37°C with 5% CO_2. After the overnight incubation, the cells were washed with 1X PBS three times and fixed in 4% paraformaldehyde (Sigma Aldrich, MO, USA) for 15 minutes. Fixed cells were washed three times again with 1X PBS. Cells were stained with DAPI (Life Technologies, NY, USA) and 1:1000 diluted Wheat Germ Agglutinin Alexa Fluor® 594 Conjugate (Life Technologies, NY, USA) for 15 minutes. After the staining, the samples were again washed three times with 1X PBS, and were stored in 50% glycerol (Sigma

Aldrich, MO, USA) for confocal imaging. Zeiss LSM700 system with ZEN microscope software was used to image the samples.

C. Elimination of direct cell-to-material contact

1. Adherent vs. non-adherent cells

All cell lines were obtained from InvivoGen (San Diego, USA). Adherent RAW-Blue™ cells were cultured as stated above. THP1-XBlue™-MD2-CD14 is non-adherent and is derived from the human monocytic THP-1 cell line. Like RAW-Blue™ cells, THP1-XBlue™-MD2-CD14 also expresses many PRRs. Both RAW-Blue™ and THP1-XBlue™-MD2-CD14 are stably transfected with a secreted embryonic alkaline phosphatase (SEAP) reporter gene inducible by NF-kB and AP-1 transcription factors. THP1-XBlue™-MD2-CD14 cells also stably express CD14 and MD2. THP1-XBlue™-MD2-CD14 cells were cultured in RPMI 1640 medium (2mM L-glutamine, 1.5g/L sodium bicarbonate, 4.5g/L glucose, 10mM HEPES, 1.0mM sodium pyruvate) supplemented with 10% heat inactivated fetal bovine serum, Pen-Strep (50U/ml), 100ug/ml Normocin™, 200ug/ml Zeocin™, and 250ug/ml of G418. Because THP1-XBlue™-MD2-CD14 is non-adherent, this cell line was further tested with free alginate molecules. To test THP1-XBlue™-MD2-CD14 with free alginate molecules, 20µl of each alginate, dissolved as stated above, was added to 180µl of the suspended cells in each well of 96 well plate and incubated overnight at 37°C 5% CO_2. RPMI 1640 medium (2mM L-glutamine, 1.5g/L sodium bicarbonate, 4.5g/L glucose, 10mM HEPES, 1.0mM sodium pyruvate) supplemented with 10% heat inactivated fetal bovine serum, Pen-Strep (50U/ml), 100ug/ml Normocin™, 200ug/ml Zeocin™, and 250ug/ml of G418 was used as a negative control for THP1-

XBlue™-MD2-CD14 cells. DMEM medium (4.5g/L glucose, 2mM L-glutamine) supplemented with 10% heat inactivated fetal bovine serum, Pen-Strep (50U/ml), 100ug/ml Normocin™, and 200ug/ml Zeocin™ was used as a negative control for RAW-Blue™ cells.

2. Elimination of cell-to-material contact with Transwell®

Tissue culture treated, sterile Corning® HTS Transwell® 96-well and permeable support with 3.0 μm pore polycarbonate membrane were used to create a barrier between the cells and alginate hydrogels (**Figure 2a**). Alginate hydrogels were synthesized in the receiver plate as described above. RAW-Blue™ cells were seeded on the Transwell® insert with the polycarbonate permeable membrane, and incubated overnight in 37°C and 5% CO_2. 50μl of cell culture supernatant from each plate well was transferred to a new 96 well plate, and 200μl of QUANTI-Blue™ was added to each well. This mixture was then incubated at 37°C for 2 hours, and SEAP activity was measured at 655 nm on TECAN Infinite M200.

3. Elimination of cell-to-material contact with PEG hydrogels

To create a barrier between the alginate hydrogels and cells, poly(ethylene glycol) (PEG) hydrogels were synthesized on top of the alginate hydrogels using a protocol described in Pritchard et al., 2011 (**Figure 2b**). Briefly, activated basic alumina flashed ethoxylated trimethylolpropane tri(3-mercaptopropionate) (ETTMP) (MW 1300 g/mol) and poly(ethylene glycol) diacrylate (PEGDA) (MW 575 g/mol) oligomers were solubilized independently in 1X PBS and then filtered using a 0.2 μm Acrodisc Supor syringe filter (Pall) under sterile conditions. To initiate gelation the individual hydrogel

precursor solutions were combined together in stoichiometric equivalency. 40 µl of mixed hydrogel solution were aliquoted into individual cell culture wells or on top of preformed alginate hydrogels and allowed to cure for 20 minutes. All PEG hydrogels were incubated with PBS overnight at 37°C and washed multiple times with media prior to cell seeding to remove any unreacted polymer sol fraction.

D. NF-κB activation of specific Toll-like receptors

1. HEK-Blue™ TLR Cell lines

To identify specific PRR receptors, human TLR specific HEK-Blue™ cell lines (InvivoGen, San Diego, USA) were used. Following HEK-Blue™ cell lines were used: HEK-Blue™ hTLR2, HEK-Blue™ hTLR4, HEK-Blue™ hTLR5, HEK-Blue™ hTLR7, HEK-Blue™ hTLR8, and HEK-Blue™ hTLR9. These HEK-Blue™ cells are derived from human embryonic kidney (HEK) 293 cells.

HEK-Blue™ hTLR2 is co-transfected with the SEAP reporter under the control of IFN-β minimal promoter fused to five NF-κB and AP-1 binding sites and the CD14 co-receptor gene. HEK-Blue™ hTLR2 was cultured in DMDM medium (4.5g/L glucose, 2mM L-glutamine) supplemented with 10% heat inactivated fetal bovine serum, Pen-Strep (50U/ml), 100ug/ml Normocin™, and 1X HEK Blue Selection™.

HEK-Blue™ hTLR4 is co-transfected with the SEAP reporter under the control of IL-12 p40 minimal promoter fused to five NF-κB and AP-1 binding sites and the MD-2/CD14 co-receptor genes. HEK-Blue™ hTLR4 was cultured in DMDM medium (4.5g/L glucose, 2mM L-glutamine) supplemented with 10% heat inactivated fetal bovine serum, Pen-Strep (50U/ml), 100ug/ml Normocin™, and 1X HEK Blue Selection™.

HEK-Blue™ hTLR5 is co-transfected with the SEAP reporter under the control of an NFκ-B and AP-1 inducible promoter. HEK-Blue™ hTLR5 was cultured in DMDM medium (4.5g/L glucose, 2mM L-glutamine) supplemented with 10% heat inactivated fetal bovine serum, Pen-Strep (50U/ml), 100ug/ml Normocin™, 30μg/ml Blasticidin, 100μg/ml Zeocin™.

HEK-Blue™ hTLR7 is co-transfected with the SEAP reporter under the control of the IFN-β minimal promoter fused to five NF-κB and AP-1 binding sites. HEK-Blue™ hTLR7 was cultured in DMDM medium (4.5g/L glucose, 2mM L-glutamine) supplemented with 10% heat inactivated fetal bovine serum, Pen-Strep (50U/ml), 100ug/ml Normocin™, 10μg/ml Blasticidin, 100μg/ml Zeocin™.

HEK-Blue™ hTLR8 is co-transfected with the SEAP reporter under the control of the IFN-β minimal promoter fused to five NF-κB and AP-1 binding sites. HEK-Blue™ hTLR7 was cultured in DMDM medium (4.5g/L glucose, 2mM L-glutamine) supplemented with 10% heat inactivated fetal bovine serum, Pen-Strep (50U/ml), 100ug/ml Normocin™, 30μg/ml Blasticidin, 100μg/ml Zeocin™.

HEK-Blue™ hTLR9 is co-transfected with the SEAP reporter under the control of the IFN-β minimal promoter fused to five NF-κB and AP-1 binding sites. HEK-Blue™ hTLR7 was cultured in DMDM medium (4.5g/L glucose, 2mM L-glutamine) supplemented with 10% heat inactivated fetal bovine serum, Pen-Strep (50U/ml), 100ug/ml Normocin™, 10μg/ml Blasticidin, 100μg/ml Zeocin™.

2. *Screening of specific PRRs with TLR specific HEK-Blue™ cell lines*

In order to investigate whether specific PRRs get activated by alginate, HEK-Blue™ cell lines (InvivoGen, San Diego, USA) expressing a specific TLR were used. Each HEK-Blue™ cells were cultured in DMEM medium (4.5g/L glucose, 2mM L-glutamine) supplemented with 10% heat inactivated fetal bovine serum, Pen-Strep (50U/ml), 100ug/ml Normocin™, and with appropriate selective antibiotics for each cell line. HEK-Blue™ hTLR2 was plated at ~280,000 cells/ml, and Pam3CSK4 (100ng/ml) was used as a positive control. HEK-Blue™ hTLR4 was plated at ~140,000 cells/ml, and LPS-EK Ultrapure (5μg/ml) was used as a positive control. HEK-Blue™ hTLR5 was plated at ~140,000 cells/ml, and FLA-ST Ultrapure (100ng/ml) was used as a positive control. HEK-Blue™ hTLR7 was plated at ~220,000 cells/ml, and R848 (100ng/ml) was used as a positive control. HEK-Blue™ hTLR8 was plated at ~220,000 cells/ml, and R848 (100ng/ml) was used as a positive control. HEK-Blue™ hTLR9 was plated at ~450,000 cells/ml, and ODN 2006 (5μM) was used as a positive control. As a negative control, DMEM medium (4.5g/L glucose, 2mM L-glutamine) supplemented with 10% heat inactivated fetal bovine serum, Pen-Strep (50U/ml), 100ug/ml Normocin™, and appropriate selective antibiotics was used in each cell line. Each cell line was plated into the individual wells of Corning® Costar® Ultra-Low attachment 96-well plate containing alginate hydrogels, and incubated overnight at 37°C 5% CO_2 to allow PRRs to be activated by alginate hydrogels. The SEAP level was monitored using QUANTI-Blue™ detection medium as stated above.

III. Results

A. Establishment of the PRR activation assays

1. Quanti-Blue™ negative control test

Presence of alkaline phosphatase in FBS can interfere with alkaline phosphatase quantification. Therefore, we tested DMEM medium (4.5g/L glucose, 2mM L-glutamine) supplemented with 10% heat inactivated fetal bovine serum, Pen-Strep (50U/ml), 100ug/ml Normocin™, and 200ug/ml Zeocin™ for the alkaline phosphatase activity. Absorbance at 655nm was measured at 2 hour and 24 hour incubation at 37°C. The measurement was then compared between blank media (50µl) plus QUANTI-Blue™ reagent (150µl) and QUANTI-Blue™ reagent (200µl) alone. As seen in **Figure 3**, very low level of SEAP activity was observed in the blank media compared to QUANTI-Blue™ reagent alone (p-value < 0.05) at 2-hour incubation. This is likely due to the fact that even though the fetal bovine serum used in this study was heat-inactivated, there may be small amount of residual alkaline phosphatase. The 24-hour incubation of the blank media showed slightly increased SEAP activity (p-value < 0.001). Based on this observation, we set the absorbance 655nm value of 0.05 as the threshold value of the negative control for the PRR activation assays.

2. Optimal agonist concentration

RAW-Blue™ cells express many pattern recognition receptors (PRRs), including all toll-like receptors (TLRs), except TLR5, and are stably transfected with a secreted embryonic alkaline phosphatase (SEAP) reporter gene inducible by NF-κB and AP-1 transcription factors. Each PRR has different agonists, so we tested various agonists at

different concentrations to determine optimal concentration for each agonist. As seen in **Figure 4**, some of the agonists, such as ODN 1826 and ORN Sa19, activate PRRs more strongly than others. Optimal concentration for each agonist was determined based on this data: TLR1/2 (Pam3CSK4, 100ng/ml), TLR3 (Poly(I:C), 5μg/ml,), TLR4 (LPS-EK, 5μg/ml), TLR5 (FLA-ST, 100ng/ml), TLR7 (Gardiquimod™ VacciGrade™, 10μg/ml), TLR7/8 (ssRNA40/LyoVec™, 5μg/ml), TLR7/8 (R848, 100ng/ml), TLR9 (ODN 1826, 1μM), TLR13 (ORN Sa19, 500ng/ml), NOD1 (Tri-DAP, 10μg/ml), and NOD2 (L18-MDP, 50ng/ml).

B. Optimization of the immunostimulation assays with alginates

1. Kinetic studies of PRR activation

In order to determine the optimal number of RAW-Blue™ cells and incubation time with QUANTI-Blue™ for PRR assay, we investigated kinetic profiles of QUANTI-Blue™ with different cell numbers and incubation times. RAW-Blue™ cells were plated at 100,000 cells/well, 200,000 cells/well, and 500,000 cells/well and treated with various PRR agonists. After 24 hours and 48 hours treatment with agonists, cell culture media of the agonist treat cells were incubated with QUANTI-Blue™ reagents, and absorbance at 655nm was measured at every 2 hours interval for 24 hours. Absorbance values were normalized with values of the untreated cell controls (**Figure 5**). QUANTI-Blue™ substrate degrades even in the absence of alkaline phosphatase once dissolved in water. Therefore, we expected the fold activation would be the highest at 2 hours time point and decrease thereafter – as seen in the **Figure 5d, 5e, 5f**. RAW-Blue™ cells incubated with agonists for 24 hours at 100,000 cells/well (**Figure 5a**) exhibited Michaelis-Menten

kinetics, and as the cell number is increased to 200,000 cells/well (**Figure 5b**), Michaelis-Menten kinetics characteristics is somewhat diminished. This is likely due to the increased secretion of SEAP in the media. Based on this kinetics data, we expected the optimal parameters for the PRR activation assay to be either 200,000 cells/well for 24-hour incubation or 100,000 cells/well for 48-hour incubation.

2. Controlling gelation kinetics

When making the alginate hydrogels in the 96 well plates, cross-linking of alginate with barium happens instantaneously, and therefore this uncontrolled gelation produces rough hydrogel surface topology. **Figure 6a** schematically illustrates how cell-seeding behaviors differ in flat vs. rough alginate hydrogel surfaces. As expected, when cells are seeded on a rough hydrogel surface, cells tend to settle in valleys of the surface (**Figure 6c, 6d**). Immunofluorescence staining of these cells (**Figure 6e, 6h**) shows clumping of cells.

Smooth surface alginate hydrogels were made by controlling gelation kinetics. Alginate hydrogels were molded into the 24 well plate with sterile Scaffdex CellCrown™ 24 well plate insert with 8μm PET filter (**Figure 6b**). These insert allowed slow diffusion of barium into alginate, producing molded alginate hydrogel surface with the identical surface smoothness as the PET filter. **Figure 6f** and **Figure 6g** shows cells seeded on these flat surface hydrogels.

When alginate hydrogels are made in the 96 well plate format without controlling the gelation kinetics, resulting hydrogel surfaces cause data variability, making it difficult to reproduce immunostimulation assay data. This is likely due to fact that the

cell seeding behavior is influenced by the surface topography which in turn affects the numbers of cells that come in contact with the alginate hydrogel. In order to determine whether smooth surface eliminates this data variability, immunostimulation assays on smooth surface hydrogels were performed with RAW-Blue™ cells. The cells were seeded on alginate hydrogels in the ultra-low attachment 24 well plate and incubated overnight in 37°C and 5% CO_2. 50µl of cell culture supernatant from each plate well was transferred to a new 96 well plate, and 200µl of QUANTI-Blue™ was added to each well. This mixture was then incubated at 37°C for 2 hours, and SEAP activity was measured at 655 nm on TECAN Infinite M200 (**Figure 7a**). Since decreased SEAP secretion can be either due to the lack of PRR activation or cell death, cell viability assays were performed parallel to all alginate PRR stimulation assays. Cell viability was determined using CellTiter-Glo® Luminescent Cell Viability Assay (Promega, Madison, WI, USA) (**Figure 7b**). The number of viable cells was calculated using a standard curve for each alginate, and the raw absorbance 655nm values were normalized with the number of viable cells (**Figure 7c**). We observed that UPVLVG and UPVLVG/SLG100 blend cause higher PRR activation compared to all other alginates we tested. SLG100 also causes PRR activation, though not as high as UPVLVG. PRR activation observed in SLG100 and UPVLVG are both statistically significant ($p < 0.001$). With smooth surface alginate hydrogels, it was possible to reliably reproduce this PRR activation data.

3. Cell adhesion assay

In order to understand how cell adhesion affects PRR activation, we investigated how many cells are adhering to the alginate hydrogels using Vybrant™ Cell Adhesion

Assay Kit (Molecular Probes, NY, USA). RAW-Blue™ cells were stained with calcein acetoxymethyl ester (calcein AM, 5μM), which is non-fluorescent but produces fluorescence once loaded into the cells when it is cleaved by endogenous esterases to produce highly fluorescent calcein, and incubated at 37°C for 30 minutes in DMEM medium (4.5g/L glucose, 2mM L-glutamine) supplemented with Pen-Strep (50U/ml), 100ug/ml Normocin™, and 200ug/ml Zeocin™. As shown in **Figure 8**, most of the cells are adhered after 8-hour incubation. Alginate hydrogels were made in ultra low adhesion plate, and as seen in the no alginate control, cells barely adhere to the plate itself, and therefore, any resulting fluorescence are from the cells adhered to the alginate hydrogels, not the plate.

At each time point of the adhesion assay, SEAP activity was quantified in parallel in order to investigate at which time point, we can obtain the optimal PRR activation profiles of alginate hydrogels. As shown in **Figure 9a**, PRR activation profile is not established just yet at 4-hour and 8-hour incubation with the alginate hydrogels. This is likely due to the fact that NF-κB and AP-1 are not able to fully induce the SEAP reporter gene expression just yet. At 12-hour incubation, PRR activation profile takes more definitive pattern. LPS-EK positive control gives a strong NF-κB activation, and the strongest PRR activation is observed with UPVLVG. At 24-hour incubation, the background noise increases, and therefore it no longer gives a distinctive PRR activation profile. This is likely caused by two factors. First, the QUANTI-Blue™ substrate breaks down with time regardless of the presence of alkaline phosphatase. Secondly, RAW-Blue™ cells doubles approximately every 12 hours, and thus after 24 hours of incubation,

the cell number likely becomes too high, causing stress-induced NF-κB activation (Baldwin, 1996). **Figure 9b** shows the PRR activation profile at 12-hour statistical significance.

4. Alginate hydrogel formats: flat vs. microcapsules

In cell replacement therapy, cells are generally encapsulated in microcapsules. Our purpose here is to study the PRR activation against alginate hydrogels *in vitro*. We investigated whether the surface format (microcapsules vs. flat) matters in terms of studying PRR activation *in vitro*. Alginate microcapsules were formulated as described above. Capsules were washed with HEPES buffer (NaCl 15.428g, KCl 0.70g, $MgCl_2 \cdot 6H_2O$ 0.488g, 50 mL of HEPES (1M) buffer solution (Gibco, Life Technologies, California, USA) in 2L of DiH2O) 4 times, and with media 3 times. 100μl volume of each capsules were placed in ultra low adhesion 96 well plate, and approximately 100,000 cells of RAW-Blue™ were seeded in each well. The plate was incubated overnight in 37°C and 5% CO_2. 50μl of cell culture supernatant from each plate well was transferred to a new 96 well plate, and 200μl of QUANTI-Blue™ was added to each well. This mixture was then incubated at 37°C for 2 hours, and SEAP activity was measured at 655 nm on TECAN Infinite M200.

Figure 10a shows light microscopy images of alginate microcapsules seeded with RAW-Blue™ cells in the 96 well plates. Because capsules floats and moves around in the media, cell-seeding behaviors is far less predictable than any other alginate hydrogel format for *in vitro* experiments. Dark spots in the image indicate cells adhered to the microcapsule surface. As shown, the amount of cells adhered to the capsules vary

significantly from one alginate to the other alginate. Therefore, it was expected that the PRR activation data from the capsules would not be in agreement with the PRR activation data from the flat alginate hydrogels. This turned out to be true, as seen in **Figure 10b**. PRR activation was observed only with SLG20 alginate ($p < 0.05$). PRR activation in all other alginates was statistically not significant ($p > 0.05$).

C. Immunostimulatory capacity of alginates

1. Alginate selection

Alginate tested in this experiments are SLG20, SLG100, UPVLVG, blend of UPVLVG and SLG100, SLM20, SLM100, UP LVM, UP VLVM, UP MVM, and UP MVG. SLG20 and SLG100 are made from alginate where over 60% of the monomer units are guluronate. The molecular weight for SLG20 is in the 75,000 – 220,000 g/mol range, and the molecular weight for SLG100 is in the 200,000 – 300,000 g/mol range. SLM20 and SLM100 are made from alginate where over 50% of the monomer units are mannuronate. The molecular weight for SLM20 is in the 75,000 – 220,000 g/ml range, and the molecular weight for SLM100 is in the 200,000 – 300,000 g/mol range. SLG20, SLG100, SLM20, are SLM100 are all highly purified, sterile, and well characterized sodium alginates. UPVLVG is a very low viscosity (<20 mPas) sodium alginate where minimum 60% of the monomer units are guluronate. UP LVM is a low viscosity (20-200mPas) sodium alginate where minimum 50% of the monomer units are mannuronate. UP VLVM is a very low viscosity (<20 mPas) sodium alginate where minimum 50% of the monomer units are mannuronate. UP MVM is a medium viscosity (>200 mPas) sodium alginate where minimum 50% of the monomer units are

mannuronate. UP MVG is also a medium viscosity (>200 mPas) sodium alginate where minimum 60% of the monomer units are guluronate. Of all the alginates tested, UPVLVG seemed to induce the strongest PRR activation, as seen in the **Figure 7a** and **Figure 9b**.

2. Adherent cells (RAW-Blue™) vs. non-adherent cells (THP1-XBlue™-MD2-CD14)

To investigate immunostimulation capacity of alginates, we incubated alginate hydrogels with RAW-Blue™ and THP1-XBlue™-MD2-CD14 cells. Both of these cell lines express many pattern recognition receptors (PRRs), and activation of PRRs in these cell lines leads to expression of secreted embryonic alkaline phosphatase (SEAP) reporter gene, which gets secreted out to the media. Production of SEAP can then be quantified by using QUANTI-Blue™, a detection and quantification medium of alkaline phosphatase. The cells were seeded on alginate hydrogels in the ultra-low attachment 96 well plate and incubated overnight in 37°C and 5% CO_2. 50µl of cell culture supernatant from each plate well was transferred to a new 96 well plate, and 200µl of QUANTI-Blue™ was added to each well. This mixture was then incubated at 37°C for 2 hours, and SEAP activity was measured at 655 nm on TECAN Infinite M200.

First, we tested the immunostimulatory capacity of alginate hydrogels with adhering RAW-Blue™ cells. As shown in **Figure 11a**, we found a profound increase of PRR activation in alginates UPVLVG and UPVLVG/SLG100 blend (p-value < 0.001). Thought not as intense as UPVLVG, SLG100 showed statistically significant PRR activation (p-value < 0.001). Next, we tested immunostimulatory capacity of alginate hydrogels with non-adhering THP1-XBlue™-MD2-CD14 cells. Unlike adhering RAW-Blue™ cells, we did not observe significant PRR activation against alginate hydrogels

(**Figure 11b**). UPVLVG displayed highest SEAP output, but this value is not statistically significant. Since THP1-XBlue™-MD2-CD14 cells are non-adhering cells, we also tested immunostimulatory capacity with free alginate solution. Free alginate solutions are not cross-linked with barium. With free alginate solution, statistically significant PRR activation is observed with LF10/60 and crude alginate (**Figure 11b**) (p-value < 0.001). When a solution of barium is added to alginate solution, the crosslinking of alginate takes place immediately, entrapping impurities present in the solution in the 3D network of highly hydrated gel. Without this cross-linking, any impurity present in the alginate solution are now free to activate PRR. Therefore, the PRR activation observed in LF10/60 and crude alginate indicates presence of endotoxin. However, no PRR activation was observed in ultrapure, clean alginates SLG20, SLG100 and UPVLVG. Based on these observations, we hypothesized that PRR activation is initiated by the cell adhesion to the materials. This hypothesis was supported in the Transwell and PEG hydrogel experiments below.

D. Effect of eliminating of direct cell-to-material contact

1. Transwell® system

Rough alginate hydrogel surface leads to uneven cell adhesion to the materials, and this seems to affect the level of PRR activation. Also, as seen in **Figure 11**, adhering RAW-Blue™ and non-adhering THP1-XBlue™-MD2-CD14 cells displayed different immunostimulatory capacity. With RAW-Blue™ cells, PRR activations against alginate hydrogels were statistically significant. However, statistically significant PRR activation was not observed with THP1-XBlue™-MD2-CD14 cells against both hydrogels and free

solutions with an exception of LF10/60 and crude alginate solution. This activation is likely due to the impurities present in the alginates, not the alginate itself.

Based on these observations, we investigated whether the direct cell-to-the material contact is required in order for the cells to activate PRR response against the alginate hydrogels. First approach to eliminate the direct cell to material contact was to utilize sterile Corning® HTS Transwell® 96 well permeable support with 3.0μm pore polycarbonate membrane to create a barrier between the cells and the alginate hydrogels. Alginate hydrogels were synthesized in the receiver plate, and the RAW-Blue™ cells were seeded on the Transwell insert with permeable membrane (**Figure 2a**). The resulting PRR activations were then compared to the PRR activations observed in RAW-Blue™ cells plated directly on top of the alginate hydrogels (**Figure 12**). In contrast to non-transwell samples, no statistically significant PRR activation was observed in SLG20, SLG100 and UPVLVG. Statistically significant PRR activation is observed in transwell samples for LF10/60 and crude alginates. As seen with THP1-XBlue™-MD2-CD14 cells in **Figure 11**, this is likely due to the presence of impurities in the alginate, not due to the alginate itself.

2. Poly(ethylene glycol) hydrogels

Second approach to eliminate direct cell to the alginate hydrogel contact was to create a barrier with poly(ethylene glycol) (PEG) by curing PEG hydrogels on top of the alginate hydrogels (**Figure 2b**). PEG is known to repel protein and cell adhesion. We utilized this characteristic of PEG to eliminate direct cell-to-material contact on the alginate hydrogels. PEG hydrogels were cured on top of alginate hydrogels for 20

minutes. After curing, PEG hydrogels were incubated with 1X PBS overnight at 37°C and washed multiple times with 1X PBS and media to remove any unreacted polymer sol fraction. RAW-Blue™ cells were seeded on the PEG topped alginate hydrogels in the ultra-low attachment 96 well plate and incubated overnight in 37°C and 5% CO_2. 50µl of cell culture supernatant from each plate well was transferred to a new 96 well plate, and 200µl of QUANTI-Blue™ was added to each well. This mixture was then incubated at 37°C for 2 hours, and SEAP activity was measured at 655 nm on TECAN Infinite M200. As seen in **Figure 13a**, PEG hydrogel alone is not immunogenic (p-value > 0.05). Some PRR activations were observed when cells were plated directly on top of the SLG100 and UPVLVG hydrogels as previously observed. High PRR activation with LF10/60 and crude alginates are expected since these are not clean alginates. When PEG hydrogels are added on top of alginate hydrogels, PRR activation is abolished in all samples even in LF10/60 and crude alginates (**Figure 13a**). In order to ensure that PEG is not causing cell death, leading to abolished PRR activation, cell viability assays were performed parallel to all alginate PRR stimulation assays. Cell viability was determined using CellTiter 96® AQ_{ueous} One Solution Cell Proliferation Assay (Promega, Madison, WI, USA). The number of viable cells was calculated using a standard curve for each sample, and the raw absorbance 655nm values of PRR assays were normalized with the number of viable cells (**Figure 13b**).

E. NF-κB activation of specific toll-like receptors

Pattern recognition receptors (PRRs) activation observed with RAW-Blue™ and THP1-XBlue™-MD2-CD14 cells can be combinatorial effect of multiple PRRs since these

cells express many PRRs. In order to identify which specific PRRs are likely activated against different alginates, particularly VLVG, we used reporter cell lines that express specific Toll-like receptors. Human TLR specific HEK-Blue™ cell lines, derived from human embryonic kidney (HEK) 293, expressing TLR2, TLR4, TLR5, TLR7, TLR8, TLR9, all of which are MyD88 dependent, were tested. Of these TLRs, TLR2, TLR4, TLR5 are located on the cell surface, and TLR7, TLR8, TLR9 are endosomal (**Figure 15**)

Given the fact that VLVG activates PRRs most strongly, we have tested immunostimulatory capacity of VLVG with human TLR specific HEK-Blue™ cell lines. **Figure 14** shows the absorbance at 650nm from QUANTI-Blue™ colorimetric assays. Of the TLRs tested, observed SEAP output values of TLR4, TLR7, TLR8, TLR9 were statistically significant ($p < 0.001$). Interestingly, contrary to strong PRR activation in RAW-Blue™ cells with VLVG, VLVG does not seem to activate TLR2 (**Figure 14a**), but activates TLR5, though weak (**Figure 14b**). As expected, both TLR2 and TLR5 are activated strongly with LF10/60, which indicates that LF10/60 impurities include TLR2 and TLR5 agonists. TLR4, TLR7, TLR8, and TLR9 are just strongly activated with VLVG as they are with LF10/60 (**Figure 14c-f**).

IV. Discussion

Microencapsulation of cells has a great therapeutic potential to treat various diseases, such as diabetes, kidney and liver failure, that require a cell replacement therapy (Aebischer et al., 1994; Chang et al., 1993; Lim and Sun, 1980; Liu et al., 1993). Even though immunoisolation technology in principal provides a protective barrier of implanted cells from the host immune system attack, long-term usage of these therapies, however, is currently hampered due to insufficient understanding of how immune system circumvents successful integration of encapsulated cells. Despite the important advances made with encapsulation technology and successful demonstration of principle applicability of such system, there exists a major hurdle that has to be overcome. Graft survival of encapsulated cells was never permanent and, the longevity of the graft survival varied significantly from case to case (Calafiore et al., 2006; Jacobs-Tulleneers-Thevissen et al., 2013; Omer et al., 2003b). It has been suggested that this variation is due to the difference of tissue responses against the materials. However, despite decades of research, it still is not clear what is responsible for this difference.

A. Present understanding of alginate-induced inflammation

Currently there are two mainstream theories of how macrophages are activated against alginate (**Figure 16**). First theory is that impurities present in alginate are responsible for the inflammation, which leads to variable success of the capsule implantation. Commercially available alginates are generally extracted from brown algae (*Phaeophyeae*), and many have speculated that there are residual impurities from the algae and various contaminants. Several studies have demonstrated that further purification of the alginate

reduces inflammation responses, yet none were able to identify and measure the impurities present in alginate. A study claimed that TLR2, 5, 8, 9 ligands are present in alginate, though they were not able to detect the ligands of TLR 8 and 9, and these impurities are responsible for triggering inflammation against alginate (Paredes-Juarez et al., 2013). Second theory is that alginate itself can directly activate macrophages, which then leads to activation of innate immunity. Many studies have shown that various biomaterials activate the innate immune mechanism that eventually leads to chronic inflammation and fibrosis of implanted biomaterials (Franz et al., 2011). In 2002, Flo et al. published a study demonstrating that TLR2 and TLR4 are involved in immune cell activation against alginate mannuronic acid polymers (Flo et al., 2002). Yang and Jones demonstrated that macrophages get activated against alginate through the NF-κB pathway, subsequently producing proinflammatory cytokines such as IL-1β, IL-6, IL-12 and TNF-α (Yang and Jones, 2009). Subsequently, Auquit-Auckbur et al. showed that TLR4 plays an important role in the foreign body response against silicone prosthesis (Auquit-Auckbur et al., 2011). Moreover, by inhibiting MyD88 pathway, Pearl et al. demonstrated that TLRs are involved in the foreign body response against orthopedic implant wear-debris particles (Pearl et al., 2011). All these studies suggest alginate somehow activates pathogen recognition receptors (PRRs), which in turn activates innate immune system against alginate. However, these studies are plagued by uncertainty of alginate purity, and whether pure alginate can truly activate macrophage has never been tested.

B. Activation of macrophages

To gain a better understanding of whether impurities present in alginate or alginate itself are responsible for innate immune system activation, we designed an *in vitro* system to study the activation of pattern recognition receptors (PRRs) against commercially available clean and dirty alginates. Of alginates we chose to study, SLG20, SLG100, SLM20, and SLM100 are ultrapure and sterile. UPVLVG, UPVLVM, UPLVM, UPMVM, and UPMVG are ultrapure but not sterilized. All of ultrapure alginates are endotoxin tested and are certified to have endotoxin level less than 100EU/g. One Endotoxin Unit (EU) is equivalent to approximately 0.1 to 0.2 ng of endotoxin/ml. As impure alginate controls, we used pharmaceutical grade alginate LF10/60 and unpurified crude sodium alginate. Typically, for *in vivo* application studies, cells are entrapped in alginate spherical microcapsules, but the use of spherical microcapsules for *in vitro* studies presents challenges that are not present *in vivo* studies. **Figure 10a** shows inconsistent cell adherence to alginate microcapsules due to three-dimensional spatial movement of the capsules, and immunostimulatory capacity of the capsules are shown in **Figure 10a**, which are not in agreement with results obtained from two-dimensional flat hydrogels. Therefore, for *in vitro* studies, we utilized flat alginate hydrogels so that cells can be plated directly on top with minimal three-dimensional spatial movement.

In order to investigate whether pattern specific receptors (PRRs) are activated against alginates we selected to study, we utilized several different cell lines. RAW-Blue™ and THP1-XBlue™-MD2-CD14 cells express many PRRs. They both are stably transfected with a secreted embryonic alkaline phosphatase (SEAP) reporter gene inducible by NF-κB and AP-

1 transcription factors. Upon activation of PRRs, signaling cascades lead to expression of nuclear factor-κB (NF-κB) and activator protein-1 (AP-1) (**Figure 17**) (O'Neill et al., 2013). The SEAP reporter gene in RAW-Blue™ and THP1-XBlue™-MD2-CD14 cells is under the control of NF-κB and AP-1 transcription factor, and therefore upon activation of PRRs, SEAP is secreted out to the cell culture supernatant, allowing us to quantify PRR activation by the use of QUANTI-Blue™ reagent, a colorimetric enzyme assay developed to determine alkaline phosphatase activity in a biological sample (**Figure 1, 17**). We have performed preliminary experiments to test and optimize the assay conditions and different experimental parameters, such as incubation time with alginates and subsequently with QUANTI-Blue™ reagent, and use of proper positive and negative controls.

We first examined immunostimulatory capacity of alginates with adhering RAW-Blue™ cells. As shown in **Figure 7, 8, 11a**, UPVLVG shows the strongest level of PRR activation. Though not as intense as UPVLVG, SLG20, SLG100, and SLM100 and UPLVM showed PRR activation as well. Given the fact that these alginates are ultrapure, observed PRR activations are likely due to the alginate itself, not any impurity. Next, we investigated immunostimulatory capacity of alginates with non-adhering THP1-XBlue™-MD2-CD14 cells. Since THP1-XBlue™-MD2-CD14 is non-adhering, we performed the experiment with free non-crosslinked alginate molecules in solution in parallel with the experiment with crosslinked alginate hydrogels. In contrast to RAW-Blue™ cells, as shown in **Figure 11b**, none of the alginates we tested activated PRRs with THP1-XBlueTM-MD2-CD14 cells except dirty alginate controls and free non-crosslinked LF10/60 and Crude alginate molecules. No PRR activation is observed with LF10/60 and Crude alginate hydrogels despite the

impurities present in these alginates. This observation leads us to hypothesize that direct cell-to-material contact is a crucial step in PRR activation.

C. Cell-contact dependent alginate-induced inflammation

To test our cell-to-material contact hypothesis, we investigated whether PRR activation is reduced or eliminated when the direct cell-to-material contact is blocked. We first eliminated cell-to-material contact by utilizing sterile Corning® HTS Transwell® 96 well permeable support with 3.0μm pore polycarbonate membrane. Alginate hydrogels were cross-linked in the receiver plate, and the RAW-Blue™ cells were seeded on the Transwell insert as shown in **Figure 2a**. In this system, the Transwell insert provides a physical barrier between the alginate hydrogels and the cells whilst allowing bi-directional diffusion of water, nutrients, and any biomolecules and impurities present through the polycarbonate membrane of the insert. In contrast to the cells plated directly on top of the alginate hydrogels, PRR activation is abolished except with LF10/60 and Crude alginates (**Figure12**). PRR activation with LF10/60 and Crude alginates are likely due to the impurities present within these alginates. For ultrapure alginates SLG20, SLG100, and UPVLVG, PRR activation is obliterated when the cells cannot directly adhere to the alginate hydrogel.

To validate this observation with this Transwell experiment, we designed another system to eliminate direct cell-to-material contact. Gene therapy delivery vehicles are often coated with poly(ethylene glycol) (PEG) in order to protect them from the host immune system and improve circulatory half-life. It has been suggested that PEG can protect the gene delivery particles from the host immune system by deterring protein and

cell adhesion to the surface (Kreppel and Kochanek, 2008). We utilized this characteristic of PEG to eliminate direct cell contact to the alginate hydrogels. After alginate hydrogel synthesis described above, PEG hydrogels were cured on top of the hydrogel again as described above, effectively creating a barrier between the cells and alginate hydrogels (**Figure 2b**). As seen in **Figure 13**, presence of PEG barrier obliterates PRR activation.

These strategies to create a barrier between the cells and alginate hydrogels allowed us to conclude that cell adhesion to the material is a key step for immune cells to initiate PRR activation in response to alginates. This finding is in line with the finding that no PRR activation is observed with non-adhering THP1-XBlue™-MD2-CD14 cells against alginates.

D. Specific TLRs in alginate-induced inflammation

Since RAW-Blue™ cells express many PRRs, NF-κB activation observed with RAW-Blue™ cells against alginate can be a combinatorial effect of multiple PRRs being activated. We also examined whether we can identify specific PRRs responsible for provoking immune response against alginates. We utilized human TLR specific HEK-Blue™ cell lines for TLR2, TLR4, TLR5, TLR7, TLR8, and TLR9 for their immunostimulatory capacity against alginates. Of these cell lines, HEK-Blue™ TLR4, HEK-Blue™ TLR5, HEK-Blue™ TLR7, and HEK-Blue™ TLR8 cells seemed to activate TLR signaling pathways against UPVLVG alginates (**Figure 14**). Interestingly, TLR2 was not activated against UPVLVG, while TLR5 was activated against UPVLVG (**Figure 14 a, b**). Involvement of TLR4 in poly-M alginate induced inflammation was previously implicated (Flo et al., 2002). However, VLVG alginate is 60% guluronic acids. It is interesting to point out that TLR7, TLR8, and TLR9 are endosomal TLRs, and their involvements in alginate-induced inflammation have yet been

demonstrated in the literature. Here, we conclude that observed TLR2 and TLR5 activation are likely related the impurities present in alginate samples, given the fact that they are much more strongly activated against LF10/60, but not so with VLVG (**Figure 14a, b**). Unlike TLR2 and TLR5, activation of TLR4, 7, 8, 9 against VLVG are just as strong as those against LF10/60, indicating that these TLR activations are likely related to the alginate material itself rather than impurities since VLVG is an ultra pure alginate (**Figure 14c-f**).

As a final note, we used clean, sterile, ultrapure alginates in our studies, and therefore our data here suggest that alginate itself can provoke immune response via PRR activation and the level of PRR activation can vary depends on the alginate material characteristics and compositions. Our data also confirmed that impurities, present in dirty alginate, such as LF10/60, could indeed trigger inflammation response via PRR activation.

V. Conclusions

Despite the fact that many studies confirmed that alginate microcapsules activate innate immune system via pattern recognition receptors (PRRs) (Flo et al., 2002; Paredes-Juarez et al., 2013; Yang and Jones, 2009), which PRRs are involved is, how they recognize alginates, and whether alginate material characteristics and compositions can elicit different responses are not very well understood. With regard to other biomaterials, a number of studies investigated the role of PRRs in response to various biomaterials. Many of these studies indicate the involvement of TLR4 (Auquit-Auckbur et al., 2011; Grandjean-Laquerriere et al., 2007; Pearl et al., 2011). However, the role of different PRRs specifically to alginate has not been extensively studied. Of note, Flo et al. showed that poly-M alginates, produced by the human pathogen *Pseudomonas aeruginosa*, can stimulate TLR2 and TLR4 pathways. They demonstrated that immune response to poly-M was completely obliterated in macrophages isolated from TLR4 knockout mice, while the response was reduced by half in macrophages from TLR2 knockout mice (Flo et al., 2002). Various other studies supported the roles of TLR2 and TLR4 in M-block alginate. However, these studies are plagued by questions of LPS contamination as alginate is produced not only by brown algae but also by bacteria.

Recently, Paredes-Juarez et al. suggested that alginate itself does not induce PRR mediated immune response against alginates and claimed that it is the impurities present in the alginates that can provoke PRR mediated immune responses (Paredes-Juarez et al., 2013). Paredes-Juarez et al. purified the alginates and showed profound reduction in NK-κB activation. They claimed that alginate activates TLR2, TLR5, TLR8, TLR9, but

surprisingly not TLR4, and the activation of these TLRs are due to the pathogen-associated molecular patterns (PAMPs) present in the alginate. However, they were only able to detect the presence of TLR2 and TLR5 ligands, but not TLR8 and TLR9 ligands. It is important to note that the alginates they used are not sterile, ultrapure alginates.

In this study, we designed an *in vitro* system to study the activation of PRRs against several clean, sterile, ultrapure alginates. Using alginates with ultra low level of endotoxin (≤ 0.5EU/ml which is equivalent to ≤ 0.1ng/ml LPS), we showed that some alginates, but not all, can indeed provoke PRR mediated immune responses. We also demonstrated that direct cell-to-material contact plays a key role in initiating PRR mediated immune response. Additionally, by testing alginates of different material characteristics and compositions, we showed that some alginates, such as UPVLVG (G ≥ 60%, viscosity < 20 mPa•s, MW < 75kDa), could induce stronger PRR activation than others, such as SLG20 (G ≥ 60%, viscosity 20-99 mPa•s, MW 75-150kDa) or SLG100 (G ≥ 60%, viscosity 100-300 mPa•s, MW 150-250kDa). Of TLR2, TLR4, TLR5, TLR7, TLR8, TLR9 studied, it seems that UPVLVG likely does not activate TLR2, but activates TLR4, TLR7, TLR8, and TLR9 signaling pathway; however, additional work needs to be done to draw more conclusive results on their roles in provoking PRR mediated immune response against alginates.

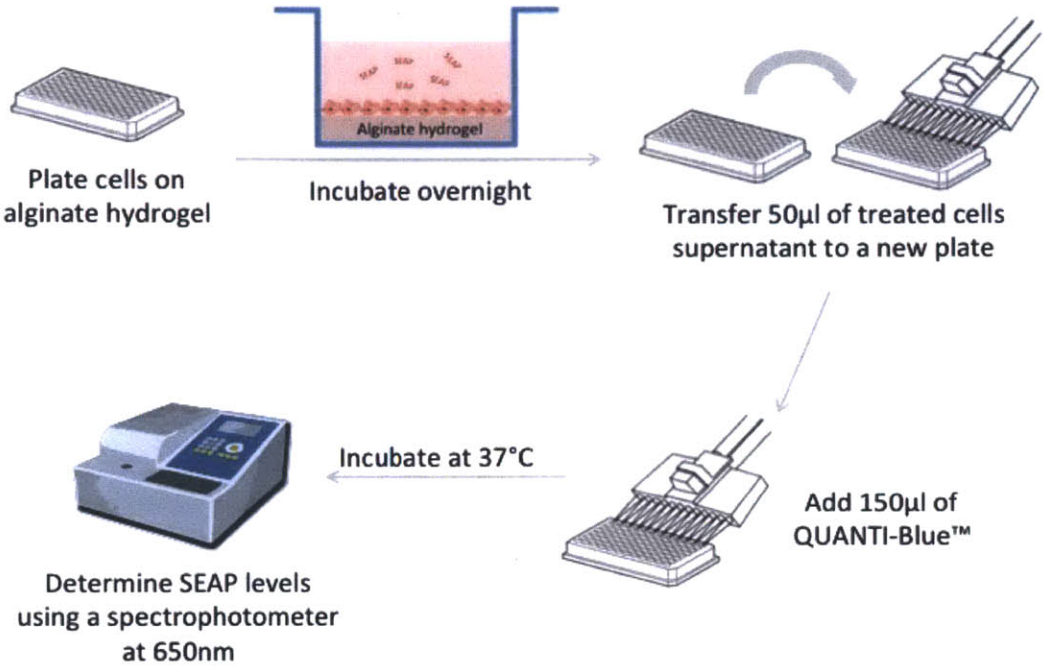

Figure 1. Schematics of colorimetric QUANTI-Blue™ assay. QUANTI-Blue™ assay allows for the detection of NF-κB/AP-1 activation following the activation of pattern recognition receptors (PRRs) by assessing secreted embryonic alkaline phosphatase (SEAP) activity in the cell culture supernatant.

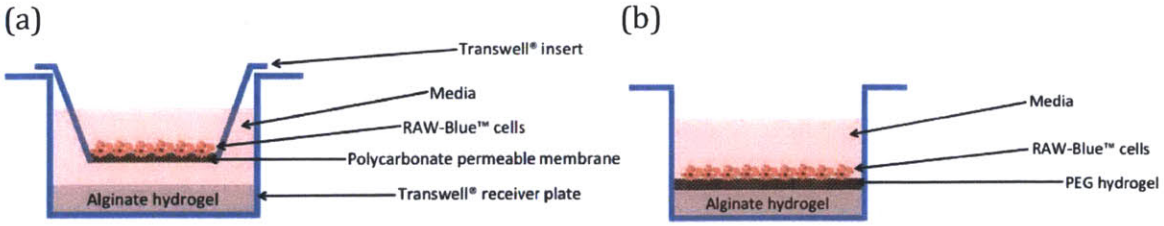

Figure 2. Systems to eliminate direct cell-to-material contact. (a) Corning® HTS Transwell® 96-well with polycarbonate permeable support was used to create a barrier between the cells and alginate. (b) Poly(ethylene glycol) (PEG) hydrogels were synthesized on top of alginate hydrogels to create a barrier between the cells and alginate.

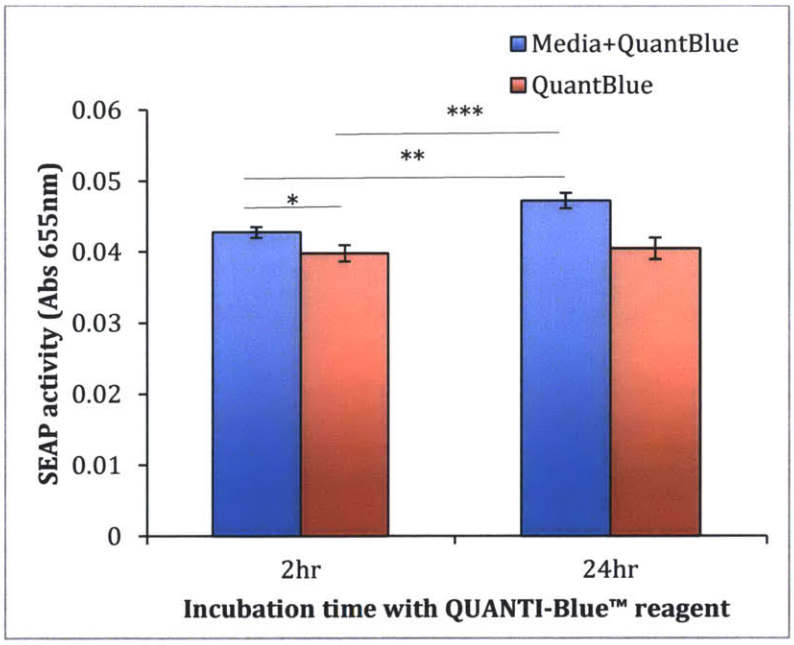

Figure 3. QUANTI-Blue™ negative control test. Media plus QUANTI-Blue™ reagent and QUANTI-Blue™ reagent alone were incubated at 37°C for 2 hours and 24 hours. SEAP level was determined by measuring absorbance at 655nm. Statistical comparison was made with Prism6 one-way ANOVA with Tukey's test. p-value < 0.001 (***), p-value < 0.01 (**), p-value < 0.05 (*).

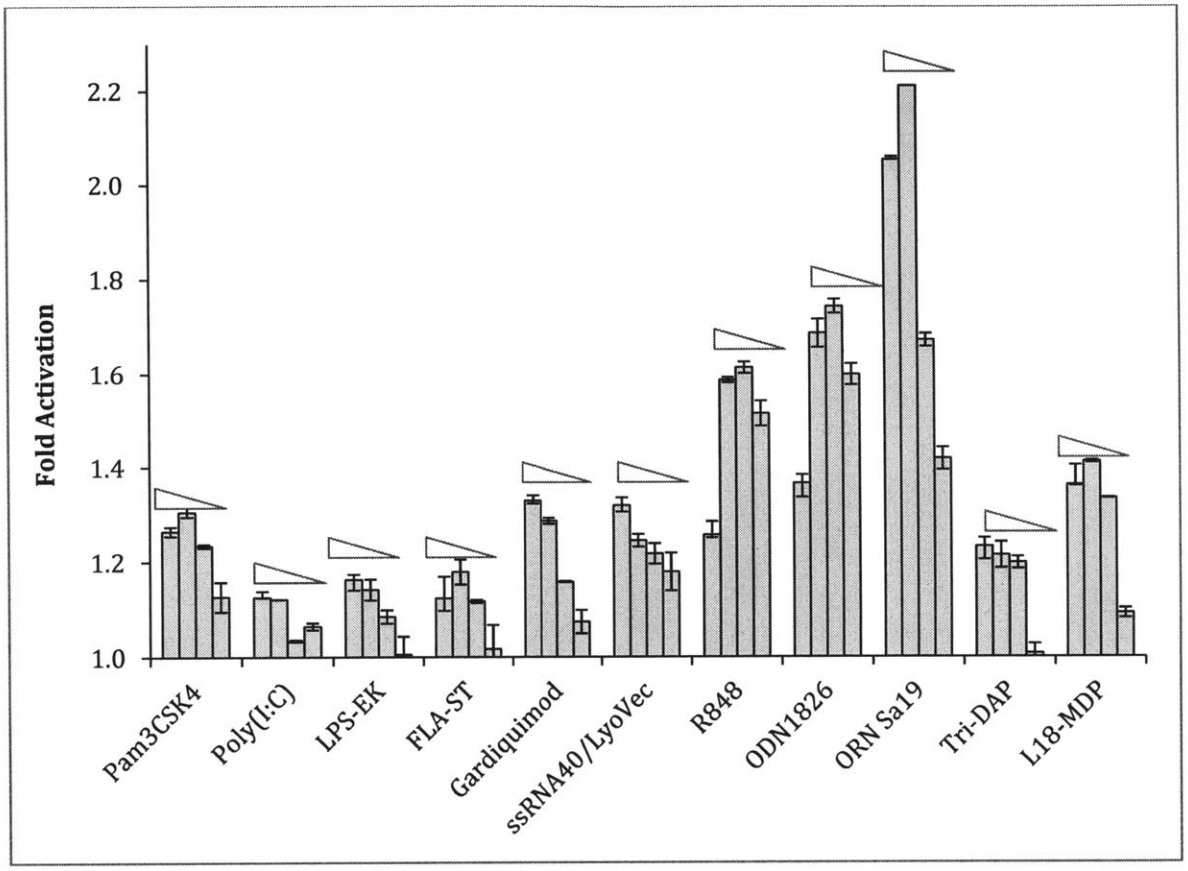

Figure 4. Determination of the optimal agonist concentration for the immunostimulatory assays. RAW-Blue™ cells were stimulated with different agonists at different concentrations. TLR1/2 (Pam3CSK4, 200ng/ml, 100ng/ml, 50ng/ml, 5ng/ml), TLR3 (Poly(I:C), 1μg/ml, 500ng/ml, 100ng/ml, 50ng/ml), TLR4 (LPS-EK, 5μg/ml, 500ng/ml, 50ng/ml, 5ng/ml), TLR5 (FLA-ST, 100ng/ml, 50ng/ml, 25ng/ml, 12.5ng/ml), TLR7 (Gardiquimod™ VacciGrade™, 10μg/ml, 1μg/ml, 100ng/ml, 10ng/ml), TLR7/8 (ssRNA40/LyoVec™, 5μg/ml, 2.5μg/ml, 1μg/ml, 250ng/ml), TLR7/8 (R848, 5μg/ml, 1μg/ml, 100ng/ml, 10ng/ml), TLR9 (ODN 1826, 5μM, 2.5μM, 1μM, 0.5μM), TLR13 (ORN Sa19, 1μg/ml, 500ng/ml, 100ng/ml, 50ng/ml), NOD1 (Tri-DAP, 10μg/ml, 5μg/ml, 2.5μg/ml, 1μg/ml), NOD2 (L18-MDP, 100ng/ml, 50ng/ml, 10ng/ml, 1ng/ml). After 24-hour incubation, PRR stimulation was assessed by quantifying the level of SEAP using QUANTI-Blue™. Absorbance at 655nm was measured after 2-hour incubation with QUANTI-Blue™. Absorbance values were normalized with blank cell control. The triangle above each cluster of bar graphs represents the gradient of agonist concentration.

(a)

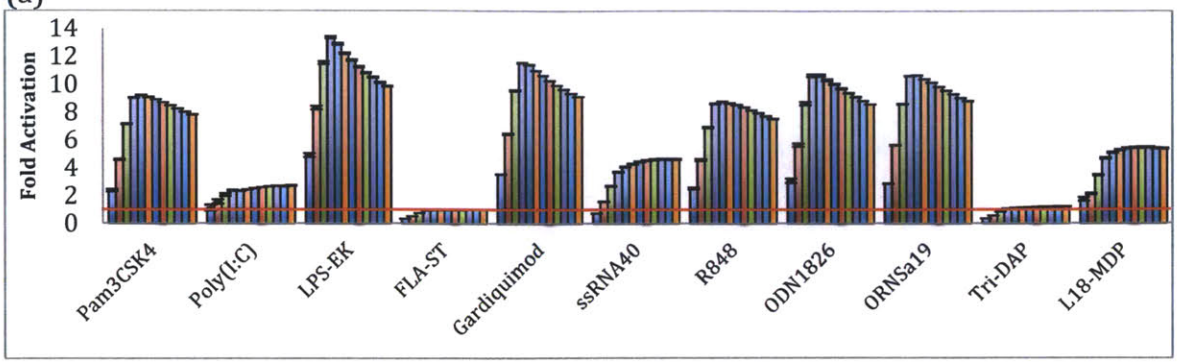
Fold Activation
14
12
10
8
6
4
2
0
Pam3CSK4
Poly(I:C)
LPS-EK
FLA-ST
Gardiquimod
ssRNA40
R848
ODN1826
ORNSa19
Tri-DAP
L18-MDP

(b)

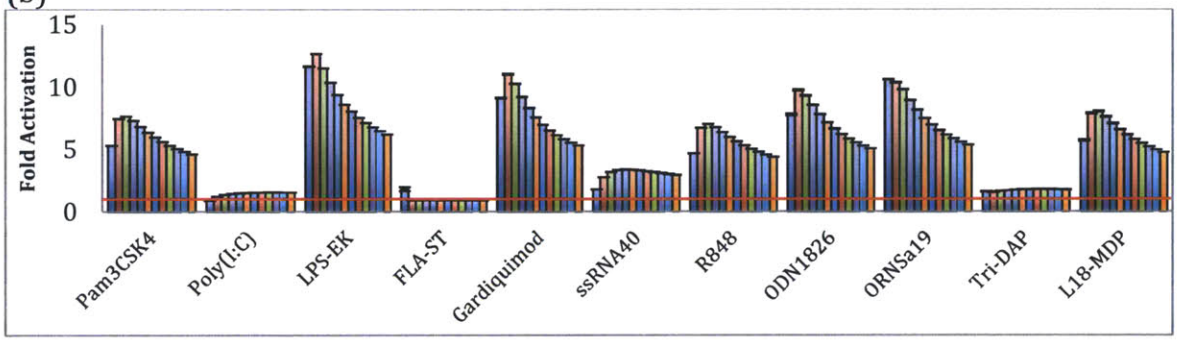
Fold Activation
15
10
5
0
Pam3CSK4
Poly(I:C)
LPS-EK
FLA-ST
Gardiquimod
ssRNA40
R848
ODN1826
ORNSa19
Tri-DAP
L18-MDP

(c)

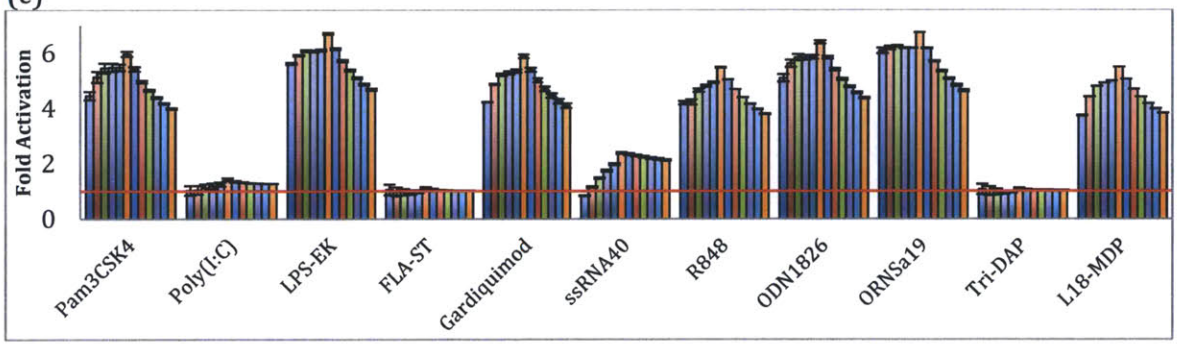
Fold Activation
6
4
2
0
Pam3CSK4
Poly(I:C)
LPS-EK
FLA-ST
Gardiquimod
ssRNA40
R848
ODN1826
ORNSa19
Tri-DAP
L18-MDP

(d)

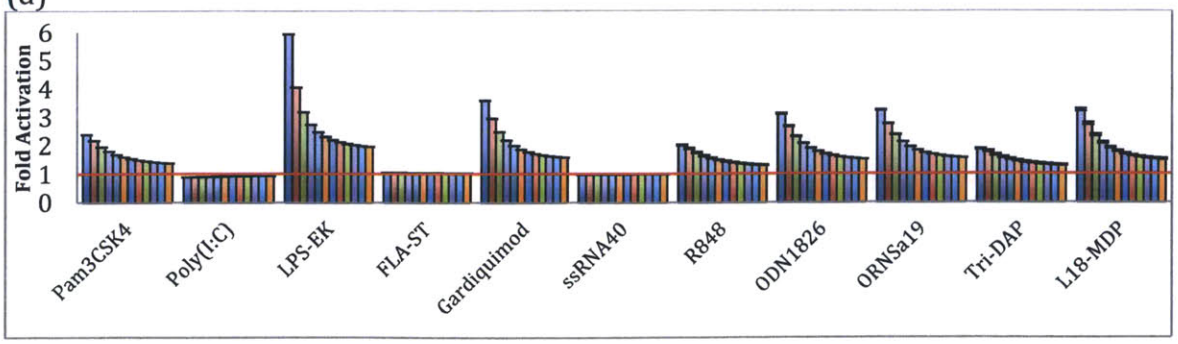
Fold Activation
6
5
4
3
2
1
0
Pam3CSK4
Poly(I:C)
LPS-EK
FLA-ST
Gardiquimod
ssRNA40
R848
ODN1826
ORNSa19
Tri-DAP
L18-MDP

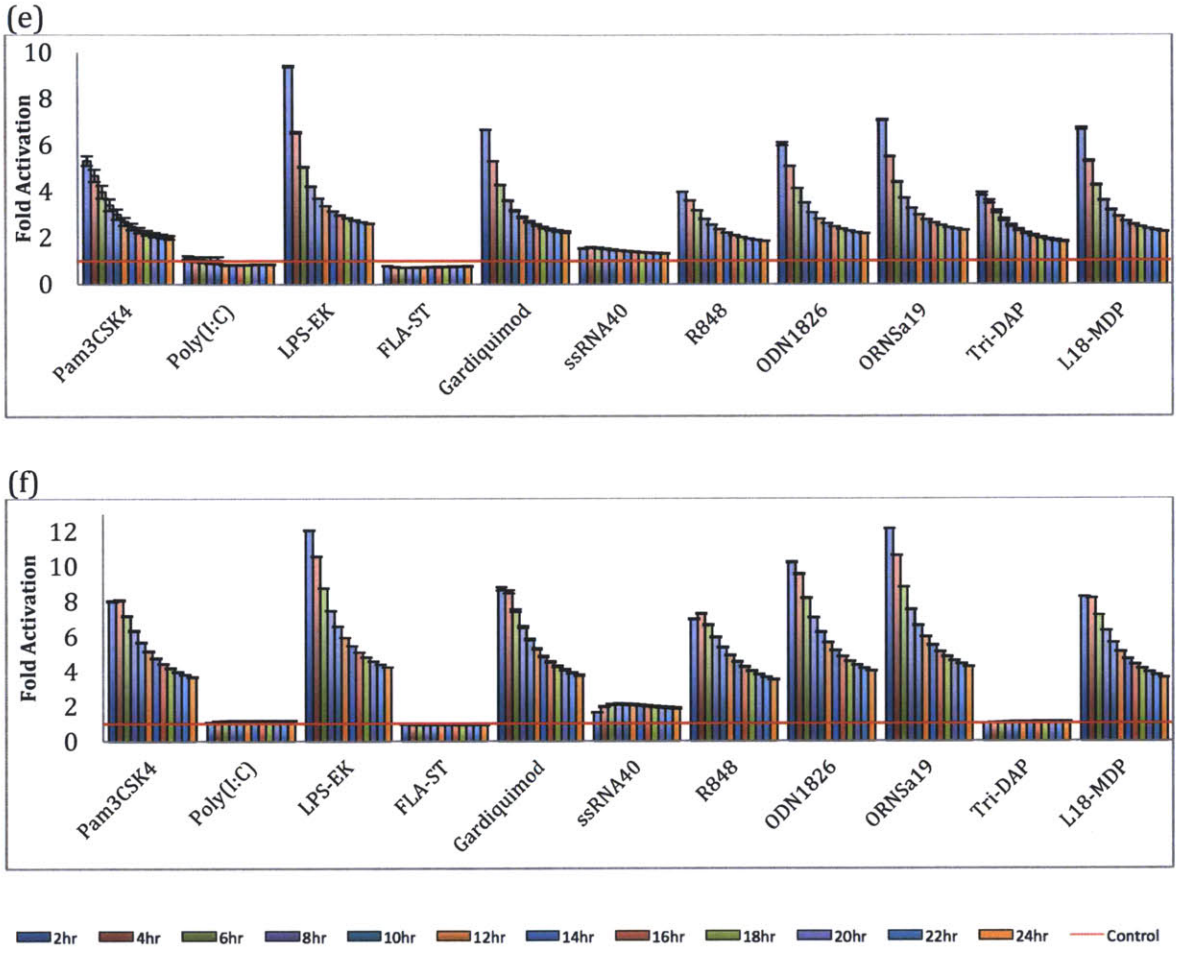

Figure 5. Kinetic profiles of PRR activation in RAW-Blue™ cells against various agonists. (a, d) 100,000 cells/well; (b, e) 200,000 cells/well; (c, f) 500,000 cells/well. (a, b, c) Cells were incubated with agonists for 24 hours and subjected to QUANTI-Blue™ kinetics assay; (d, e, f) Cells were incubated with agonists for 48 hours, and subjected to QUANTI-Blue™ kinetics assay. SEAP level was measured every 2-hours for 24 hours by recording the absorbance at 655nm. Absorbance values were normalized with the blank cell control, which was not treated with any agonist. Fold activation was calculated by normalizing each value with the blank cell control. Data represent the average ± standard deviation of duplicate samples. Red horizontal line indicates 1 fold. Following agonists were used: TLR1/2 (Pam3CSK4, 100ng/ml), TLR3 (Poly(I:C), 5μg/ml,), TLR4 (LPS-EK, 5μg/ml), TLR5 (FLA-ST, 100ng/ml), TLR7 (Gardiquimod™ VacciGrade™, 10μg/ml), TLR7/8 (ssRNA40/LyoVec™, 5μg/ml), TLR7/8 (R848, 100ng/ml), TLR9 (ODN 1826, 1μM), TLR13 (ORN Sa19, 500ng/ml), NOD1 (Tri-DAP, 10μg/ml), NOD2 (L18-MDP, 50ng/ml).

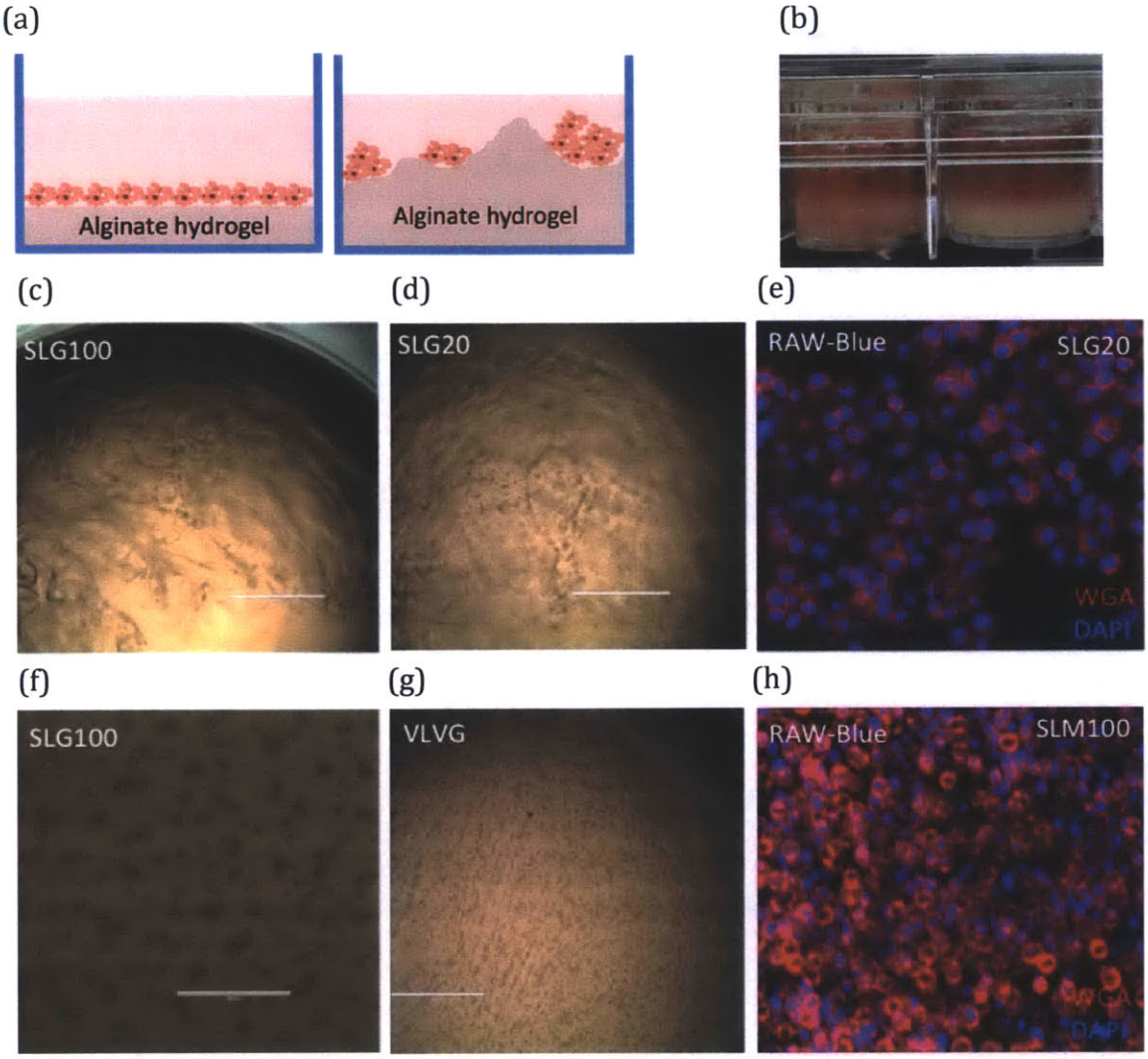

Figure 6. Alginate hydrogel surface topology and cell seeding behaviors. (a) Schematic illustration of cell seeding behaviors on the smooth surface vs. rough surface hydrogels. (b) Molding of smooth surface hydrogels with Scaffdex CellCrown™ 24 well plate insert with 8μm PET filter. (c, d) Light microscopy images of RAW-Blue™ cells seeded on rough surface alginate hydrogels made in 96 well plate format. (f, g) Light microscopy images of RAW-Blue™ cells seeded on flat surface alginate hydrogels molded with Scaffdex CellCrown™ 24 well plate insert. (e, h) Confocal microscopy images of seeded RAW-Blue™ cells stained with DAPI (blue) and Wheat Germ Agglutinin Alexa Fluor® 594 Conjugate (red). Zeiss LSM700 system with ZEN microscope software was used to image the samples.

(a)

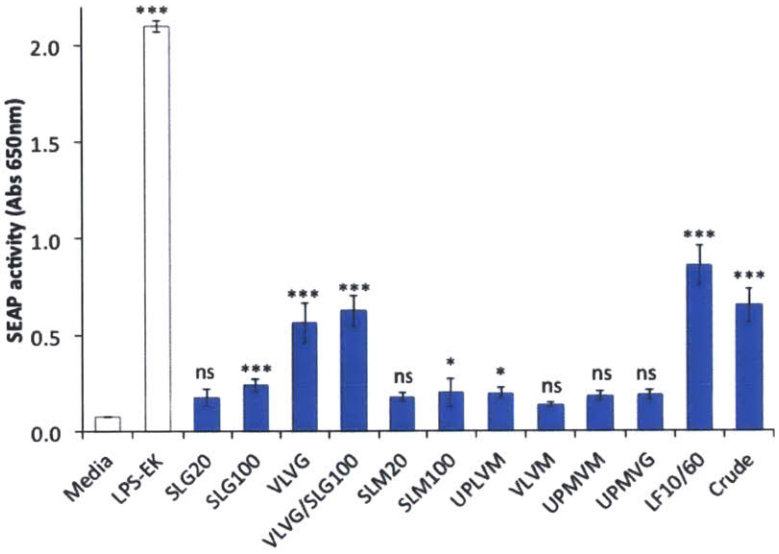
SEAP activity (Abs 650nm)
2.0
1.5
1.0
0.5
0.0
***
ns
***
***
***
ns
*
*
ns
ns
ns
***
***
Media
LPS-EK
SLG20
SLG100
VLVG
VLVG/SLG100
SLM20
SLM100
UPLVM
VLVM
UPMVM
UPMVG
LF10/60
Crude

(b)

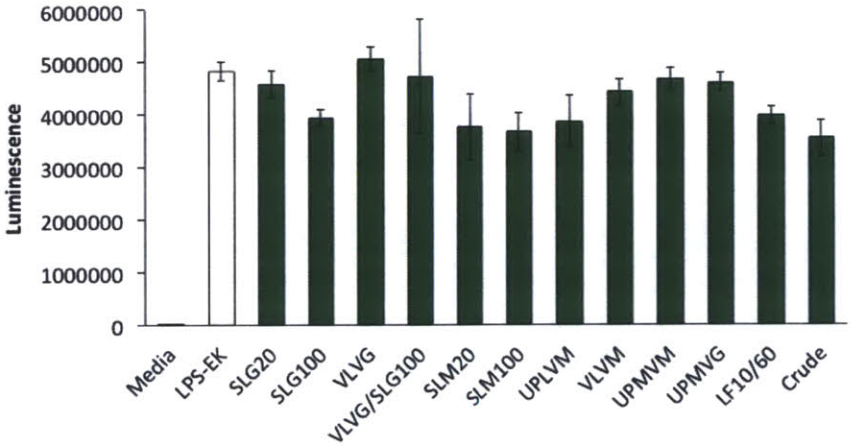
Luminescence
6000000
5000000
4000000
3000000
2000000
1000000
0
Media
LPS-EK
SLG20
SLG100
VLVG
VLVG/SLG100
SLM20
SLM100
UPLVM
VLVM
UPMVM
UPMVG
LF10/60
Crude

(c)

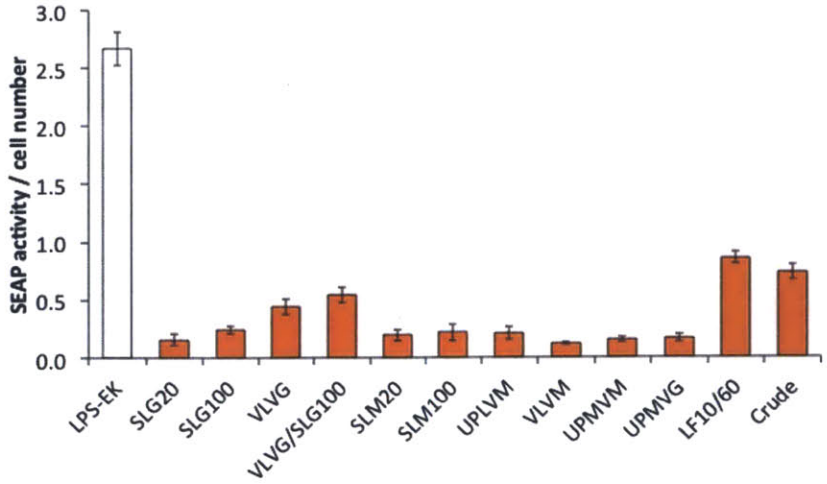
SEAP activity / cell number
3.0
2.5
2.0
1.5
1.0
0.5
0.0
LPS-EK
SLG20
SLG100
VLVG
VLVG/SLG100
SLM20
SLM100
UPLVM
VLVM
UPMVM
UPMVG
LF10/60
Crude

Figure 7. PRR stimulation of RAW-Blue™ cells seeded on smooth surface alginate hydrogels. (a) Quantification SEAP activities of cells plated on each alginate, measured at absorbance 650nm. (b) Cell viability assay to determine toxicity of alginate hydrogels with CellTiter-Glo® Luminescent Cell Viability Assay (Promega, Madison, WI, USA). Luminescence is directly proportional to the number of viable cells. (c) Level of SEAP activity in (a) was normalized with the viable cell number from (b) for each alginate. LPS-EK (5μg/ml) was used as a positive control, and the blank media was used as a negative control. After 24-hour incubation, PRR stimulation was assessed by quantifying SEAP with QUANTI-Blue™. Absorbance at 650nm was measured after 2 hours of incubation with QUANTI-Blue™. Statistical comparison of each alginate value to the negative control was made using Prizm one-way ANOVA with Tukey's test. p-value < 0.001 (***), p-value < 0.01 (**), p-value < 0.05 (*), p-value > 0.05 (ns).

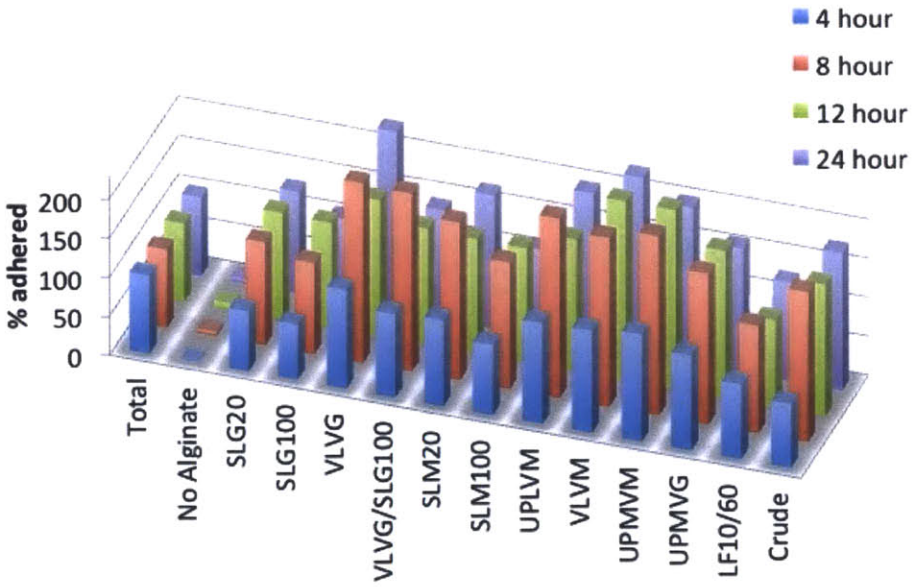

Figure 8. Percentage of cell adhesion to alginate hydrogels. The percentage of adhesion was determined by dividing the corrected (background subtracted) fluorescence of adhered cells by the total corrected fluorescence of cells. In total control, fluorescence of cells was measured without washing steps. In no alginate control, cells were plated in the low adhesion plate without any alginate. For all of the alginate hydrogels, non-adhered cells were washed after 4, 8, 12, and 24-hour incubation. Fluorescence was measured using TECAN Infinite M200 (absorbance 494nm and emission 517nm).

(a)

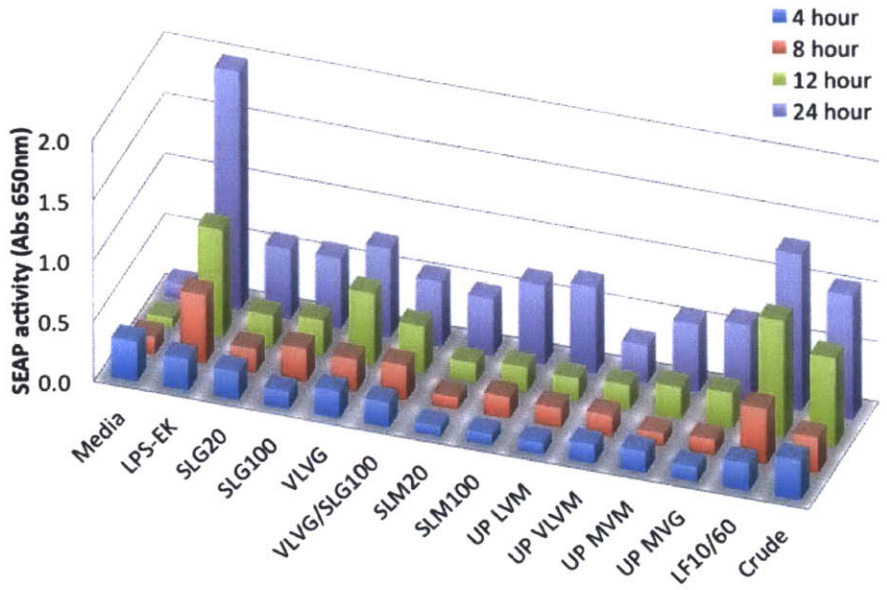

(b)

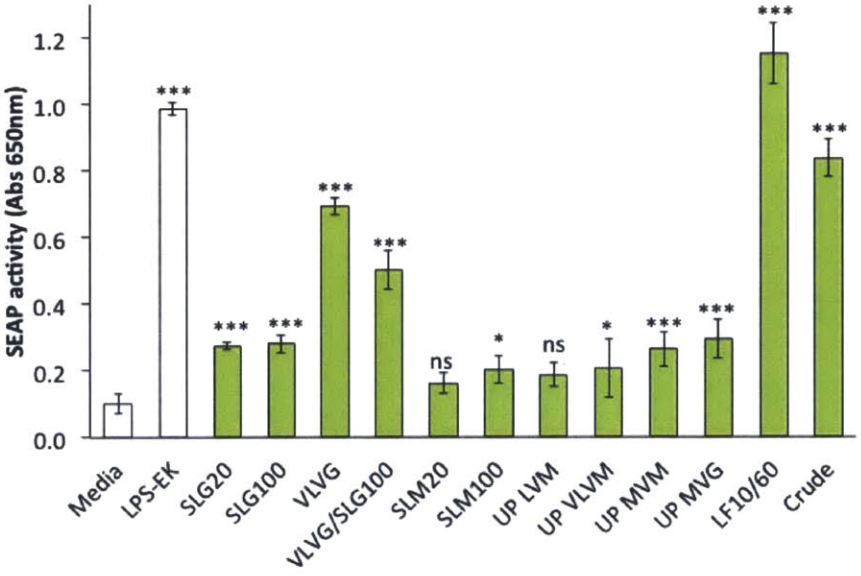

Figure 9. Stimulation of PRRs in RAW-Blue™ cells on alginate hydrogels at 4, 8, 12, and 24-hour incubation. (a) Quantification of SEAP activity with RAW-Blue™ cells seeded on alginate hydrogels after 4, 8, 12, and 24-hours incubation. (b) Quantification of SEAP activity with RAW-Blue™ cells incubated on alginate hydrogels for 12 hours. LPS-EK (5μg/ml) was used as a positive control, and the blank media was used as a negative controls. After 4, 8, 12, and 24-hour incubation, PRR stimulation was assessed by quantifying the level of SEAP with QUANTI-Blue™. Absorbance at 650nm was measured after 2 hours of incubation with QUANTI-Blue™. Statistical comparison of each alginate values to the negative control was made using Prism one-way ANOVA with Tukey's test. p-value < 0.001 (***), p-value < 0.01 (**), p-value < 0.05 (*), p-value > 0.05 (ns).

(a)

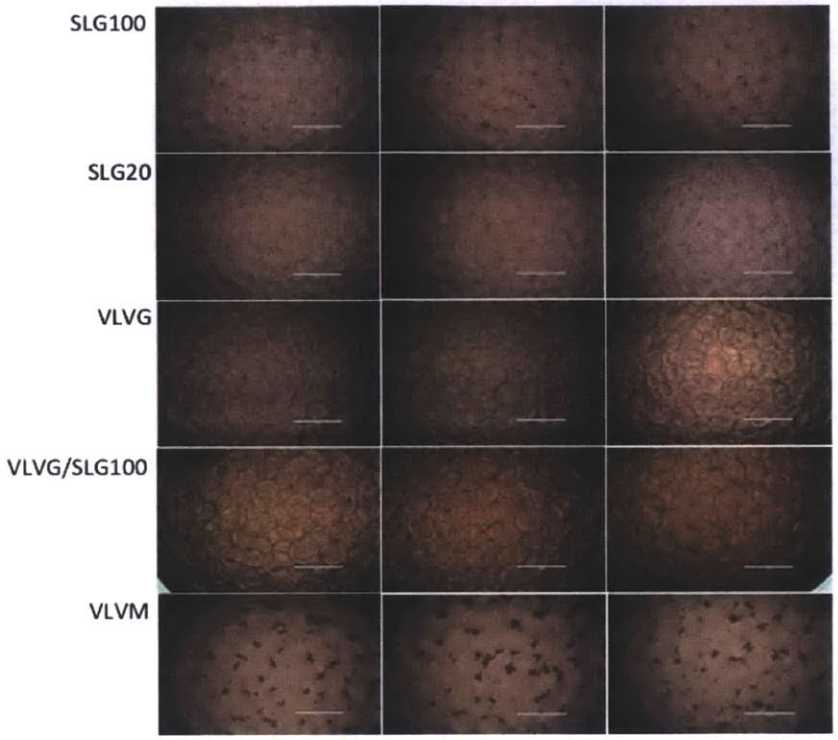

(b)

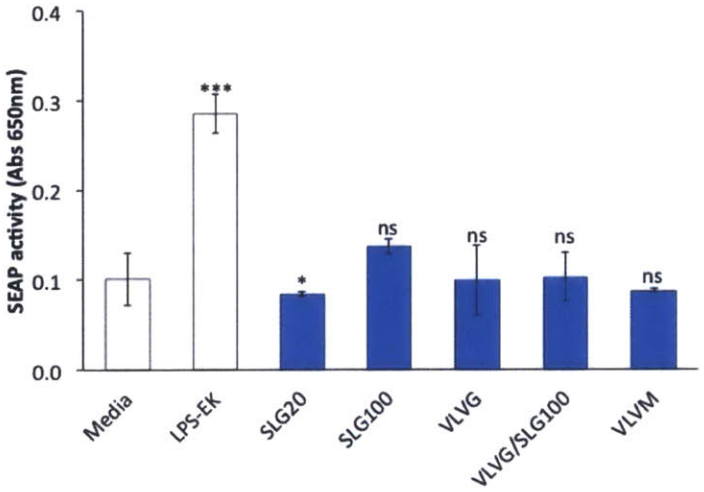

Figure 10. Stimulation of PRRs with RAW-Blue™ on alginate microcapsules. (a) Light microscope image of alginate microcapsules seeded with RAW-Blue™ cells. Dark spots indicate cells adhered to the microcapsule surface. As shown, the amount of cells that adhered to the capsules vary significantly from one alginate to the other alginate. (b) Quantification of SEAP activity with RAW-Blue™ cells seeded on alginate microcapsules. LPS-EK (5μg/ml) was used as a positive control, and the blank media was used as a negative controls. Statistical comparison of each alginate values to the negative control was made using Prism one-way ANOVA with Tukey's test. p-value < 0.001 (***), p-value < 0.01 (**), p-value < 0.05 (*), p-value > 0.05 (ns).

(a)

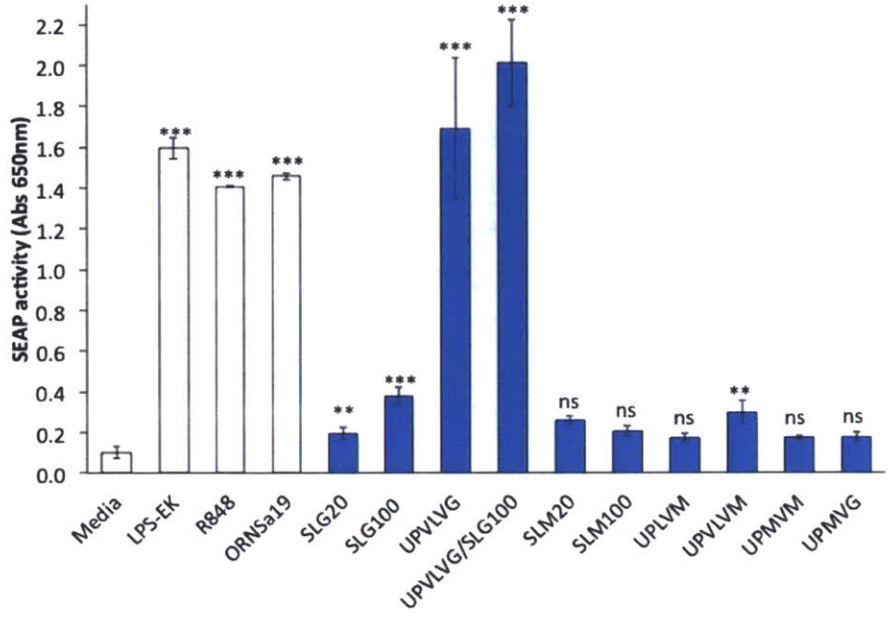

(b)

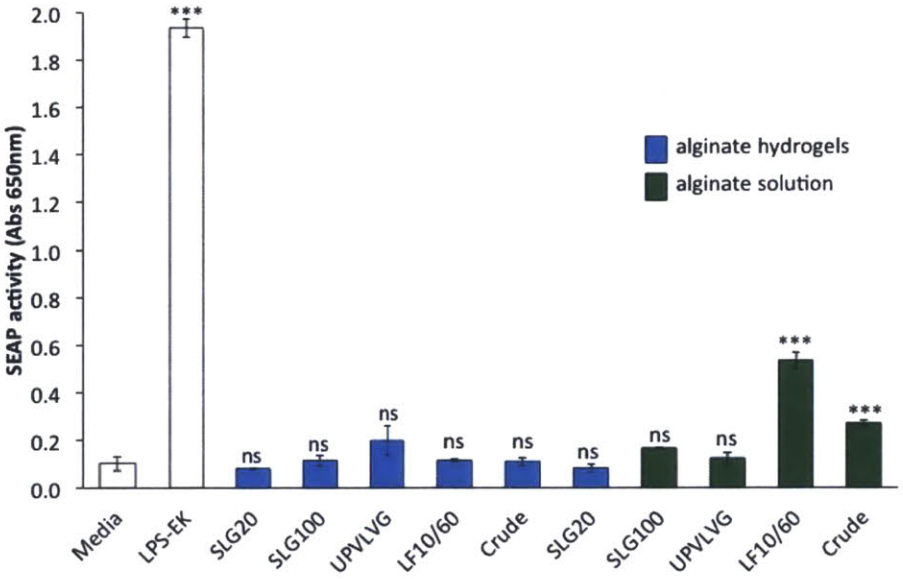

Figure 11. Stimulation of PRR in adherent and non-adherent cells. (a) Quantification of SEAP activity with adhering RAW-Blue™ cells seeded on alginate hydrogels. LPS-EK (5µg/ml), R848 (5µg/ml), and ORN Sa19 (1µg/ml) were used as positive controls, and the blank media was used as a negative control. (b) Quantification of SEAP activity with non-adhering THP1-XBlue™-MD2-CD14 cells on both alginate hydrogels (blue) and alginate solution (green). LPS-EK (5µg/ml) were used as a positive control, and the blank media was used as a negative control. PRR stimulation was assessed by quantifying SEAP with QUANTI-Blue™. Absorbance at 655nm was measured after 2 hours of incubation with QUANTI-Blue™. Statistical comparison was made with Prizm one-way ANOVA with Tukey's test. p-value < 0.001 (***), p-value < 0.01 (**), p-value < 0.05 (*), p-value > 0.05 (ns).

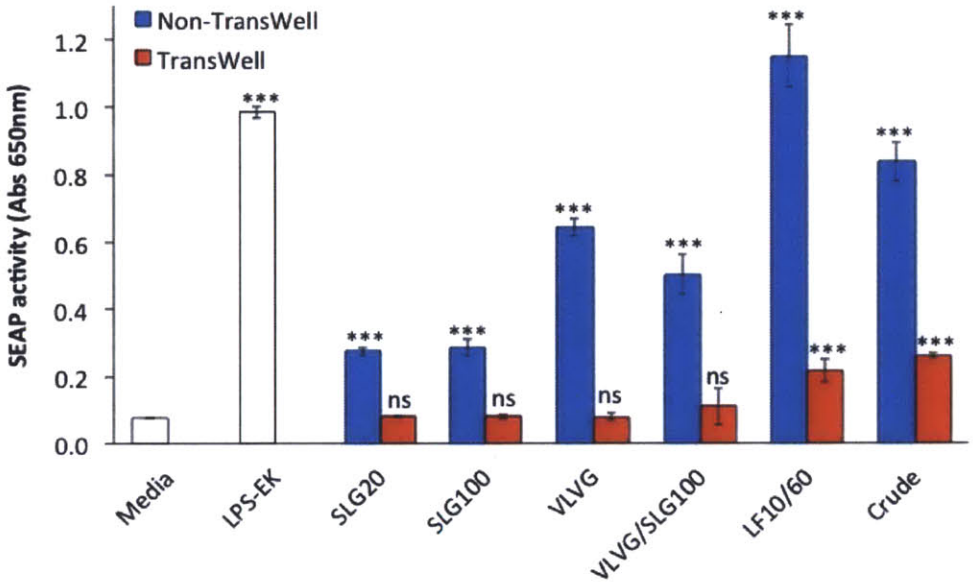

Figure 12. Stimulation of PRR activation with RAW-Blue™ cells in the Transwell® system. Blue: Quantification of SEAP activity with RAW-Blue™ cells seeded directly on top of the alginate hydrogels. Red: Quantification of SEAP activity with RAW-Blue™ cells seeded on the Transwell insert with permeable membrane, preventing direct cell-to-alginate contact. LPS-EK (5μg/ml) was used as a positive control, and the blank media was used as a negative control. PRR stimulation was assessed by quantifying the level of SEAP using QUANTI-Blue™. Absorbance at 650nm was measured after 2 hours of incubation with QUANTI-Blue™. Statistical comparison of each alginate values to the negative control was made using Prizm one-way ANOVA with Tukey's test. p-value < 0.001 (***), p-value < 0.01 (**), p-value < 0.05 (*), p-value > 0.05 (ns).

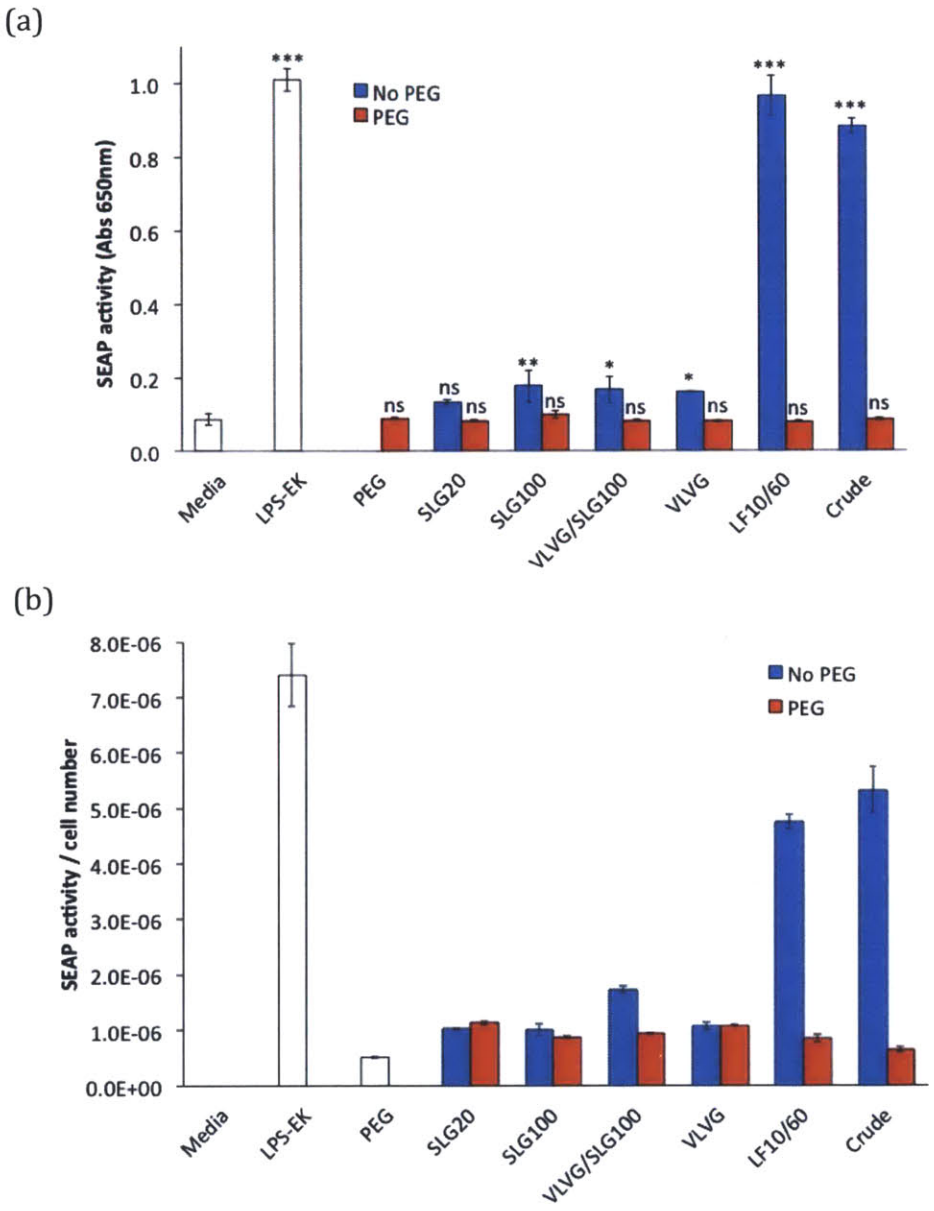

Figure 13. Stimulation of PRR activation with RAW-Blue™ cells on PEG + alginate hydrogels. Blue: RAW-Blue™ cells seeded directly on top of the alginate hydrogels. Red: RAW-Blue™ cells seeded on the PEG + alginate hydrogels. (a) Quantification of SEAP activity. (b) Level of SEAP activity in (a) was normalized with the cell viability assay for each alginate. LPS-EK (5μg/ml) was used as a positive control, and the blank media was used as a negative control. PRR stimulation was assessed by quantifying the level of SEAP using QUANTI-Blue™. Absorbance at 650nm was measured after 2 hours of incubation with QUANTI-Blue™. Statistical comparison of each alginate values to the negative control was made using Prizm one-way ANOVA with Tukey's test. p-value < 0.001 (***), p-value < 0.01 (**), p-value < 0.05 (*), p-value > 0.05 (ns).

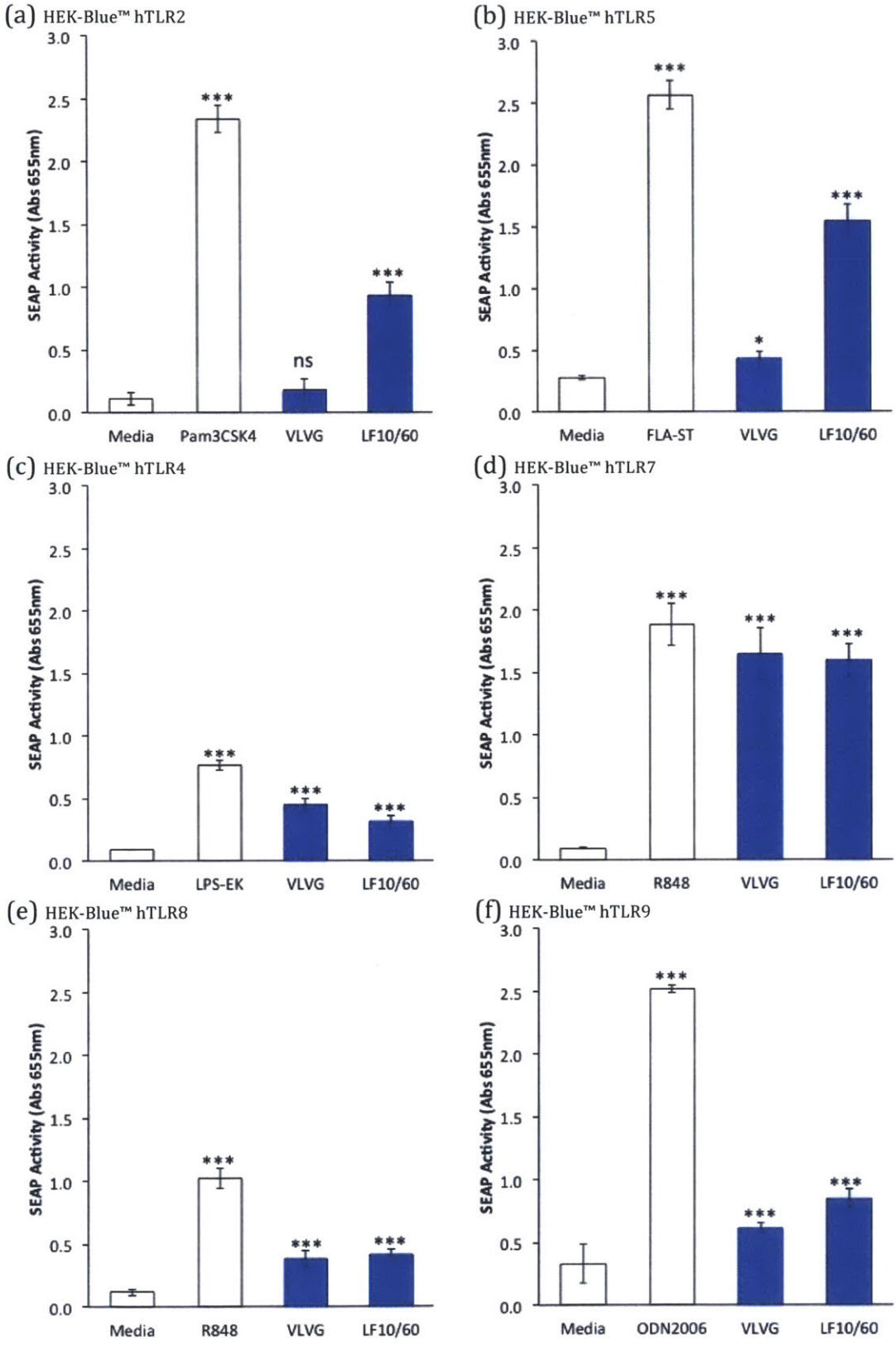
(a) HEK-Blue™ hTLR2
SEAP Activity (Abs 655nm)
3.0
2.5
2.0
1.5
1.0
0.5
0.0
***
ns
***
Media
Pam3CSK4
VLVG
LF10/60
(b) HEK-Blue™ hTLR5
SEAP Activity (Abs 655nm)
***
*
***
Media
FLA-ST
VLVG
LF10/60
(c) HEK-Blue™ hTLR4
SEAP Activity (Abs 655nm)
***
***
***
Media
LPS-EK
VLVG
LF10/60
(d) HEK-Blue™ hTLR7
SEAP Activity (Abs 655nm)
***
***
***
Media
R848
VLVG
LF10/60
(e) HEK-Blue™ hTLR8
SEAP Activity (Abs 655nm)
***
***
***
Media
R848
VLVG
LF10/60
(f) HEK-Blue™ hTLR9
SEAP Activity (Abs 655nm)
***
***
***
Media
ODN2006
VLVG
LF10/60

Figure 14. Stimulation of PRR activation with human HEK-Blue™ cells on alginate hydrogels. HEK-Blue™ hTLR2, 4, 5, 7, 8, 9 cells were seeded on the alginate hydrogels. (a) Quantification of SEAP activity with HEK-Blue™ hTLR2 cells. Pam3CSK4 (100ng/ml) was used as a positive control with HEK-Blue™ hTLR2 cells. (b) Quantification of SEAP activity with HEK-Blue™ hTLR5 cells. FLA-ST (100ng/ml) was used as a positive control with HEK-Blue™ hTLR5 cells. (c) Quantification of SEAP activity with HEK-Blue™ hTLR4 cells. LPS-EK (5μg/ml) was used as a positive control with HEK-Blue™ hTLR4 cells. (d) Quantification of SEAP activity with HEK-Blue™ hTLR7 cells. R848 (100ng/ml) was used as a positive control with HEK-Blue™ hTLR7. (e) Quantification of SEAP activity with HEK-Blue™ hTLR8 cells. R848 (100ng/ml) was used as a positive control with HEK-Blue™ hTLR8. (f) Quantification of SEAP activity with HEK-Blue™ hTLR9 cells. ODN2006 (5μM) was used as a positive control with HEK-Blue™ hTLR9 cells. Blank media was used as a negative control with all cell types. PRR stimulation was assessed by quantifying the level of SEAP using QUANTI-Blue™. Absorbance at 650nm was measured after 2 hours of incubation with QUANTI-Blue™. Values are presented as mean ± SD (n = 12). Statistical comparison of each alginate values to the negative control was made using Prizm one-way ANOVA with Tukey's test. p-value < 0.001 (***), p-value < 0.01 (**), p-value < 0.05 (*), p-value > 0.05 (ns).

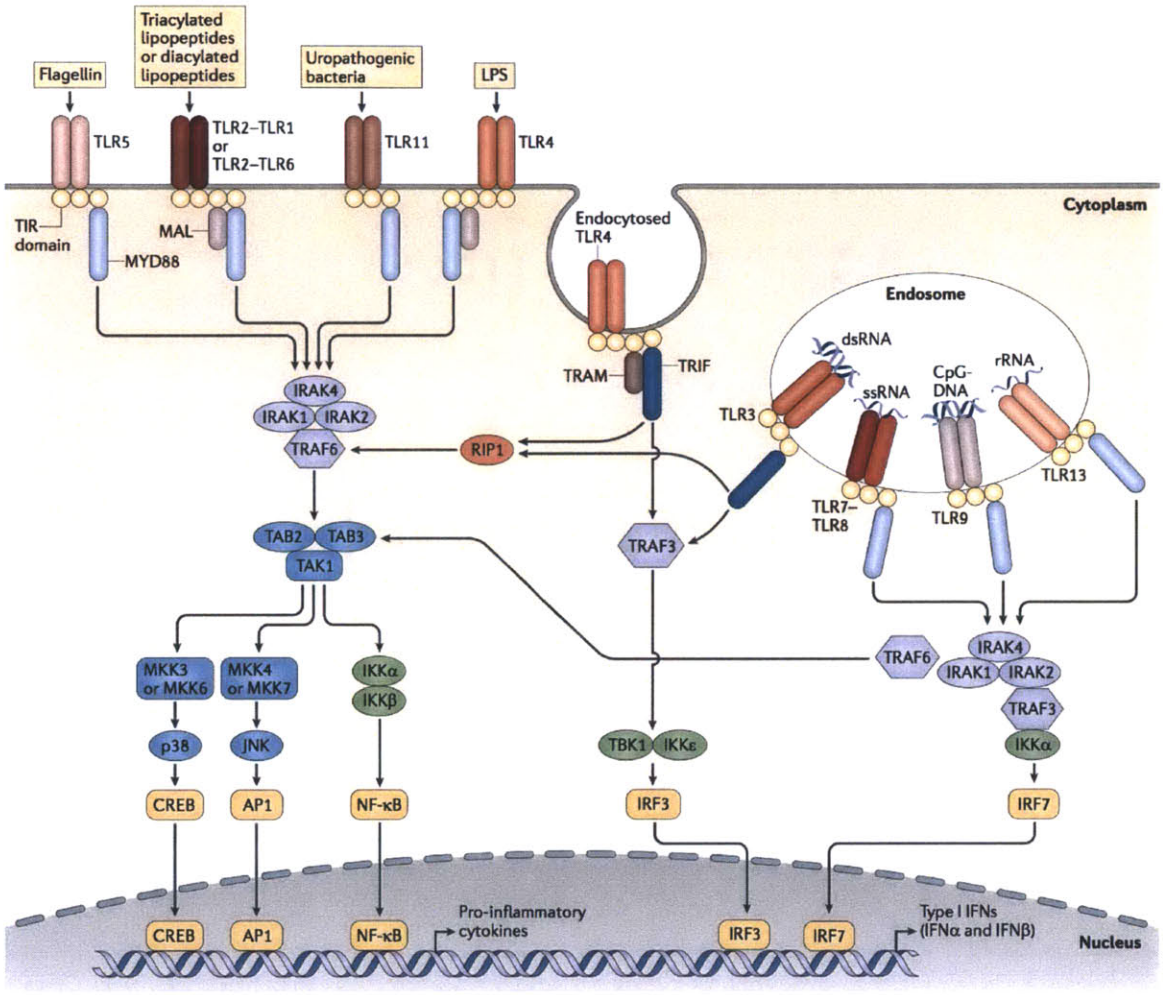

Figure 15. Mammalian TLR signaling pathways. Upon binding of ligands, cascades of signaling pathways leads to a few important transcription factors downstream, such as nuclear factor-κB (NF-κB) and activator protein-1 (AP-1). Figure adapted from O'Neill et al., 2013.

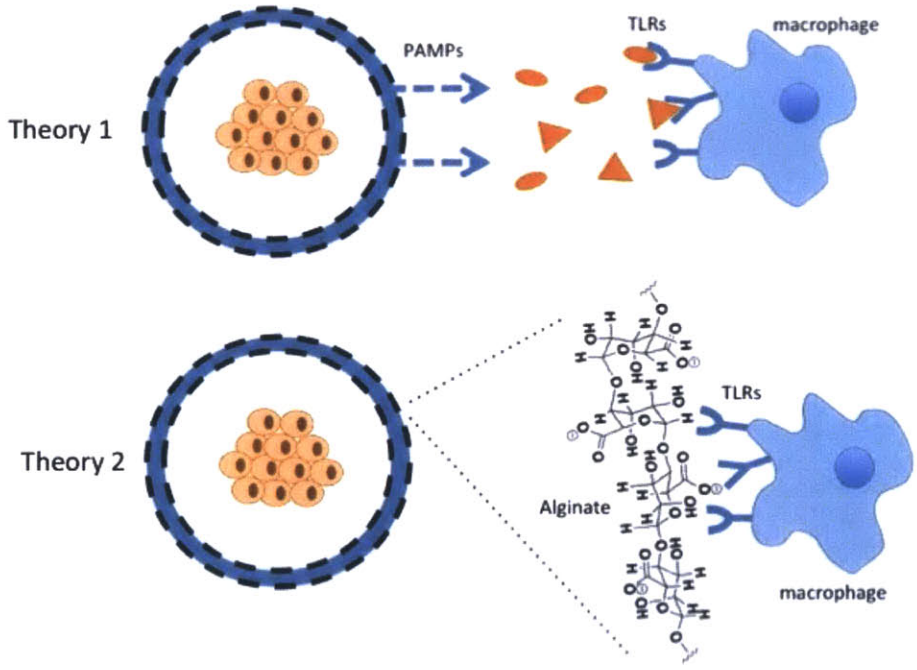

Figure 16. Two mainstream theories of how macrophages are activated by alginate. Theory 1: Impurities present in alginate, not the alginate itself, are responsible for the inflammation. Theory 2: The alginate itself can somehow directly activate macrophages, which then leads to activation of innate immunity.

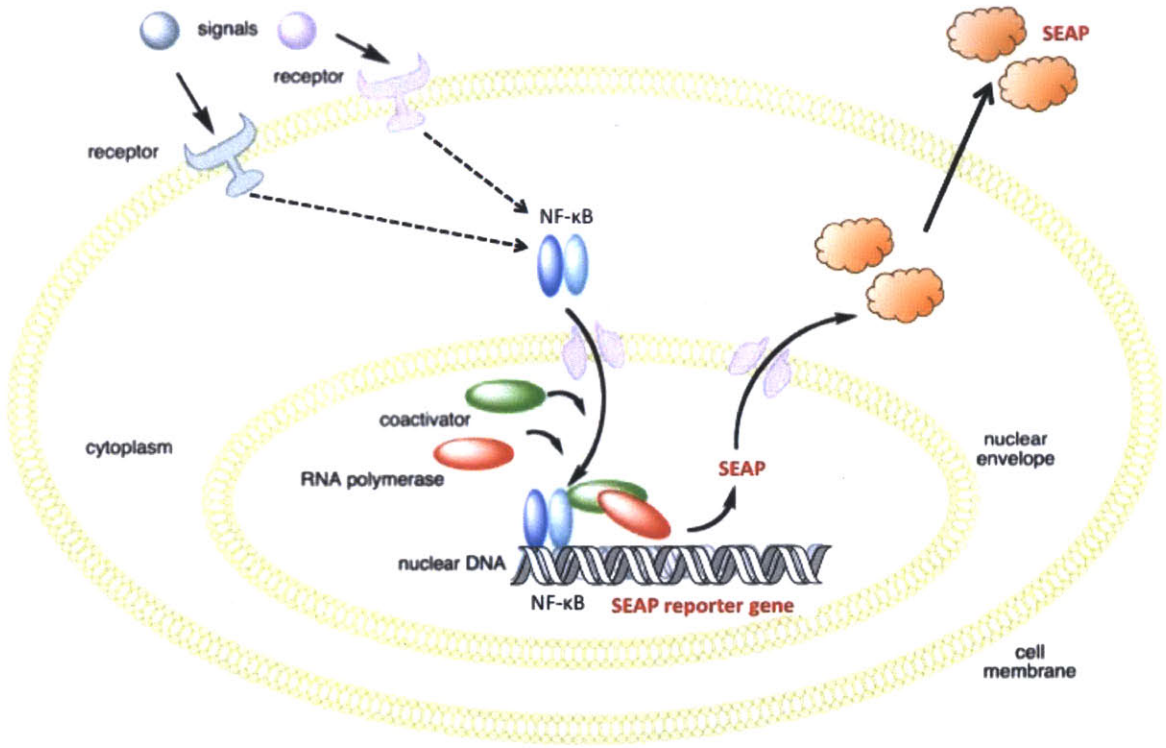

Figure 17. Secreted embryonic alkaline phosphatase (SEAP) reporter system. RAW-Blue™, THP1-XBlue™-MD2-CD14 cells express many PRRs. They both are stably transfected with a secreted embryonic alkaline phosphatase (SEAP) reporter gene inducible by NF-κB and AP-1 transcription factors. Upon activation of pattern recognition receptors (PRRs), signaling cascades lead to expression of nuclear factor-κB (NF-κB). The SEAP reporter gene is placed under the control of NF-κB, and therefore upon activation of PRRs, SEAP is secreted out to the cell culture supernatant. SEAP can then be quantified with QUANTI-Blue™ reagent, a colorimetric enzyme assay developed to determine alkaline phosphatase activity in a biological sample.

References

Aebischer, P., Goddard, M., Signore, A.P., and Timpson, R.L. (1994). Functional recovery in hemiparkinsonian primates transplanted with polymer-encapsulated PC12 cells. Exp. Neurol. *126*, 151–158.

Alexopoulou, L., Holt, A.C., Medzhitov, R., and Flavell, R.A. (2001). Recognition of double-stranded RNA and activation of NF-kappaB by Toll-like receptor 3. Nature *413*, 732–738.

Algire, G.H., Weaver, J.M., and Prehn, R.T. (1954). Growth of cells in vivo in diffusion chambers. I. Survival of homografts in immunized mice. J. Natl. Cancer Inst. *15*, 493–507.

Aliprantis, A.O. (1999). Cell Activation and Apoptosis by Bacterial Lipoproteins Through Toll-like Receptor-2. Science (80-.). *285*, 736–739.

Andersen, T., Strand, B.L., Formo, K., Alsberg, E., and Christensen, B.E. (2012). Chapter 9 Alginates as biomaterials in tissue engineering. In Carbohydrate Chemistry: Volume 37, (The Royal Society of Chemistry), pp. 227–258.

Anderson, J.M., Rodriguez, A., and Chang, D.T. (2008). Foreign body reaction to biomaterials. Semin. Immunol. *20*, 86–100.

Auquit-Auckbur, I., Caillot, F., Arnoult, C., Menard, J.F., Drouot, L., Courville, P., Tron, F., and Musette, P. (2011). Role of toll-like receptor 4 in the inflammation reaction surrounding silicone prosthesis. Acta Biomater *7*, 2047–2052.

Baldwin, A.S. (1996). The NF-kappa B and I kappa B proteins: new discoveries and insights. Annu. Rev. Immunol. *14*, 649–683.

Basta, G., Montanucci, P., Luca, G., Boselli, C., Noya, G., Barbaro, B., Qi, M., Kinzer, K.P., Oberholzer, J., and Calafiore, R. (2011). Long-term metabolic and immunological follow-up of nonimmunosuppressed patients with type 1 diabetes treated with microencapsulated islet allografts: four cases. Diabetes Care *34*, 2406–2409.

Bauer, S., Kirschning, C.J., Häcker, H., Redecke, V., Hausmann, S., Akira, S., Wagner, H., and Lipford, G.B. (2001). Human TLR9 confers responsiveness to bacterial DNA via species-specific CpG motif recognition. Proc. Natl. Acad. Sci. U. S. A. *98*, 9237–9242.

Beck, J., Angus, R., Madsen, B., Britt, D., Vernon, B., and Nguyen, K.T. (2007). Islet encapsulation: strategies to enhance islet cell functions. Tissue Eng. *13*, 589–599.

Braccini, I., and Perez, S. (2001). Molecular basis of C(2+)-induced gelation in alginates and pectins: the egg-box model revisited. Biomacromolecules *2*, 1089–1096.

Bridges, A.W., and García, A.J. (2008). Anti-inflammatory polymeric coatings for implantable biomaterials and devices. J. Diabetes Sci. Technol. *2*, 984–994.

Calafiore, R., Basta, G., Luca, G., Lemmi, A., Montanucci, M.P., Calabrese, G., Racanicchi, L., Mancuso, F., and Brunetti, P. (2006). Microencapsulated pancreatic islet allografts into nonimmunosuppressed patients with type 1 diabetes: first two cases. Diabetes Care *29*, 137–138.

Chamaillard, M., Hashimoto, M., Horie, Y., Masumoto, J., Qiu, S., Saab, L., Ogura, Y., Kawasaki, A., Fukase, K., Kusumoto, S., et al. (2003). An essential role for NOD1 in host recognition of bacterial peptidoglycan containing diaminopimelic acid. Nat. Immunol. *4*, 702–707.

Chang, T.M.. (1964). Semipermeable microcapsules. Science (80-.). *146*, 524–525.

Chang, P.L., Shen, N., and Westcott, A.J. (1993). Delivery of recombinant gene products with microencapsulated cells in vivo. Hum. Gene Ther. *4*, 433–440.

Chatenoud, L. (2008). Chemical Immunosuppression in Islet Transplantation — Friend or Foe? N. Engl. J. Med. *358*, 1192–1193.

Diebold, S.S., Kaisho, T., Hemmi, H., Akira, S., and Reis e Sousa, C. (2004). Innate antiviral responses by means of TLR7-mediated recognition of single-stranded RNA. Science *303*, 1529–1531.

Drouin, P., Blickle, J.F., Charbonnel, B., Eschwege, E., Guillausseau, P.J., Plouin, P.F., Daninos, J.M., Balarac, N., and Sauvanet, J.P. (2009). Diagnosis and classification of diabetes mellitus. Diabetes Care *32 Suppl 1*, S62–S67.

Flo, T.H., Ryan, L., Latz, E., Takeuchi, O., Monks, B.G., Lien, E., Halaas, O., Akira, S., Skjak-Braek, G., Golenbock, D.T., et al. (2002). Involvement of toll-like receptor TLR2 and TLR4 in cell activation by mannuronic acid polymers. J Biol Chem *277*, 35489–35495.

Franz, S., Rammelt, S., Scharnweber, D., and Simon, J.C. (2011). Immune responses to implants - a review of the implications for the design of immunomodulatory biomaterials. Biomaterials *32*, 6692–6709.

Fujihara, M., Muroi, M., Tanamoto, K., Suzuki, T., Azuma, H., and Ikeda, H. (2003). Molecular mechanisms of macrophage activation and deactivation by lipopolysaccharide: roles of the receptor complex. Pharmacol. Ther. *100*, 171–194.

Gallucci, S., and Matzinger, P. (2001). Danger signals: SOS to the immune system. Curr. Opin. Immunol. *13*, 114–119.

Girardin, S.E., Boneca, I.G., Viala, J., Chamaillard, M., Labigne, A., Thomas, G., Philpott, D.J., and Sansonetti, P.J. (2003). Nod2 is a general sensor of peptidoglycan through muramyl dipeptide (MDP) detection. J. Biol. Chem. *278*, 8869–8872.

Gorbet, M.B., and Sefton, M. V (2005). Endotoxin: the uninvited guest. Biomaterials *26*, 6811–6817.

Grandjean-Laquerriere, A., Tabary, O., Jacquot, J., Richard, D., Frayssinet, P., Guenounou, M., Laurent-Maquin, D., Laquerriere, P., and Gangloff, S. (2007). Involvement of toll-like receptor 4 in the inflammatory reaction induced by hydroxyapatite particles. Biomaterials *28*, 400–404.

Hasse, C., Klöck, G., Schlosser, A., Zimmermann, U., and Rothmund, M. (1997). Parathyroid allotransplantation without immunosuppression. Lancet *350*, 1296–1297.

Hayashi, F., Smith, K.D., Ozinsky, A., Hawn, T.R., Yi, E.C., Goodlett, D.R., Eng, J.K., Akira, S., Underhill, D.M., and Aderem, A. (2001). The innate immune response to bacterial flagellin is mediated by Toll-like receptor 5. Nature *410*, 1099–1103.

Heil, F., Hemmi, H., Hochrein, H., Ampenberger, F., Kirschning, C., Akira, S., Lipford, G., Wagner, H., and Bauer, S. (2004). Species-specific recognition of single-stranded RNA via toll-like receptor 7 and 8. Science *303*, 1526–1529.

Hemmi, H., Kaisho, T., Takeuchi, O., Sato, S., Sanjo, H., Hoshino, K., Horiuchi, T., Tomizawa, H., Takeda, K., and Akira, S. (2002). Small anti-viral compounds activate immune cells via the TLR7 MyD88-dependent signaling pathway. Nat. Immunol. *3*, 196–200.

Hidmark, A., von Saint Paul, A., and Dalpke, A.H. (2012). Cutting edge: TLR13 is a receptor for bacterial RNA. J. Immunol. *189*, 2717–2721.

Jacobs-Tulleneers-Thevissen, D., Chintinne, M., Ling, Z., Gillard, P., Schoonjans, L., Delvaux, G., Strand, B.L., Gorus, F., Keymeulen, B., Pipeleers, D., et al. (2013). Sustained function of alginate-encapsulated human islet cell implants in the peritoneal cavity of mice leading to a pilot study in a type 1 diabetic patient. Diabetologia *56*, 1605–1614.

Jurk, M., Heil, F., Vollmer, J., Schetter, C., Krieg, A.M., Wagner, H., Lipford, G., and Bauer, S. (2002). Human TLR7 or TLR8 independently confer responsiveness to the antiviral compound R-848. Nat. Immunol. *3*, 499.

Kawai, T., and Akira, S. (2008). Toll-like receptor and RIG-I-like receptor signaling. Ann. N. Y. Acad. Sci. *1143*, 1–20.

Kreppel, F., and Kochanek, S. (2008). Modification of adenovirus gene transfer vectors with synthetic polymers: a scientific review and technical guide. Mol. Ther. *16*, 16–29.

Krieg, A.M., Yi, A.K., Matson, S., Waldschmidt, T.J., Bishop, G.A., Teasdale, R., Koretzky, G.A., and Klinman, D.M. (1995). CpG motifs in bacterial DNA trigger direct B-cell activation. Nature *374*, 546–549.

Lakey, J.R.T., Mirbolooki, M., and Shapiro, A.M.J. (2006). Current status of clinical islet cell transplantation. Methods Mol. Biol. *333*, 47–104.

Lee, K.Y., and Mooney, D.J. (2012). Alginate: properties and biomedical applications. Prog Polym Sci *37*, 106–126.

Li, X.-D., and Chen, Z.J. (2012). Sequence specific detection of bacterial 23S ribosomal RNA by TLR13. Elife *1*, e00102.

Lim, F., and Sun, A.M. (1980). Microencapsulated islets as bioartificial endocrine pancreas. Science (80-.). *210*, 908–910.

Liu, H.W., Ofosu, F.A., and Chang, P.L. (1993). Expression of human factor IX by microencapsulated recombinant fibroblasts. Hum. Gene Ther. *4*, 291–301.

Ma, F., Zhang, J., Zhang, J., and Zhang, C. (2010). The TLR7 agonists imiquimod and gardiquimod improve DC-based immunotherapy for melanoma in mice. Cell. Mol. Immunol. *7*, 381–388.

Matsumoto, M., Kikkawa, S., Kohase, M., Miyake, K., and Seya, T. (2002). Establishment of a monoclonal antibody against human Toll-like receptor 3 that blocks double-stranded RNA-mediated signaling. Biochem. Biophys. Res. Commun. *293*, 1364–1369.

Mizel, S.B., Honko, A.N., Moors, M.A., Smith, P.S., and West, A.P. (2003). Induction of Macrophage Nitric Oxide Production by Gram-Negative Flagellin Involves Signaling Via Heteromeric Toll-Like Receptor 5/Toll-Like Receptor 4 Complexes. J. Immunol. *170*, 6217–6223.

Mørch, Y.A., Donati, I., Strand, B.L., and Skjåk-Braek, G. (2007). Molecular engineering as an approach to design new functional properties of alginate. Biomacromolecules *8*, 2809–2814.

Narang, A.S., and Mahato, R.I. (2006). Biological and biomaterial approaches for improved islet transplantation. Pharmacol. Rev. *58*, 194–243.

O'Neill, L.A., Golenbock, D., and Bowie, A.G. (2013). The history of Toll-like receptors - redefining innate immunity. Nat Rev Immunol *13*, 453–460.

Oldenburg, M., Krüger, A., Ferstl, R., Kaufmann, A., Nees, G., Sigmund, A., Bathke, B., Lauterbach, H., Suter, M., Dreher, S., et al. (2012). TLR13 recognizes bacterial 23S rRNA devoid of erythromycin resistance-forming modification. Science *337*, 1111–1115.

Omer, A., Keegan, M., Czismadia, E., De Vos, P., Van Rooijen, N., Bonner-Weir, S., and Weir, G.C. (2003a). Macrophage depletion improves survival of porcine neonatal pancreatic cell clusters contained in alginate macrocapsules transplanted into rats. Xenotransplantation *10*, 240–251.

Omer, A., Duvivier-Kali, V.F., Trivedi, N., Wilmot, K., Bonner-Weir, S., and Weir, G.C. (2003b). Survival and maturation of microencapsulated porcine neonatal pancreatic cell clusters transplanted into immunocompetent diabetic mice. Diabetes *52*, 69–75.

Orive, G., Carcaboso, A.M., Hernández, R.M., Gascón, A.R., and Pedraz, J.L. (2003a). Biocompatibility evaluation of different alginates and alginate-based microcapsules. Biomacromolecules *6*, 927–931.

Orive, G., Gascón, A.R., Hernández, R.M., Igartua, M., and Luis Pedraz, J. (2003b). Cell microencapsulation technology for biomedical purposes: novel insights and challenges. Trends Pharmacol. Sci. *24*, 207–210.

Ozinsky, A., Underhill, D.M., Fontenot, J.D., Hajjar, A.M., Smith, K.D., Wilson, C.B., Schroeder, L., and Aderem, A. (2000). The repertoire for pattern recognition of pathogens by the innate immune system is defined by cooperation between toll-like receptors. Proc. Natl. Acad. Sci. U. S. A. *97*, 13766–13771.

Paredes-Juarez, G.A., de Haan, B.J., Faas, M.M., and de Vos, P. (2013). The role of pathogen-associated molecular patterns in inflammatory responses against alginate based microcapsules. J Control Release *172*, 983–992.

Park, J.-H., Kim, Y.-G., McDonald, C., Kanneganti, T.-D., Hasegawa, M., Body-Malapel, M., Inohara, N., and Nunez, G. (2007). RICK/RIP2 Mediates Innate Immune Responses Induced through Nod1 and Nod2 but Not TLRs. J. Immunol. *178*, 2380–2386.

Pearl, J.I., Ma, T., Irani, A.R., Huang, Z., Robinson, W.H., Smith, R.L., and Goodman, S.B. (2011). Role of the Toll-like receptor pathway in the recognition of orthopedic implant wear-debris particles. Biomaterials *32*, 5535–5542.

Poltorak, A. (1998). Defective LPS Signaling in C3H/HeJ and C57BL/10ScCr Mice: Mutations in Tlr4 Gene. Science (80-.). *282*, 2085–2088.

Pritchard, C.D., O'Shea, T.M., Siegwart, D.J., Calo, E., Anderson, D.G., Reynolds, F.M., Thomas, J.A., Slotkin, J.R., Woodard, E.J., and Langer, R. (2011). An injectable thiol-acrylate

poly(ethylene glycol) hydrogel for sustained release of methylprednisolone sodium succinate. Biomaterials *32*, 587–597.

Weir, G.C. (2013). Islet encapsulation: advances and obstacles. Diabetologia *56*, 1458–1461.

Yamamoto, M., Sato, S., Hemmi, H., Hoshino, K., Kaisho, T., Sanjo, H., Takeuchi, O., Sugiyama, M., Okabe, M., Takeda, K., et al. (2003). Role of adaptor TRIF in the MyD88-independent toll-like receptor signaling pathway. Science *301*, 640–643.

Yang, D., and Jones, K.S. (2009). Effect of alginate on innate immune activation of macrophages. J. Biomed. Mater. Res. A *90*, 411–418.

Zimmermann, H., Shirley, S.G., and Zimmermann, U. (2007). Alginate-based encapsulation of cells: past, present, and future. Curr Diab Rep *7*, 314–320.

Chapter 3

Closing Remarks

Current Status of Islet Encapsulation and Development of Novel Alginate Analogs

The content of this chapter in part refers to a recently submitted paper for publication:

Vegas, A.J., Veiseh, O., Doloff, J.C., Ma, M., Tam, H.H., Bratlie, K., Li, J., Bader, A.R., Langan, E., Olejnik, K., Fenton, P., Kang, J.W., Hollister-Locke, J., Bochenek, M.A., Chiu, A., Siebert, S., Tang, K., Jhunjhunwala, S., Aresta-Dasilva, S., Dholokia, N., Thakrar, R., Vietti, T., Cohen, J., Siniakowicz, K., Qi, M., Lyle, S., Harlan, D.M., Greiner, D.L., Oberholzer, J., Weir, G.C., Langer, R., and Anderson, D.G. Combinatorial Development of Hydrogels that Mitigate the Foreign Body Response in Primates. Manuscript submitted for publication to *Science* (2014).

Since Lim and Sun first demonstrated that alginate encapsulated islets corrected diabetic state for 2 to 3 weeks and remained functionally viable over 15 weeks in rats in the 1980s, cell encapsulation technology has remained an attractive therapeutic approach to treat type 1 diabetes (Lim and Sun, 1980). Many subsequent studies advanced this technique since its first inception. But, a great deal of research by many yielded only variable success with rodents, and it proved to be difficult to extend the success to large animals and humans (Calafiore et al., 2006; Elliott et al., 2007; Jacobs-Tulleneers-Thevissen et al., 2013; Omer et al., 2003a; Scharp et al., 1991; Tuch et al., 2009). Although the reports with humans are encouraging, much more work has to be done, particularly in the area of graft rejection, in order to achieve long-term treatment success of diabetic patients with islet cell encapsulation.

Alginate microcapsules, even those without islet cells, can elicit an immune response, which eventually results in fibrosis of the implants and hypoxic death of the enclosed islet cells, and macrophages play an important role in initiating this foreign body response (Omer et al., 2003b). In Chapter 2, we demonstrated that activation of pattern recognition receptors (PRRs) are involved in activating macrophages *in vitro*, and that different alginates can provoke PRR mediated immune response at varying degrees *in vitro*. We showed that UPVLVG (ultrapure, high G) induces the strongest PRR activation, while SLG20 (sterile, high G) and SLG100 (sterile, high G) do so weakly. To follow up on these *in vitro* observations *in vivo*, we examined *in vivo* fibrotic profiling of alginate microcapsules. Alginate microcapsules were made as previously described in Chapter 2, and transplanted into the intraperitoneal (IP) space of C57BL/6 mice. Capsules were retrieved after two

weeks and evaluated for the fibrotic tissue accumulation using dark film microscopy (**Figure 1**). We demonstrated that UPVLVG activates PRR in Chapter 2, and as expected, the retrieved UPVLVG microcapsules are covered with fibrotic cellular debris, as seen in **Figure 2b**. LF10/60 is a middle-grade pharmaceutical alginate, which we utilized as a dirty alginate control in Chapter 2. As expected, LF10/60 microcapsules are heavily fibrosed (**Figure 2b**). Interestingly, the *in vitro* PRR stimulatory profiles of SLG20 and SLG100 are not in agreement with the *in vivo* fibrotic profiles of the microcapsules. We demonstrated that SLG20 and SLG100 are not strong immunostimulatory alginates *in vitro*; however, retrieved SLG20 and SLG100 microcapsules are heavily fibrosed (see **Appendix A**). Disagreement between *in vitro* and *in vivo* data is not a rare occurrence in biological sciences, and we can only speculate that the difference is likely due to a myriad of complicated biological reactions happening *in vivo* that are not present in a simplified *in vitro* experiment.

Alginate is by far the most reliable and most widely used material for microencapsulation of islet cells; however, in order to eliminate variability and achieve long-term success of encapsulated islet cell transplantation, the need for more reliable biomaterials that can provide reproducible results is undeniable. In our lab, there was a consorted effort to generate a library of novel, chemically modified alginates. A total of 902 polymer library was generated, and their fibrotic responses *in vivo* were profiled using a rapid subcutaneous mouse model. The top nine alginate analogs with superior *in vivo* performances resisting the foreign body responses were identified: E9, RZA15, RZA19, RN7, RN8, OH6, OH9, OP3, and OH11 (see **Appendix A**). We tested *in vitro*

immunostimulatory capacity of these modified alginate analogs. We subsequently investigated how *in vitro* immunostimulatory profile of these modified alginate analogs compares to the *in vivo* fibrotic profiles. Hydrogels were made, using the same experimental procedures described in **Chapter 2**, and RAW-Blue™ cells were plated on top (see **Appendix B**). As seen in **Figure 3**, no PRR activation was observed against E9 and RZA15 – in agreement with *in vivo* capsule retrieval data. However, even though RZA19 retrieved capsules did not have significant fibrous deposition, *in vitro* PRR activation against RZA19 was statistically significant ($p < 0.001$). RN8, OH6, and OH1 displayed statistically significant level of PRR activation as expected based on *in vivo* retrieval data. However, no PRR activation was observed with OH9 and OH3 despite the fact that some fibrous deposition was observed on the retrieved capsules.

We performed these experiments to investigate how these modified alginate analogs can mitigate foreign body response. Both *in vivo* and *in vitro* results support that E9 is the top performing alginate analog with the least amount of fibrotic deposition and low immune cell recruitment *in vivo* and no PRR activation *in vitro* (**Figure 2**), yet understanding how it can mitigate foreign body response requires further studies. The Arturo et al. hypothesized that chemical modification of the polymer chain may create distinctive surface on E9. In the paper submitted for publication, they investigated surface features of these modified analogs, and found that E9 capsules have fewer cratered features compared to SLG20 capsules. This surface topology may contribute to how cells and adhere to the capsule surface. As we demonstrated in Chapter 2, cell-to-material direct contact is an important step in initiating PRR mediated immune response against alginate.

When alginate capsules are implanted, the material surface gets immediately coated with proteins from blood/serum and interstitial fluids, subsequently recruiting a host of inflammatory cells to the implant site (Anderson et al., 2008; Bridges and García, 2008; Franz et al., 2011). The different surface topology of E9 analog may alter this very first adsorption step, ultimately mitigating foreign body response.

Cell encapsulation technique undoubtedly remains an attractive therapeutic option to treat not only diabetes, but also other diseases that require replacement of diseased cells. Many challenges remains to be addressed, but the novel alginate analogs developed in our lab promises a major therapeutic advance in improving cell encapsulation technology. Cell replacement therapy without systemic immunosuppression may not be that far out of reach after all.

The situation with regard to insulin is particularly clear. In many parts of the world diabetic children still die from lack of this hormone. ... [T]hose of us who search for new biological facts and for new and better therapeutic weapons should appreciate that one of the central problems of the world is the more equitable distribution and use of the medical and nutritional advances which have already been established. The observations which I have recently made in parts of Africa and South America have brought this fact very forcible to my attention.

~ Charles Best, 1952

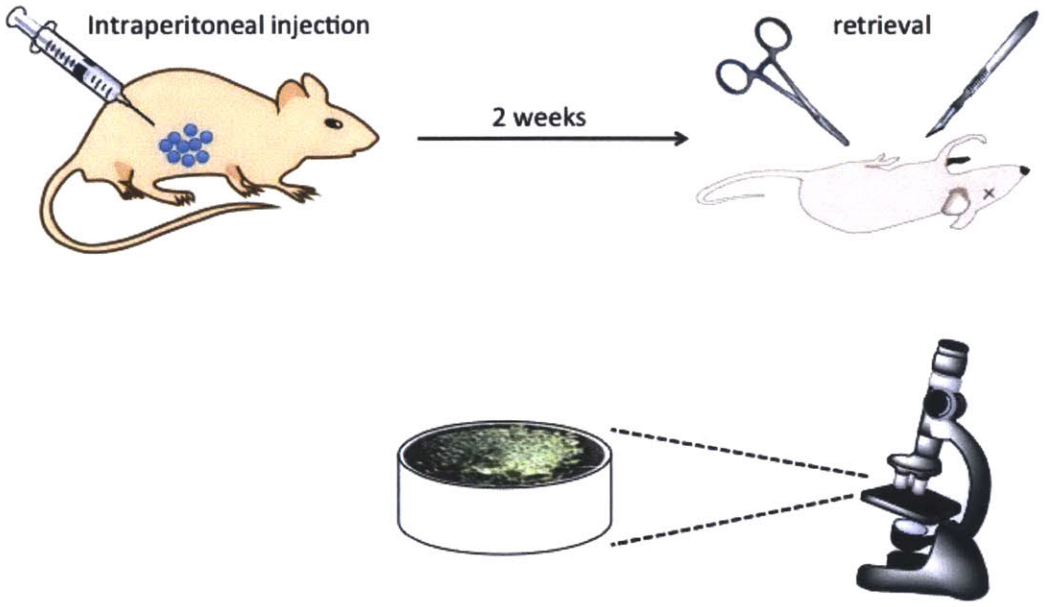

Figure 1. Schematic diagram of the method to examine fibrotic profiling of alginate microcapsules *in vivo*. Alginate microcapsules are transplanted into the intraperitoneal (IP) space of C57BL/6 mice. Capsules are retried after two weeks and evaluated for the fibrotic tissue accumulation with dark film microscopy.

(a)

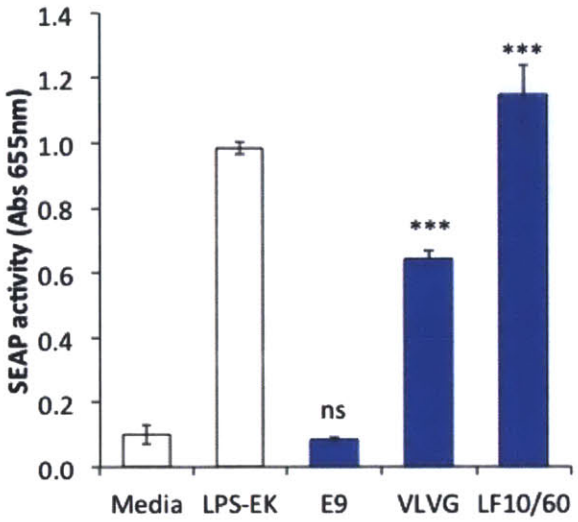

(b)

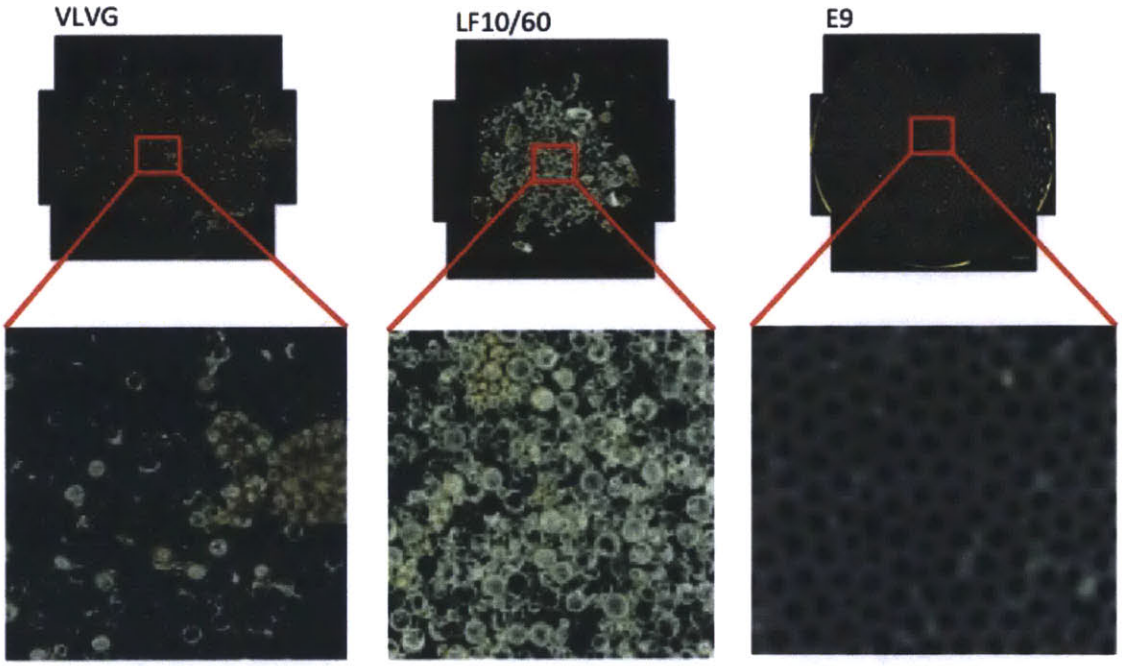

Figure 2. *In vitro* immunostimulatory capacity and *in vivo* fibrotic profiling of UPVLVG, E9, and LF10/60. (a) Stimulation of PRR activation with RAW-Blue™ cells on alginate hydrogels. (b) Phase contrast images of alginate microcapsules retrieved after two weeks. The brownish debris on the capsule surface is the cellular and collagenous fibrotic deposition.

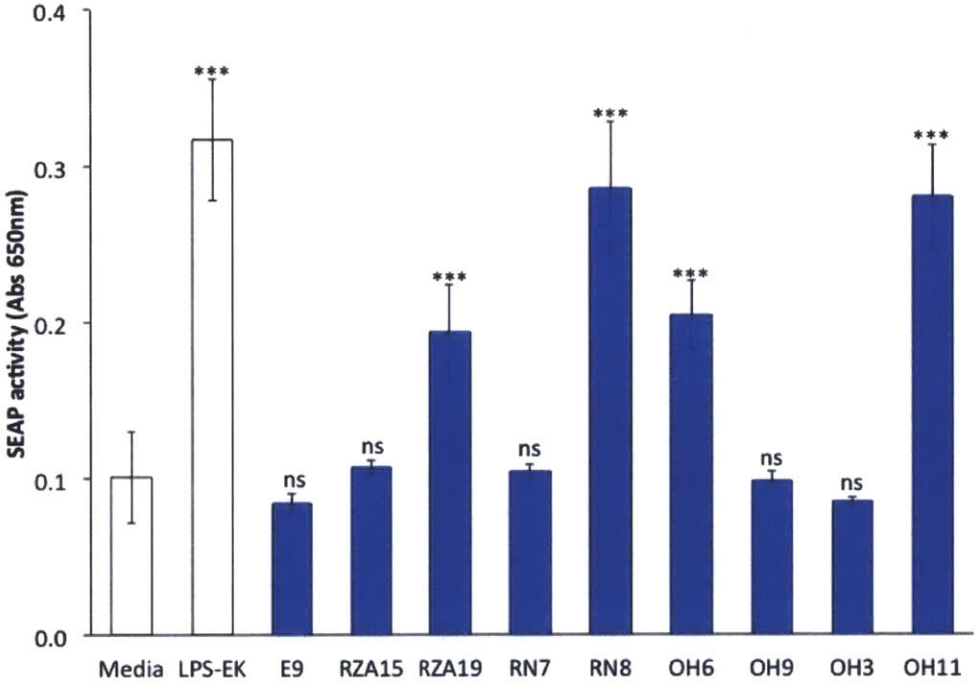

Figure 3. *In vitro* immunostimulatory profiles of modified alginate analogs. NF-κB activation of pattern recognition receptors (PRRs) by modified alginate hydrogels. LPS-EK (5μg/ml) was used as a positive control, and blank media was used as a negative control. Values are presented as mean ± SD (n = 7). Cells were incubated overnight with the hydrogels, and absorbance at 655nm was measured after 2-hour incubation with QUANTI-Blue™. Statistical comparison of each alginate analog value to the negative control media was made using Prism one way ANOVA analysis with Tukey's test. p-value < 0.001 (***), p-value < 0.01 (**), p-value < 0.05 (*), p-value > 0.05 (ns).

References

Anderson, J.M., Rodriguez, A., and Chang, D.T. (2008). Foreign body reaction to biomaterials. Semin. Immunol. *20*, 86–100.

Bridges, A.W., and García, A.J. (2008). Anti-inflammatory polymeric coatings for implantable biomaterials and devices. J. Diabetes Sci. Technol. *2*, 984–994.

Calafiore, R., Basta, G., Luca, G., Lemmi, A., Montanucci, M.P., Calabrese, G., Racanicchi, L., Mancuso, F., and Brunetti, P. (2006). Microencapsulated pancreatic islet allografts into nonimmunosuppressed patients with type 1 diabetes: first two cases. Diabetes Care *29*, 137–138.

Elliott, R.B., Escobar, L., Tan, P.L.J., Muzina, M., Zwain, S., and Buchanan, C. (2007). Live encapsulated porcine islets from a type 1 diabetic patient 9.5 yr after xenotransplantation. Xenotransplantation *14*, 157–161.

Franz, S., Rammelt, S., Scharnweber, D., and Simon, J.C. (2011). Immune responses to implants - a review of the implications for the design of immunomodulatory biomaterials. Biomaterials *32*, 6692–6709.

Jacobs-Tulleneers-Thevissen, D., Chintinne, M., Ling, Z., Gillard, P., Schoonjans, L., Delvaux, G., Strand, B.L., Gorus, F., Keymeulen, B., Pipeleers, D., et al. (2013). Sustained function of alginate-encapsulated human islet cell implants in the peritoneal cavity of mice leading to a pilot study in a type 1 diabetic patient. Diabetologia *56*, 1605–1614.

Lim, F., and Sun, A.M. (1980). Microencapsulated islets as bioartificial endocrine pancreas. Science (80-.). *210*, 908–910.

Omer, A., Duvivier-Kali, V.F., Trivedi, N., Wilmot, K., Bonner-Weir, S., and Weir, G.C. (2003a). Survival and maturation of microencapsulated porcine neonatal pancreatic cell clusters transplanted into immunocompetent diabetic mice. Diabetes *52*, 69–75.

Omer, A., Keegan, M., Czismadia, E., De Vos, P., Van Rooijen, N., Bonner-Weir, S., and Weir, G.C. (2003b). Macrophage depletion improves survival of porcine neonatal pancreatic cell clusters contained in alginate macrocapsules transplanted into rats. Xenotransplantation *10*, 240–251.

Scharp, D.W., Lacy, P.E., Santiago, J. V, McCullough, C.S., Weide, L.G., Boyle, P.J., Falqui, L., Marchetti, P., Ricordi, C., and Gingerich, R.L. (1991). Results of our first nine intraportal islet allografts in type 1, insulin-dependent diabetic patients. Transplantation *51*, 76–85.

Tuch, B.E., Keogh, G.W., Williams, L.J., Wu, W., Foster, J.L., Vaithilingam, V., and Philips, R. (2009). Safety and viability of microencapsulated human islets transplanted into diabetic humans. Diabetes Care *32*, 1887–1889.

Appendix A

In vivo fibrotic profiling of commercial and modified alginate microcapsules

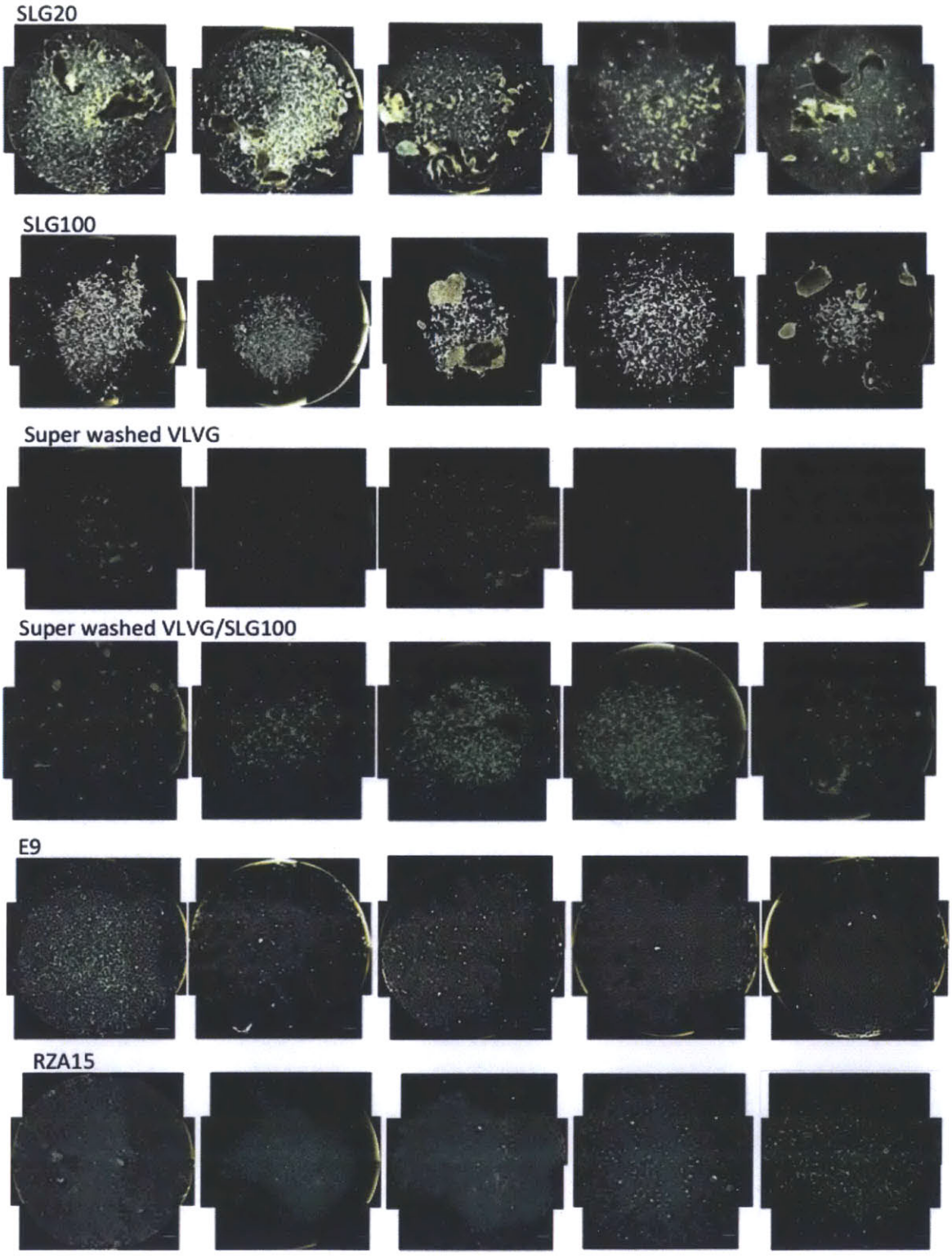
SLG20
SLG100
Super washed VLVG
Super washed VLVG/SLG100
E9
RZA15

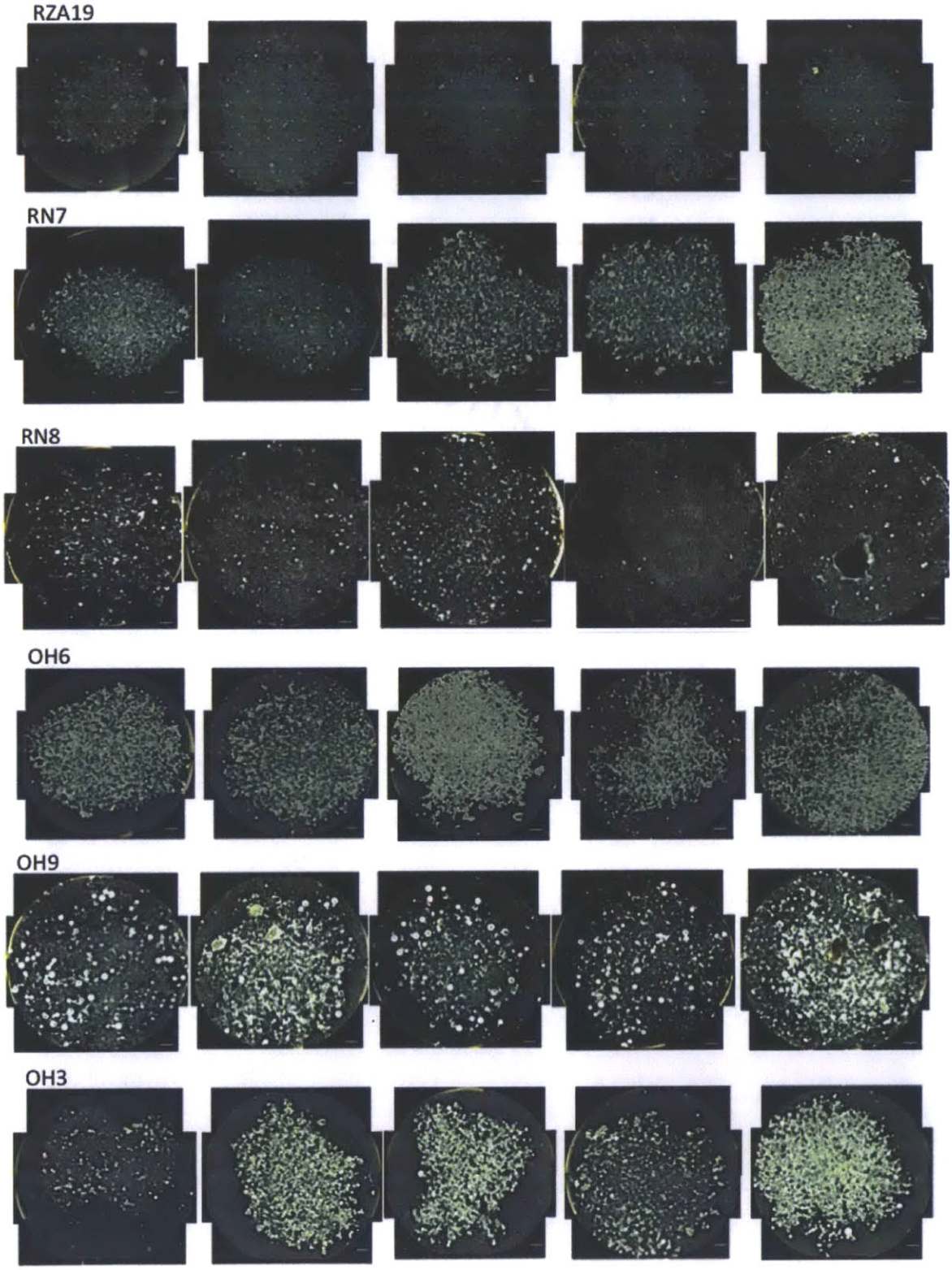
RZA19
RN7
RN8
OH6
OH9
OH3

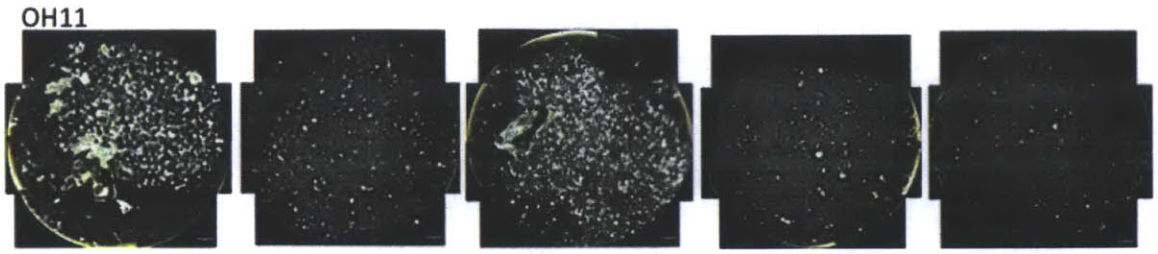

Phase contrast images of microcapsules retrieved from IP. Capsules of commercial alginate SLG20, SLG100, UPVLVG and UPVLVG/SLG100, and capsules of top nine alginate analogs were transplanted in the intraperitoneal (IP) space of C57BL/6 mice, and were retrieved after two weeks. Fibrotic tissue accumulation was evaluated with dark film microscopy. The brownish debris on the capsule surface is the cellular and collagenous fibrotic deposition.

Appendix B

Bright field microscopy images of RAW-Blue™ cells seeded modified alginate hydrogels

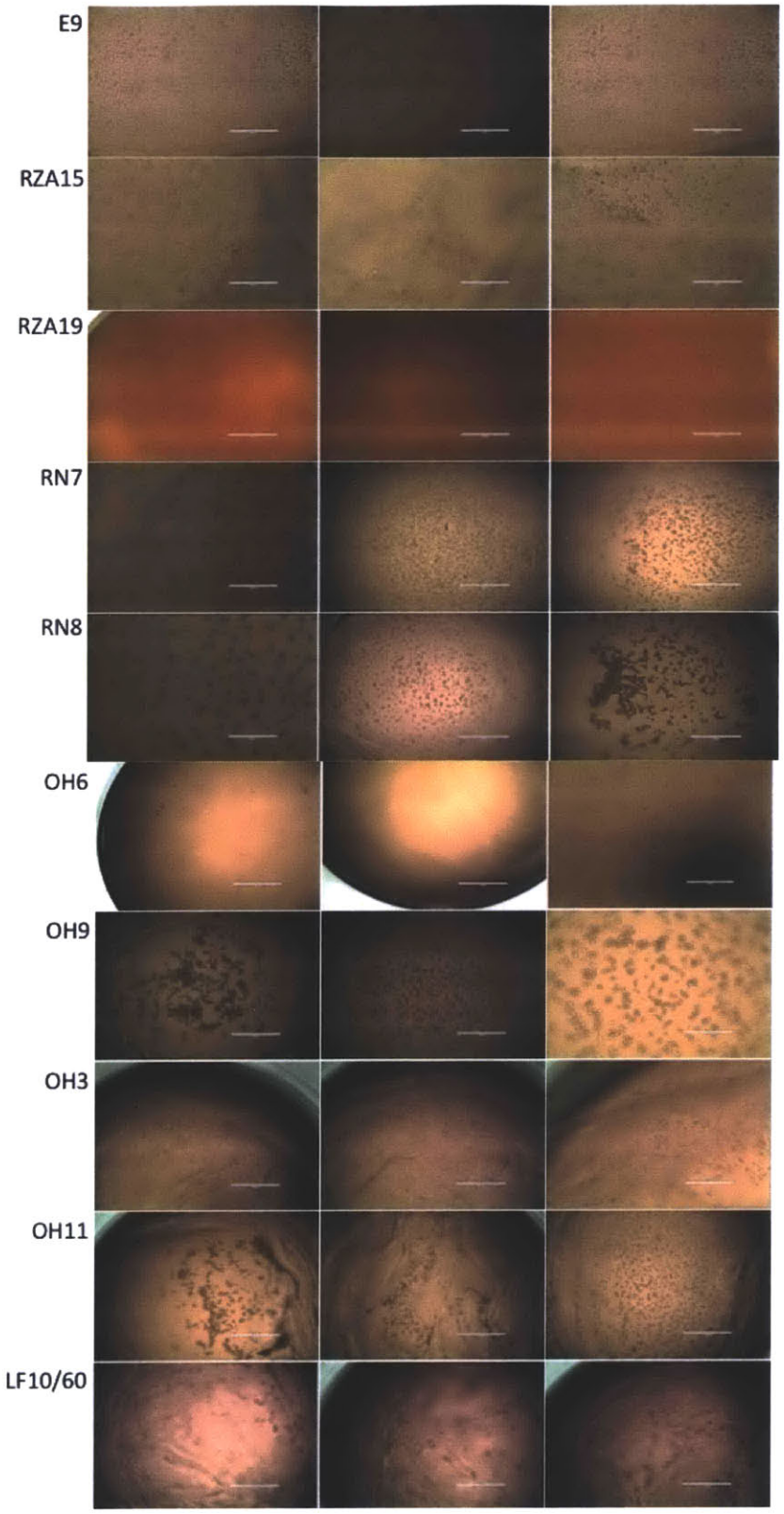
E9
RZA15
RZA19
RN7
RN8
OH6
OH9
OH3
OH11
LF10/60